Receiver Design for OFDM Transmission with Insufficient Cyclic Prefix

Tri Pham

Electrical and Computer Engineering Department

University of Canterbury

A thesis submitted for the degree of

Doctor of Philosophy (Ph.D)

May 2016

Abstract

Orthogonal frequency division multiplexing (OFDM) is desirable for broadband communication because of its high spectral efficiency and resistance to multipath fading. The latter is achieved by adding a cyclic prefix to the beginning of each OFDM symbol. The cyclic prefix length must be equal to or greater than the channel delay spread to avoid multipath interference. For long range transmission, this criterion leads to bandwidth inefficiency. If a shorter cyclic prefix is used, the interference caused corrupts both pilot and data sub-carriers leading to degradation in channel estimation and data detection.

This thesis focuses on developing effective receiver designs for multiple antenna orthogonal frequency division multiplexing systems when the cyclic prefix is insufficient. Closed form expressions for the short cyclic prefix induced interference are formulated and analyzed. Based on the analysis, we propose an iterative structure for channel estimation and data detection using a limited number of pilot sub-carriers. First, the number of channel paths is estimated from the channel least squares estimates at the pilot sub-carriers. We then formulate a maximum likelihood process to approximate the channel delay profile and subsequently the individual path coefficients. A search procedure is designed to reduce the estimator's complexity.

High performance trellis based equalization schemes are proposed. Two additional data detection methods based on the zero forcing and minimum mean square error criteria are introduced with lower complexity than the trellis equalizers at the cost of performance. Simulation results indicate that the proposed techniques outperform conventional receivers, especially when the trellis equalizer is utilized for data detection. The mean square error of the channel estimate converges to the Cramer-Rao bound after two iterations; and the achieved bit error rate can reach that of the sufficient cyclic prefix case even when the delay spread is significantly longer than the cyclic prefix.

This thesis is dedicated to my family, especially my mother Lan Jones, whose love and support have given me the strength to continue along the research journey.

Acknowledgements

It is an honour for me to acknowledge the help of many people, without which this thesis would not have been possible.

Firstly, I would like to show my deep gratitude to Associative Professor Philippa Martin, my senior supervisor, whose outstanding help provided me with great insight into the area of multiple antenna systems and iterative receiver design. Her caring attitude and her constant encouragement and inspiration kept me on task throughout.

I am indebted to Dr. Graeme Woodward, my senior supervisor, whose admirable knowledge and supervision guided me through to the completion of this research. Dr. Graeme Woodward supported me in many ways and gave me lots of invaluable suggestions and research materials in the area of channel estimation and data detection in OFDM systems.

I am fortunate to have had Dr. Clive Horn and Dr. Krishna Prasad as my industrial supervisors. The many constructive discussions on practical applications of my research I had with Dr. Clive Horn were important to my research direction. Dr. Krishna Prasad's great assistance, especially with channel and communication systems modelling, and the many constructive discussions on radio systems I had with him were definitely indispensable to my research.

I would like to thank my supervisor at McGill University, Professor Tho Le-Ngoc, for the opportunity he gave me to conduct my research in the Broadband Communications laboratory at McGill University and his enlightening advice in the research progression.

I appreciate the generous funding I received from the Tait Communications Research Scholarship and the Broadband Communications laboratory. I am also grateful to the Wireless Research Centre and Tait

Communications (particularly the innovation team), who provided me with the necessary resources and assistance throughout the course of my research.

My special acknowledgement to Khoa Phan, whose ideas were very valuable for my research. My sincere thanks to Yuan Chen, Duy Nguyen, Hung Vu, Sanjeewa Herath, Imtiaz Ahmed, Minh Huynh, Hanh Nguyen and Joanne Lee, who offered me a lot of help for this project and thesis writing.

Most importantly, my special mention must go to my family, including my little sister - Hannah Jones, for providing me with a caring home environment. I am thankful for the support of my step-relatives, Lynette Jones and Ian Hunter, over the years of my study. I acknowledge my stepfather, Greg Jones, for his frequent help, especially with my English writing. I never forget the regular encouragements my father, Cuong Pham, has given me since I first started school. I owe much to my mother, Lan Jones, for her endless care and love, bringing me to where I am in my life journey.

Lastly, my thanks to all those whose names I am unable to mention here but supported me in many respects during the completion of the thesis.

Contents

List of Figures

List of Tables

Abbreviations and Acronyms

A-QAM A-ary Quadrature Amplitude Modulation

AWGN Additive White Gaussian Noise

BDMA Bi-Directional M-Algorithm

BER Bit Error Rate

EPSB-MMSE Enhanced PSB-MMSE

ETU Extended Typical Urban

FD Frequency Domain

ICI Inter-Channel Interference

IJEP Iterative Joint Estimation Procedure

ISCP Insufficient Cyclic Prefix

ISI Inter-Symbol Interference

LS Least Square

LSI Least Square-Interpolation

MAP Maximum a Posteriori

MIMO Multiple Input Multiple Output

MLSE Maximum Likelihood Sequence Detection

MMSE Minimum Mean Square Error

MRC Maximal Likelihood Combining

OFDM Orthogonal Frequency Division Multiplexing

PDP Power Delay Profile

PSB-MMSE Pilot Sub-carrier Based MMSE

RISIC Residual ISI Cancellation

RLS Recursive Least Squares

RS Reference Signal

S/P Serial to Parallel

SCP Sufficient Cyclic Prefix

SIMO Single Input Multiple Output

SINR Signal to Interference and Noise Ratio

SIRF Shortened Impulse Response Filter

SISO Single Input Single Output

SNR Signal to Noise Ratio

SS Symmetric Sequence

TD Time Domain

ZF Zero Forcing

Common Mathematical Symbols

A	Order of the sub-carrier modulation.
$\boldsymbol{A}$	A-ary constellation set of the sub-carrier modulation.
$\boldsymbol{C}$	Channel covariance matrix.
d	Number of sub-carrier tracing back on one side of the sub-carrier of interest.
D	Number of channel paths with delays smaller than CP length.
G	CP length.
$h_{u,v,l}$	l^{th} path gain of the channel between the u^{th} receive and v^{th} transmit antennas.
$\boldsymbol{h}_u$	Vector containing all paths coefficients corresponding to receive antenna u.
$H_{u,v}(k)$	k^{th} channel gain at sub-carrier k of the channel between the u^{th} receive and v^{th} transmit antennas.
I	Number of iterations.
$\boldsymbol{I}$	Identity matrix.
L	The number of channel paths.
M	M-factor considered in the BDMA algorithm.
$n(a)$	Noise at sub-carrier a.
N	FFT size.
N_T	Number of transmit antennas.
N_R	Number of receive antennas.
N_p	Number of pilot sub-carriers.
$R_u(k)$	Total received signal corresponding to sub-carrier k at the u^{th} receive antenna.
$R_{d,u}(k)$	Desire component of $R_u(k)$.
$R_{ici,u}(k)$	ICI component of $R_u(k)$.
$R_{isi,u}(k)$	ISI component of $R_u(k)$.
$R_{u,v}(k)$	Received signal at the u^{th} receive antenna corresponding to sub-carrier k and transmit antenna v.
$X_{v,m}(k)$	Complex symbol transmitted on sub-carrier k of the m^{th} OFDM symbol from the v^{th} transmit antenna.
$\boldsymbol{X}$	Vector containing all data symbols transmitted over a transmission frame.
Y_u	Signal from receive antenna u after ISI and ICI mitigation.
τ_l	Delay in sample intervals of path l.
τ_{rms}	RMS delay spread of the transmission channel.
τ_{max}	Maximum delay spread of the transmission channel.
τ_{PD}	Predefined maximum channel delay spread for an OFDM network.
σ_l	Average amplitude of path l.

Chapter 1

Introduction

1.1 Motivation

Today's information society has a heavy demand for communication systems that are cheaper, faster, mobile, more reliable and higher quality. The proliferation of wireless communication services for voice, video and data, has necessitated the development of systems that have greater capacity and can operate reliably over the often hostile wireless channel. In order to increase the quality of service, we can employ larger channel bandwidth, larger transmit power and/or more spectrally efficient methods for transferring information. *Orthogonal frequency division multiplexing (OFDM)* [3] has numerous advantages for mobile communication because it has a high spectral efficiency and a natural immunity to multipath propagation. Hence, OFDM has become a core technology in many wireless standards including 802.11 WiFi for local area networks [4], 802.16 WiMAX [5] for wireless metropolitan area network, and 3GPP LTE and LTE-Advanced for 3G and 4G mobile communication [1, 6].

OFDM is a multi-carrier modulation method in which a large number of closely spaced orthogonal sub-carrier signals are used to carry data on several parallel data streams or channels [3, 7]. This allows the technique to achieve spectral efficiency. However, a certain amount of transmission time must be reserved for the *cyclic prefix (CP)*, which provides OFDM's resistance to multipath interference. The CP length must be greater than (or equal to) the channel delay spread for a total immunity to the multipath interference [8, 9]. For long range transmission, the channel

delay spread can become significant leading to a long CP, which causes causes lower total data rates and communications inefficiencies. For example, the CP length in WiFi and LTE can be up to 25% of the length of the data component of an OFDM symbol [4, 6]; this is equivalent to having 20% of the system bandwidth reserved for CP.

Insufficient CP in OFDM transmission leads to interference in the form of *inter-symbol interference (ISI)* and *inter-channel interference (ICI)*, which destroys the sub-carrier orthogonality [10]. ISI is caused by the last part of the previous OFDM symbol overlapping with the current OFDM symbol while ICI is caused by the energy of a sub-carrier leaking to other sub-carriers. Hence, the original OFDM symbol cannot be reconstructed without distortion by means of the standard one-tap equalizer at the receiver [11]. The channel estimation process is also affected as pilot sub-carriers are contaminated by interference. Standard channel estimators such as the *least squares-interpolation (LSI)* method are not able to provide an accurate channel estimate, which is important for the subsequent data detection process. The addition of multiple antenna technology can further increase the interference and hence further complicates the receiver design [12].

A system might be able to mitigate such effects by increasing the CP length. However, this results in a reduction of spectral efficiency, which is undesirable. Also, existing standards only permit a CP length up to a pre-set limit. Therefore, sophisticated channel estimation and equalization for eliminating the effects of insufficient CP are important in maintaining OFDM spectral efficiency, especially for long range transmission. This also helps to increase the OFDM transmission range for a fixed CP value.

1.2 Literature Overview

Insufficient CP in OFDM transmission leads to interference in the form of ISI and ICI, which affects both channel estimation and data detection processes. It was shown in [13–15] that the interference increases with respect to the amount that the channel delay spread exceeds the CP. Hence, in the case of long range transmission, the interference can lead to a large reception error. To alleviate this problem, a number of channel estimation and data detection methods for insufficient CP systems

have been proposed in the literature as summarized below.

1.2.1 Channel Estimation

In terms of channel estimation, many schemes assume a pilot signal that consists of a few OFDM symbols (called pilot OFDM symbols) with all sub-carriers dedicated for pilots [2, 16–26]. One strategy is to design 2 consecutive pilot OFDM symbols in such a way that ISI and ICI are forced to cancel each other in the second OFDM symbol; and channel estimation can be done at the second pilot OFDM symbol [17, 18]. Alternatively, channel estimation can rely on a single symmetric pilot OFDM symbol, whose second half part is free from interference. The initial channel estimate can be calculated from this second part [2, 19–22]. The designs of such algorithms are described in detail in Section 2.3. In [16, 23–26], channel estimation algorithms are proposed for a non-symmetric pilot OFDM symbol. The method proposed in [27] utilizes pilot OFDM symbols with variable CP length to avoid pilot corruption from insufficient CP interference. Although these methods can provide accurate channel approximation, there are practical limitations in mobile systems. This is because major mobile OFDM systems such as LTE do not support pilot OFDM symbols. For example, LTE pilot sub-carriers are instead mixed with data sub-carriers [1], thus making the process of channel estimation significantly more difficult. In addition, due to mobility, the channel needs to be estimated frequently, requiring frequent pilot transmission. Since a pilot OFDM symbol consumes a large amount of bandwidth, a significant part of the system bandwidth would be spent on pilots leading to bandwidth inefficiency. This counters the purpose of using insufficient CP for improving the bandwidth efficiency.

To reduce the bandwidth usage for piloting, a blind channel estimation scheme for insufficient CP OFDM systems is shown in [28–31]. The method utilizes the redundancy introduced by the CP or the un-used/virtual sub-carriers within the system for identifying the channel. However, the method requires the channel to be invariant over a very high number of OFDM symbols. Therefore, it is not suitable for mobile systems. In [32], a *recursive least squares (RLS)* channel estimator is proposed for insufficient CP *single input multiple output (SIMO)* OFDM systems using scattered pilot sub-carriers. The method requires a high number of iterations (6 iterations) to achieve good channel estimate. There are also a number of channel

estimation methods that utilize pilot sub-carriers to estimate the Doppler induced ICI channel such as [33–39]. However, for mobile systems such as LTE, the Doppler induced ICI is negligible [37] while insufficient CP induced interference is significant. These approaches have not been designed for the interference resulting from insufficient CP, which is significant for high delay spread channels. To the best of our knowledge, there is currently no high performance channel estimation method for insufficient CP MIMO-OFDM with a limited number of pilot sub-carriers.

1.2.2 Data Detection - Equalization

There are a number of techniques for mitigating the effects of insufficient CP induced interference available in literature. Realizing that the source of interference is caused by the channel delay exceeding the CP length, one of the equalization approaches is to shorten the channel response before the demodulation takes place. In order to achieve that, a *time domain (TD)* equalizer in the form of a finite impulse response filter (denoted as the *shortened impulse response filter (SIRF)*) is designed so that the effective channel, which is the convolution of transmit filters, physical channel, receive filters and the SIRF, is shorter than or equal to the CP length [40–50]. A *frequency domain (FD)* equivalent design of SIRF is shown in [51, 52]. In general, regardless of how the SIRF is designed, it is not possible to shorten the channel perfectly. The effective response still has some energy lying outside the CP length. Moreover, it has been shown that equalization techniques with channel shortening are sensitive to parameters, such as the channel-shortening equalizer length and the channel delay, which can vary over time for mobile channels [53].

The second technique is a TD statistics-based technique previously proposed by the authors in [54, 55]. The method is based on some structural properties of the received OFDM symbols, which contain redundancy due to the presence of the CP. A TD equalizer, which is designed using the second-order statistics of the received OFDM symbols, is applied to partially cancel the ICI and ISI. However, in order to achieve accurate data reception, a significantly large number of OFDM symbols need to be involved in the detection process. In [56], a beamforming technique with adaptive antenna array is utilized to null out the interference. The technique can provide good interference cancellation; however, it is impractical to have antenna array on mobile devices. A blind beamforming scheme for multiuser OFDM systems

is shown in [57].

In [58–62], a pre-coding technique is also used to remove the distortion due to insufficient CP. The main disadvantage of the technique is the addition of a pre-coding process in the transmitter. Such modification may not be applicable to the existing wireless communication standards. A frequency domain equalization technique employing a hybrid detection criterion is shown in [63]. The hybrid criterion is based on the *zero-forcing (ZF)* criterion for compensating desired sub-carriers and the *minimum mean square error (MMSE)* criterion for suppressing interference. Another approach is to employ iterative tail cancellation and cyclic reconstruction to eliminate ISI and ICI as shown in [2,64–72]. Most of these techniques require a complex iterative process between an equalizer and a channel decoder with soft decoding for reliable data detection, especially when the channel delay spread is significantly higher than the CP length. The procedure of such algorithms will be described in detail in Section 2.3.2.1.

Another important group of equalization methods available in literature are the trellis-based schemes [73–76]. The design in [73] utilizes a smoothing window to concentrate the ICI energy to adjacent sub-carriers for *maximum likelihood sequence estimation (MLSE)*. However, the performance of the smoothing window deteriorates quickly when the channel delay spread becomes significant leading to high *bit error rate (BER)*. The two stage advanced receiver in [75] employs the combination of a sub-carrier combiner and MLSE equalizer to enhance the equalization process. A turbo detection structure of a *maximum a posteriori (MAP)* equalizer and a channel decoder is shown in [74, 76]. It achieves accurate data reception with few iterations even for high channel delay spread. In general, the trellis based techniques are attractive because they can offer accurate symbol by symbol detection for channels with significant delay spread without the need for modifying existing OFDM transmitters. Yet, this can be achieved with a low number of iterations. However, the existing techniques are limited to single antenna systems. In addition, they can not be easily extended to multiple antenna systems due to impractical complexity. The operation of these trellis equalizers will be described in detail in Section 2.3.2.2 as their designs motivate the proposed trellis based equalizers.

1.3 Scope

The core of this research is to develop an effective receiver for insufficient CP OFDM systems with multiple transmit/receive antennas. Here, we focus on the channel estimation and data detection within the reception process. Other elements of the receiver such as synchronization and error control coding are not considered.

An important part of this work is that the developed receiver design must be compatible with existing wireless standards such as LTE for mobile communications. This means that the developed scheme must be able to provide accurate channel estimates using a limited number of pilot sub-carriers for mobile channels. In terms of data detection, due to the advantage of trellis-based equalizers, we focus on designing such equalizers for multiple antenna systems with a constraint on complexity for practical applications. The developed channel estimator and equalizer are then incorporated to form an iterative structure of interference cancellation, channel estimation, and detection for achieving reliable data reception. The proposed design is evaluated using theoretical performance analysis, complexity analysis and simulations.

The examples and performance results presented in this thesis are focused on OFDM systems with LTE parameters [1]. A multipath Rayleigh fading channel model with *additive white Gaussian noise (AWGN)* is assumed. The proposed designs are for mobile and long range communication. Therefore, a fast fading Rayleigh channel model is considered with a delay spread exceeding that of the OFDM system CP. Additionally, the receiver is assumed to have perfect knowledge of symbol timing, carrier frequency and carrier phase as the estimation of such synchronization parameters are beyond the scope of this thesis. The proposed design will be implemented and tested in Matlab as a proof of concept.

1.4 Research Contributions

Our work in this thesis aims to keep short CP (shorter than the actual delay spread in real scenarios) for high OFDM transmission efficiency (and hence high spectral efficiency), and to develop efficient channel estimation and data detection techniques for insufficient CP OFDM systems. In other words, the practical application value

of this paper is about (i) compensating for cases in which the delay spread is higher than the CP length, or (ii) improving the MIMO-OFDM system spectral efficiency by reducing the CP length. An example for (i) is in the area of LTE broadcasting. As identified in [77], the current CP specifications in LTE may not be able to handle the long channel delay spread occurred in broadcasting systems. An example for (ii) is that, in LTE systems, the extended CP is often utilized when the channel delay spread is longer than the standard CP. Depending on channel conditions, the proposed receiver design can allow the system to utilize the standard CP instead of the extended CP while keeping a reliable communication link. Our proposed design can allow the channel delay spread up to 3 times the CP length. The original contributions in this thesis include:

- A detailed investigation of insufficient CP induced interference in SIMO and *multiple input multiple output (MIMO)* OFDM systems under fast fading and high delay spread multipath channel conditions [78].

- Development of accurate-LTE compatible channel estimation schemes for insufficient CP SIMO and MIMO-OFDM systems using a limited number of pilot sub-carriers [78, 79]. Performance analysis (in the form of the *Cramer Rao bound (CRB)*) and complexity analysis for the developed estimators are also performed.

- Development of high performance trellis-based equalizers for insufficient CP SIMO and MIMO-OFDM systems with practical complexity and LTE compatibility [80, 81]. Complexity analysis for the developed schemes is also given.

- Development of an effective iterative reception process from the developed channel estimators and equalizers [78, 79]. Simulation results show that the *mean square error (MSE)* of the channel estimate converges to the CRB after a few iterations. At the same time, the achieved BER can reach that of the sufficient CP case even when the delay spread is much longer than the CP.

The above contribution resulted in the following publications:

- Pham, T.M., Le, N.T., Woodward, G., Martin, P.A. (2016) *Channel Estimation and Data Detection for Insufficient Cyclic Prefix MIMO-OFDM*. Accepted to IEEE Trans. Veh. Tech., 2016. [78]

- Pham, T.M., Le, N.T., Woodward, G., Martin, P.A., Phan, T.K. (2015) *Equalization for MIMO-OFDM Systems with Insufficient Cyclic Prefix.* Nanjing, China: IEEE 83rd VTC, 15-18 May 2016. [81]
- Pham, T.M., Woodward, G., Martin, P.A. (2015) *Channel Estimation and Data Detection for Insufficient Cyclic Prefix SIMO-OFDM with Pilot Subcarriers.* Melbourne, Australia: IEEE 16th AusCTW, 20-22 Jan 2016. [79] (Best poster awarded paper)
- Pham, T.M., Martin, P.A., Woodward, G., Kongara, K.P. and Horn, C. (2014) *Receiver Design for SIMO-OFDM Systems with Insufficient Cyclic Prefix.* Vancouver, Canada: IEEE 80th VTC, 14-17 Sep 2014. [80]

1.5 Thesis Outline

Chapter 2 begins by introducing the wireless channel and its different models. In particular, attention is paid to the Rayleigh multipath fading channel, which can be represented by a discrete multipath model as shown in [82]. This model is based on the assumption that the delay power profile and the Doppler spectrum of the channel are separable. In other words, the complex path gains are uncorrelated with each other. This is followed by a description of general baseband OFDM communication systems with descriptions of the standard OFDM transmitter and receiver. OFDM is then reviewed with the addition of SIMO and MIMO technology. The final section explains the pilot arrangement in LTE systems and the standard interpolation method for channel estimation.

Chapter 3 contains a detailed analysis of the insufficient CP induced interference in OFDM systems. This includes the derivation of the mathematical model for the interference from first principles and a discussion of the interference distribution. A proof is given to show that ICI is also a major source of interference (not just ISI) and most of the ICI energy inflicted on a sub-carrier comes from the sub-carriers close to it. The final section shows the formulation of the received *signal to interference and noise ratio (SINR)* with respect to the channel delay spread.

A multi-step channel estimator and different equalizers for insufficient CP SIMO-OFDM systems are derived in Chapter 4. As the number of pilot sub-carriers is

limited, the proposed channel estimator estimates the number of channel paths and their corresponding delays before computing the complex path gains. Various equalization schemes based on ZF, MMSE and MLSE criterions are designed. An effective multi-stage equalization structure is developed by combining the schemes together. Lastly, an iterative reception process of channel estimation and equalization is given from the developed methods. The performance of these methods are evaluated by simulation with OFDM parameters compatible to LTE systems.

In Chapter 5, the proposed channel estimator and trellis-based detector are extended to MIMO. The proposed MIMO channel estimator utilizes both pilot subcarriers and hard data decisions from previous iterations to improve the estimation accuracy. The new equalization algorithm contains a bi-directional process for enhancing the detection quality and it employs the M-algorithm [83] for complexity reduction. The chapter continues with the development of the CRB and the complexity analysis of the methods.

The pertinent results of the thesis are summarized and some ideas for future research related to the work completed in this thesis are presented in Chapter 6.

Chapter 2

General Background

This chapter presents the relevant background information for the wireless channel models and OFDM systems considered in this thesis. First, a description of the wireless multipath channel and the fading environment is given. The multipath fading found on wireless channels can have devastating effects on the performance of communication systems and it is important to know the channel characteristics. After describing the wireless channel, we introduce a general baseband OFDM communication link, which employs various signal processing techniques to transmit and receive data. Here, a pilot sub-carrier arrangement for channel estimation is also described. The following section introduces the standard receivers for SIMO and MIMO-OFDM systems with sufficient CP. An overview of iterative receivers for insufficient CP OFDM is also given in this chapter.

2.1 Wireless Channel

The performance attainable by wireless communication systems is limited by the effects of the radio channel. The channel has a time-varying nature, and hence transmission and analysis is more difficult than for fixed wired channels [84]. Transmission paths may be obstructed by natural or man-made objects such as hills or buildings. Such obstructions in the environment cause multiple reflections of the transmitted signal to be received from different directions and with different propagation delays. Interaction between the radio signals (constructive/destructive superposition) causes a phenomenon known as multipath fading, which can result in severe and rapidly fluctuating attenuation of the transmitted signal and phase

shifts [85]. This may result in an inability to reliably transfer information. In the following sub-sections, we discuss possible forms of the multipath fading channel.

2.1.1 Time Selective Fading

Relative motion between the transmitter and receiver causes a transmitted signal and its reflections to undergo different frequency shifts, which are known as Doppler shifts. A received signal transmitted at frequency f_c will experience a Doppler shift given by [85]

$$f_d = \frac{f_c v_m}{c} \cos\beta, \tag{2.1}$$

where β is the incident angle of the received signal with respect to the direction of the receiver's motion, v_m is the velocity of the receiver towards the transmitter and c is the speed of light. In a multipath channel, the signal is spread over the frequency range

$$f_c \pm f_{d_{max}}, \tag{2.2}$$

where $f_{d_{max}}$ is the maximum Doppler shift. This effect is known as frequency dispersion or time selective fading and is measured by the Doppler spread, which is defined as $D_s = 2f_{d_{max}}$ [86, 87].

A channel is considered to be slow fading if the channel impulse response changes at a much slower rate than the transmitted baseband signal [84]. This means that the channel can be assumed to be static over one or more symbol intervals. Equivalently, the channel coherence time is longer than the duration of one or more symbols. Let us consider $f_c = 700$ MHz, $v_m = 500$ km/h, then $f_{d_{max}} = 325\ Hz$ or $D_s = 650\ Hz$. The channel coherence time is given by [85]

$$T_c = \frac{1}{4D_s} \approx 385(us). \tag{2.3}$$

In LTE systems, the maximum TD spacing between OFDM symbols containing pilot sub-carriers is 4 and an OFDM symbol duration $T_s \approx 72\ us$ (for normal mode CP) [88]. Since $T_c > 4T_s$, we can assume that the channel does not change significantly during the time interval corresponding to T_c. This implies that the channel estimates obtained using an OFDM symbol containing pilots can also be used for equalization of the following 3 data OFDM symbols in LTE systems. Note: From (2.1) and (2.3), it can be seen that as the carrier frequency f_c increases, the coherence time reduces.

2.1.2 Multipath Fading

As mentioned earlier, there are often obstacles between a transmitter and its corresponding receiver; this causes multiple reflected copies of the transmitted signal to arrive at the receiver at different times and hence overlap each other. This effect is known as time dispersion, which results in frequency flat or frequency selective fading [84] of the transmitted signal. If all of the spectral components are similarly affected, the fading is frequency non-selective or flat. Conversely, if distinct spectral components experience different magnitudes of fading, the fading is frequency selective. The coherence bandwidth is a statistical measure of the range of frequencies over which the fading may be considered flat, and is inversely proportional to the time delay spread of the fading channel. Spectral components within the band are passed with approximately the same gain and change in phase [85].

Frequency selective fading happens when the bandwidth of the transmitted signal is significant in comparison to the channel coherence bandwidth. Transforming this into the time domain, we can see that a frequency selective signal will have a high multipath delay spread in comparison to a symbol period. Different gains are experienced over the transmitted signal band resulting in a variable frequency response. This is characteristic of wideband systems or long range communication. Frequency selective fading induces ISI, which requires equalization to mitigate its effect [89]. On the other hand, flat fading occurs when the symbol period is much greater than the multipath delay spread of the channel. In flat fading conditions, channel fading causes negligible ISI because the signal bandwidth is narrow relative to the coherence bandwidth of the channel. Flat fading channels often experience deep fades, but the ISI distortion is usually negligible due to the small delay spread, making it much easier to decode. Figure 2.1 illustrates the frequency responses ($H(f)$) of flat and frequency selective channels relative to signal bandwidth (W) and coherence bandwidth (ΔW_c). In this thesis, we consider frequency selective channels, which have high delay spread (longer than the available CP).

2.1.3 Rayleigh Fading Channel Model

There are a large number of fading channel models available in the literature to cover different scenarios. The most commonly used models for land mobile radio

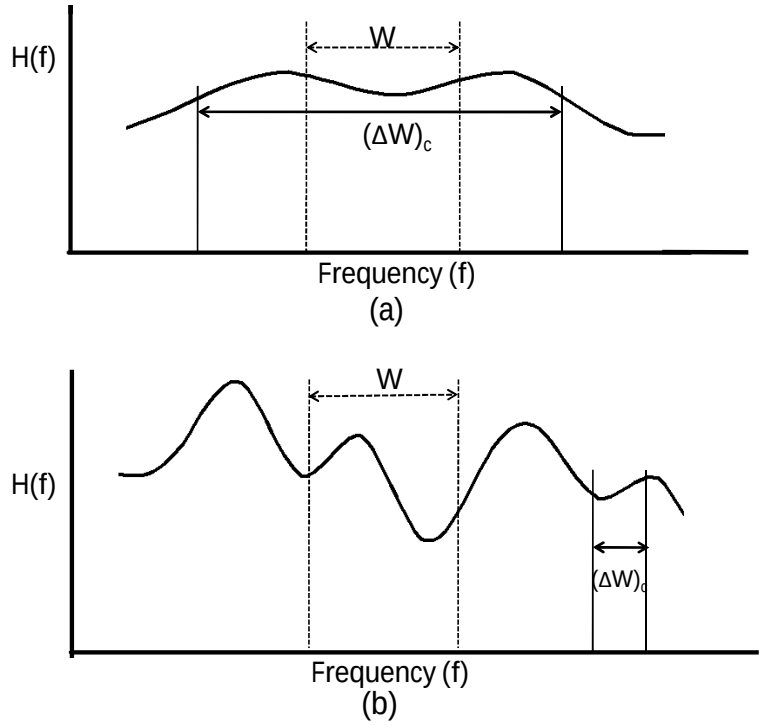

Figure 2.1: Frequency response of (a) frequency flat channel (b) and frequency selective channel.

channels are Rayleigh and Rician because they are easy to analyze and are fairly realistic [90–92]. In urban environments, there are a large number of scatterers affecting propagation. If there is a dominant stationary (non-fading) signal component, such as occurs with line of sight propagation, the Rician fading channel is an appropriate model. If there is no line of sight between the transmitter and the receiver, the Rayleigh fading channel may be used [87]. In practice, there are often obstacles between transmitters and receivers in land mobile communication; hence, the presence of the line of sight path is quite rare. Therefore, in this research we model the channel as multipath Rayleigh fading.

A Rayleigh multipath fading channel can be represented by a discrete multipath model, for which the channel coefficients vary once every K OFDM symbols (block fading). In [82], the channel between the u^{th} receive antenna and the v^{th} transmit antenna can be represented by a complex baseband model of L discrete Rayleigh

fading paths

$$h_{u,v}(\tau) = \sum_{l=0}^{L-1} h_{u,v,l}\delta(n - \tau_l), \tag{2.4}$$

where the path gains $h_{u,v,l}$ are zero mean complex random values with variance σ_l^2, τ_l is the delay in sample intervals of path l, $\delta(n)$ is the unit impulse response and n is the TD sample index. The full TD channel response can be presented by a $1 \times \tau_{L-1}$ vector $\boldsymbol{h}_{u,v}^{td} = [h_{u,v,0}, 0, \ldots, 0, h_{u,v,l}, 0, \ldots, 0, h_{u,v,L-1}]$, where the corresponding index of the non-zero element $h_{u,v,l}$ is τ_l. As we consider point to point communication, we can assume a common power delay profile for all channels between any pair of receive and transmit antennas. On the other hand, for most fading media, $h_{u,v,l}$ can be assumed independent [93], meaning $E\{h_{u,v,l}h_{u,v,l'}\} = 0$, $l \neq l'$. We also assume uncorrelated antennas so $E\{h_{u,v,l}h_{u',v',l}\} = 0$ for $u \neq u'$ or $v \neq v'$.

In this research, for simulation purposes, we consider the channel having either a double-spike or exponential *power delay profile (PDP)*. The double-spike PDF is based on the assumption that $L = 2$ since the second path can be considered to be the sum of all the delayed signals relative to the first one. In most situations, the second arrival signal has weaker energy than the first arrival one because of its longer traveling distance; this has the natural effect of decreasing the interference in the received signal [84]. However, to test the limitation of the systems, we will consider the challenging case of the second path having the same average gain as the first path. Let $\sigma_l^2 = E\{|h_{u,v,l}|^2\}$, then we have

$$\sigma_0^2 = \sigma_1^2. \tag{2.5}$$

In addition, we will simulate an exponential PDP with more than 2 paths. According to [94–97], on average, the decay of signal power can be modelled as an exponential function of delay. Hence, the average path power can be expressed as [98]

$$\sigma_l^2 = \alpha_l e^{-\tau_l/\tau_{rms}}, \tag{2.6}$$

where τ_{rms} is the *root mean square (RMS)* delay of the channel and α_l is the normalization factor so that $\sigma_0^2 + \sigma_1^2 + \cdots + \sigma_{L-1}^2 = 1$. We assume that the receiver has knowledge of τ_{rms} from pre-transmission channel measurements or applying available algorithms such as [99].

2.2 OFDM System Overview

Orthogonal frequency division multiplexing (OFDM) is a multi-carrier modulation technique with a natural resistance to multipath interference as long as its CP is sufficient [8, 9]. This makes OFDM well suited for transmission of digital signals over broadband channels. Figure 2.2 shows a simplified block diagram of an uncoded MIMO-OFDM transmitter using N_t transmit antennas and *A-ary quadrature amplitude modulation (A-QAM)* [100]. The input bit stream is grouped by the *serial-to-parallel (S/P)* converter to yield N_t parallel bit sequences. Data bits are mapped to a complex valued symbol $X_{v,m}(k) \in \boldsymbol{A}$, where $\boldsymbol{A}$ is the A-ary constellation set, and v, m, and k denote the indices of the transmit antenna, OFDM symbol, and sub-carrier, respectively. We assume that the entire transmission burst can be divided into smaller groups of M_s consecutive OFDM symbols. Within each group, the first symbol is inserted with N_p pilot sub-carriers ($N_p < N$), where N is the *fast Fourier transform (FFT)* size, while the other symbols contain only information bearing sub-carriers. For the case of sufficient CP, it is assumed that the pilot sub-carriers are distributed so that pilots from one transmit antenna do not interfere with other pilots or data sub-carriers from other antennas. Note that the OFDM transmitter with a single transmit antenna can be considered as a branch of the MIMO transmitter.

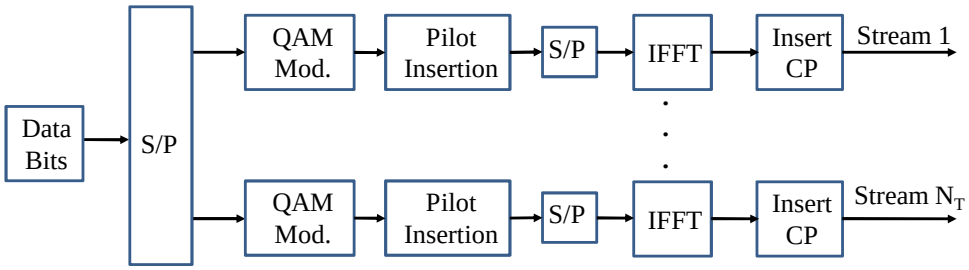

Figure 2.2: MIMO-OFDM baseband transmitter.

2.2.1 SIMO-OFDM Receiver for Sufficient CP Transmission

Figure 2.3 shows the simplified block diagram of a standard SIMO-OFDM receiver for sufficient CP transmission with one transmit antenna and N_R receive antennas.

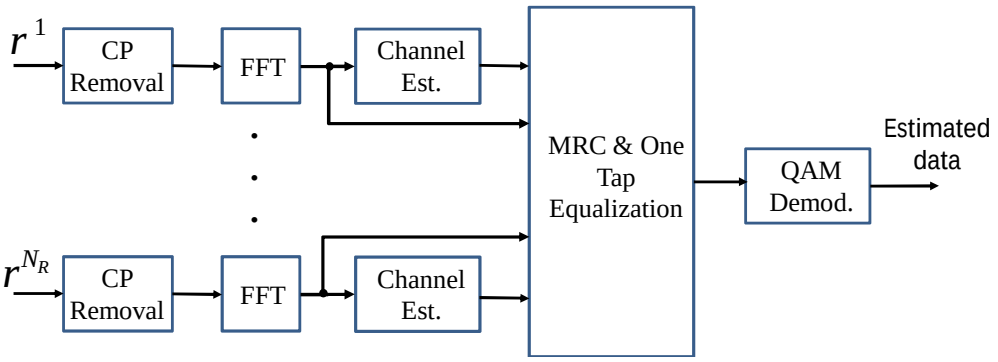

Figure 2.3: SIMO-OFDM standard receiver.

Since the CP is sufficient, the SIMO channel can be reliably estimated by a linear LSI estimator [101] using pilot sub-carriers. The channel estimates are used in the subsequent detection, which consists of one-tap equalizers and *maximum ratio combining (MRC)* [102]. The FD received signal corresponding to sub-carrier k and the u^{th} receive antenna can be written as

$$R_{u,m}(k) = H_{u,1,m}(k)X_{1,m}(k) + n_u(k), \tag{2.7}$$

where $H_{u,1,m}(k)$ is the FD channel coefficient for sub-carrier k and the u^{th} receive antenna and $n_u(k)$ represents additive white Gaussian noise. Using a one tap equalizer, $X_{1,m}(k)$ can be estimated by

$$\ddot{X}_{u,1,m}(k) = \frac{R_{u,m}(k)}{\widehat{H}_{u,1,m}(k)}, \tag{2.8}$$

where $\widehat{H}_{u,1,m}(k)$ is the estimate of $H_{u,1,m}(k)$. The values of $\ddot{X}_{u,1,m}(k)$ from different antennas are MRC combined according to

$$\widehat{X}_{1,m}(k) = \frac{1}{\sum_{u=1}^{N_R} |\widehat{H}_{u,1,m}(k)|^2} \sum_{u=1}^{N_R} |\widehat{H}_{u,1,m}(k)|^2 \ddot{X}_{u,1,m}(k). \tag{2.9}$$

$\widehat{X}_{1,m}(k)$ is a soft likelihood, which is rounded to the nearest QAM symbol for QAM detection.

2.2.2 MIMO-OFDM Receiver for Sufficient CP Transmission

Figure 2.4 shows a standard MIMO-OFDM receiver for sufficient CP transmission with N_R receive antennas. This receiver also utilizes LSI channel estimators given

that the pilot sub-carriers from one transmit antenna do not interfere with other pilot or data sub-carriers from other antennas for sufficient CP. Here, the combination of one-tap equalizers and MRC combiner for SIMO-OFDM detection is extended to a ML detector for MIMO-OFDM.

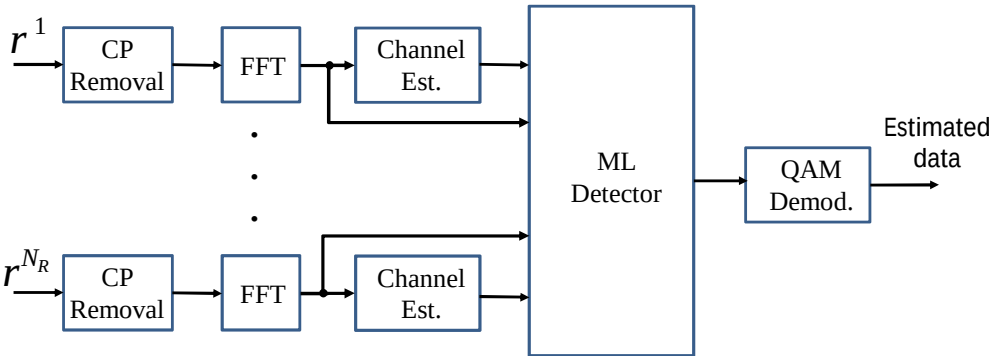

Figure 2.4: MIMO-OFDM standard receiver.

In this case, the FD received signal corresponding to sub-carrier k and the u^{th} receive antenna becomes

$$R_{u,m}(k) = \sum_{v=1}^{N_T} H_{u,v,m}(k) X_{v,m}(k) + n_u(k). \tag{2.10}$$

The ML detector searches over all the possible values of the vector $[X_{1,m}(k), X_{2,m}(k), \ldots, X_{N_T,m}(k)]$, which contains all the symbols transmitted by the k^{th} sub-carrier. The detection is done by finding the vector, which minimizes the mean square error given by

$$\min_{\{X_{1,m}(k),\ldots,X_{N_T,m}(k)\}} \left| R_{u,m}(k) - \sum_{v=1}^{N_T} \widehat{H}_{u,v,m}(k) \tilde{X}_{v,m}(k) \right|^2, \tag{2.11}$$

where $\tilde{X}_{v,m}(k)$ is a possible value for $X_{v,m}(k)$. The performance of this receiver with sufficient CP acts as a reference for comparison to the proposed receiver for insufficient CP transmission.

2.3 Overview of Receiver Design for Insufficient CP OFDM

Recall from Section 1.2 that the problem of designing reliable receivers for insufficient CP OFDM systems is the corruption of both pilot and data sub-carriers due to interference. Let $r_{u,v}(n)$ be the TD transmitted signal sample between the u^{th} receive antenna and the v^{th} transmit antenna after CP removal. It can be expressed as [14, 15]

$$r_{u,v}(n) = r_{d,u,v}(n) + r_{ici,u,v}(n) + r_{isi,u,v}(n) + n_u(n), \tag{2.12}$$

where $r_{d,u,v}(n)$, $r_{ici,u,v}(n)$, $r_{isi,u,v}(n)$ and $n_u(n)$ represent the useful signal, ICI, ISI and white Gaussian noise, respectively. Alternatively, the FD received signal at sub-carrier a can be written as

$$R_{u,v}(a) = R_{d,u,v}(a) + R_{ici,u,v}(a) + R_{isi,u,v}(a) + n_u(a), \tag{2.13}$$

where $R_{d,u,v}(a)$, $R_{ici,u,v}(a)$, $R_{isi,u,v}(a)$ and $n_u(a)$ are the FD counterparts of $r_{d,u,v}(n)$, $r_{d,u,v}(n)$, $r_{isi,u,v}(n)$ and $n_u(n)$ at sub-carrier a, respectively. Recalling that $r_u(n)$ and $R_{ici,u,v}(a)$ are the total received TD and FD signal from all transmit antennas, the objective in receiver design is to mitigate $r_{ici,u,v}(n)$ and $r_{isi,u,v}(n)$ in $r_u(n)$ (or $R_{ici,u,v}(a)$ and $R_{isi,u,v}$ in $R_u(n)$) for better channel estimation and data detection quality.

2.3.1 Iterative Design Techniques

Iterative reception is an effective reception strategy, which performs interference mitigation, channel estimation and data detection together to improve the overall performance [2, 22, 64, 74, 75]. Here, both channel estimation and equalization can be in the TD [74] or in the FD [64]. On the other hand, the receiver operations can alter between the TD and the FD to achieve good performance [2, 22, 75]. This is because channel estimation is easier in the TD, where the number of independent parameters is minimal. A single tap channel in the TD is a single amplitude and phase, whereas the equivalent in the FD, it is N amplitudes and phases.

Figure 2.5 illustrates the high performance *single input single output (SISO)* receiver proposed in [75] that motivates our proposed designs. There are two parallel data processing stages. The main decoder provides the final output while the early decoder assists with interference cancellation and channel estimation. Both

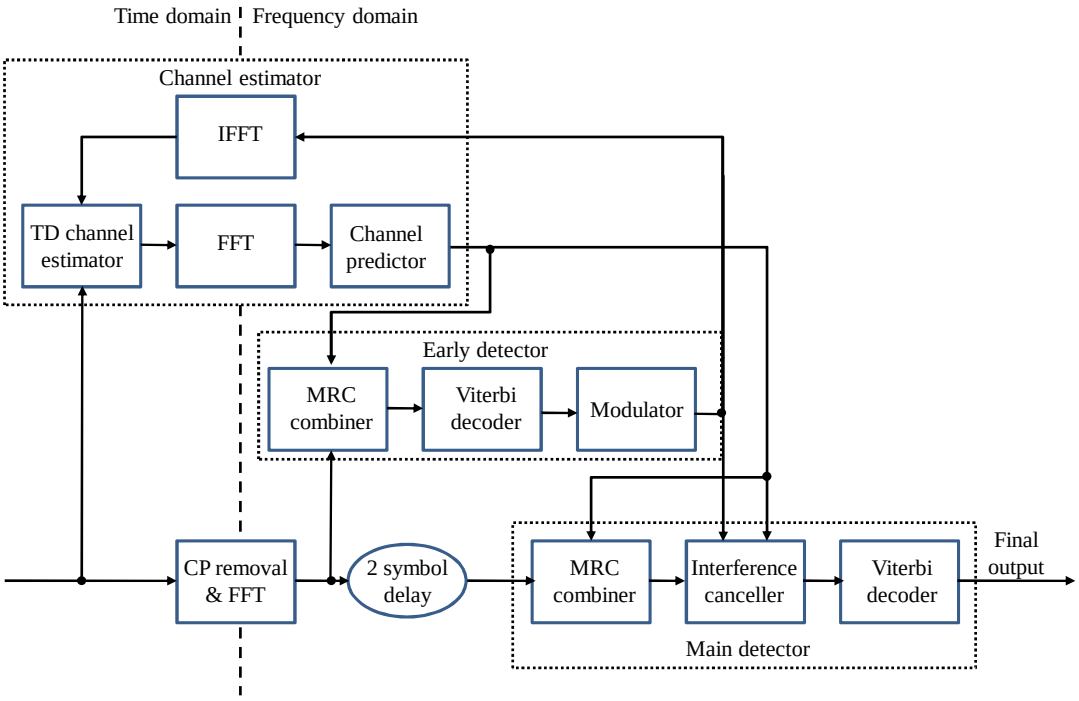

Figure 2.5: Advanced receiver for insufficient CP 802.11 OFDM [75].

decoders utilize MRC to combine two adjacent OFDM symbols in a per-subcarrier basis allowing Viterbi detection on the combined signal. The MRC combiner in the main decoder benefits from more recent/more accurate channel estimates. Using the early decoder outputs, FD interference mitigation is carried out in the main decoder before Viterbi detection.

The actual process of interference cancellation is not described in [75]. Interference mitigation is likely carried out as in [74]. This cancellation process contains two steps: First, ISI is approximated from the previous detected OFDM symbol and its corresponding channel estimate; then ISI cancellation is simply carried out by

$$\breve{R}_u(a) = R_u(a) - \widehat{R}_{isi,u}(a), \tag{2.14}$$

where $\widehat{R}_{isi,u}(a)$ is the ISI estimate. Similarly, ICI mitigation is achieved with the estimates of the current OFDM symbol and the current channel. Then the ICI cancellation process is

$$\dot{Y}_u(a) = \breve{R}_u(a) - \widehat{R}_{ici,u}(a), \tag{2.15}$$

where $\widehat{R}_{ici,u}(a)$ is the ICI estimate.

Unlike many other designs that only rely on pilots for channel estimation, this receiver uses data aided TD channel estimation and the channel is tracked in FD. The initial channel estimates are computed based on the 802.11 preamble, which is effectively a pilot OFDM symbol [4]. These estimates are transformed to the FD, where they drive a per-subcarrier channel predictor. This predictor provides channel estimates for the next two (as yet un-decoded) symbols. For the subsequent data OFDM symbol, the early decoder outputs are transformed to TD and supports the TD channel estimator resulting in improved channel estimates.

The main advantage of this design is that it can provide excellent detection accuracy with a limited number of pilot sub-carriers required in an OFDM symbol for channel estimation. The receiver processing is per OFDM symbol, rather than per frame, reducing latency [75]. However, this receiver is designed specifically for 802.11 OFDM systems, so it has a number of major limitations that prevent it from being applicable to LTE systems. First, the receiver relies on the 802.11 preamble, which contains a pilot OFDM symbol dedicated for computing initial channel estimates [4]. However, such preamble is not available in LTE systems, which rely on distributed pilot sub-carriers mixing data sub-carriers [6]. Yet, the combination of MRC and Viterbi decoder proposed in such designs are considered for SISO transmissions. With MIMO transmissions, this would lead to impractical complexity as the Viterbi decoder's trellis becomes large. In addition, due to the lack of distributed pilot symbols, the channel predictor may not perform very well with high velocity channel conditions such as those considered in LTE systems.

Motivated by [75], the receivers proposed in this thesis also utilize data aided TD channel estimation and FD detection with trellis-based equalization. However, they provide significantly more robust and reliable reception for insufficient CP OFDM systems. This is because they can operate with a generic MIMO-OFDM systems using a limited number of pilot sub-carriers distributed over time and frequency. This means that the design is compatible with LTE. They are also able to achieve accurate detection with practical complexity even if the channel delay spread far exceeds the CP.

2.3.2 Data Detection/Equalization Techniques

In this section, we focus on describing the detection strategies that are often employed within an iterative receiver for insufficient CP transmissions.

2.3.2.1 Residual ISI Cancellation Algorithm

In terms of iterative detection techniques, most of them are variants of the *residual ISI cancellation (RISIC)* algorithm, [2, 65, 67, 70, 71]. The original RISIC algorithm consists of two procedures called tail cancellation and cyclic reconstruction, which are effectively the TD versions of the ISI and ICI mitigation process. These procedures are based on the knowledge that the ISI and ICI in the TD of the m^{th} OFDM symbol can be expressed as [2, 65]

$$r_{isi,u,v}(n) = \sum_{l=G+1}^{\tau_{max}} h_{u,v,l,m-1} x_{v,m-1}([n-\tau_l+G]_N)(1-\mu(n-\tau_l+G)) \tag{2.16}$$

and

$$r_{ici,u,v}(n) = \sum_{l=G+1}^{\tau_{max}} h_{u,v,l,m} x_{v,m}([n-\tau_l]_N)\mu(n-\tau_l+G), \tag{2.17}$$

where $x_{v,m}(n)$ is the TD data sample of the m^{th} OFDM symbol transmitted from antenna v, $(n)_N$ is the residual of n modulo N, $\mu(n)$ denotes the unit step function, $h_{u,v,l,m}$ indicates the corresponding channel realization of channel path l and G is the CP length. The RISIC algorithm can be summarized in the following [2]: For all values of u and v,

1. An estimate of the channel impulse response $\widehat{h}_{u,v,l,m-1}$, is obtained from available pilots.

2. Decisions on the transmitted data $[\widehat{X}_{v,m-1}(0), \ldots, \widehat{X}_{v,m-1}(N-1)]$ from the previous OFDM symbol is obtained for use in tail cancellation. These symbols are converted back to the TD using IFFT giving $[\widehat{x}_{v,m-1}(0), \ldots, \widehat{x}_{v,m-1}(N-1)]$.

3. From (2.16), the tail cancellation process is done by calculating the ISI and subtracting it from $r_{u,v}(n)$, to give

$$r^{(0)}_{u,v}(n) = r_{u,v}(n) - \sum_{l=G+1}^{\tau_{max}} \widehat{h}_{u,v,l,m-1}\widehat{x}_{v,m-1}(n-\tau_l+G)_N(1-\mu(n-\tau_l+G)). \tag{2.18}$$

4. Each vector $[r_{u,v}^{(0)}(0), \ldots, r_{u,v}^{(0)}(N-1)]$ obtained in Step 3 is converted to the FD using FFT and decisions are made using a one tap equalizer or the ML detector in Section 2.2.2. Afterwards, the decisions are converted back to the TD to give $[\widehat{x}_{v,m}^{(0)}(0), \ldots, \widehat{x}_{v,m}^{(0)}(N-1)]$.

5. From (2.17), the cyclic reconstruction is performed by forming

$$r_{u,v}^{(I)}(n) = r_{u,v}^{(0)}(n) + \sum_{l=G+1}^{\tau_{max}} \widehat{h}_{u,v,l,m} \widehat{x}_{v,m}^{(I-1)}(n-\tau_l)_N \mu(n-\tau_l+G), \tag{2.19}$$

   where I represents iteration number with an initial value of $I = 1$.

6. Each vector $[r_{u,v}^{(I)}(0), \ldots, r_{u,v}^{(I)}(N-1)]$ is converted to the FD and decisions are made yielding $[\widehat{X}_{v,m}^{(I)}(0), \ldots, \widehat{X}_{v,m}^{(I)}(N-1)]$. This completes the I^{th} iteration in the RISIC algorithm.

7. To continue iterations, convert the vector $[\widehat{X}_{v,m}^{(I)}(0), \ldots, \widehat{X}_{v,m}^{(I)}(N-1)]$ to the FD forming $[\widehat{x}_{v,m}^{(I)}(0), \ldots, \widehat{x}_{v,m}^{(I)}(N-1)]$ and repeat Steps 5-7 with $I \leftarrow I+1$.

Due to the performance limitation of the one tap equalizer and the ML detector, the RISIC algorithm is not able to provide accurate data estimate. Thus, the iterative process may not converge, especially when the channel delay spread is significantly longer than the CP length. For performance improvement, another variant of the RISIC algorithm includes error control decoding in the iterative detection process [67,70,71]. However, this considerably increases the receiver complexity. The RISIC algorithm's performance will be compared with our proposed designs in Chapters IV and V.

2.3.2.2 Trellis-based Equalization

Trellis-based equalization [73, 76] can provide better detection accuracy than the original RISIC algorithms. It is based on the idea that the majority of ICI comes from the two adjacent sub-carriers [73]. Hence, a trellis state can be defined as consisting of a given sub-carrier and its two adjacent sub-carriers. A section of the equalizer trellis is shown in Fig. 2.6. The MLSE or MAP algorithms can then be applied for FD detection. The main disadvantage of this method is that the ICI energy, which the trellis does not account for, can become significant with long delay spread (exceeding the CP) leading to detection degradation. In [73], a filtering process is applied to concentrate ICI energy to the adjacent sub-carriers but it can only

offer good performance when the channel delay spread does not exceed twice the CP length. The design is considered for SISO systems and would be impractically complex if directly extended to MIMO systems. Let A be the order of the sub-carrier modulation. In the case of SISO systems, the number of different trellis states is determined by A^3 so it would be A^{3N_T} states for MIMO systems. For example, if we consider a 2×2 MIMO-OFDM systems with 4-QAM as the sub-carrier modulation, the corresponding trellis would need to have $4^{2\times 3} = 4096$ different states, which would lead to a very computational demanding equalization process.

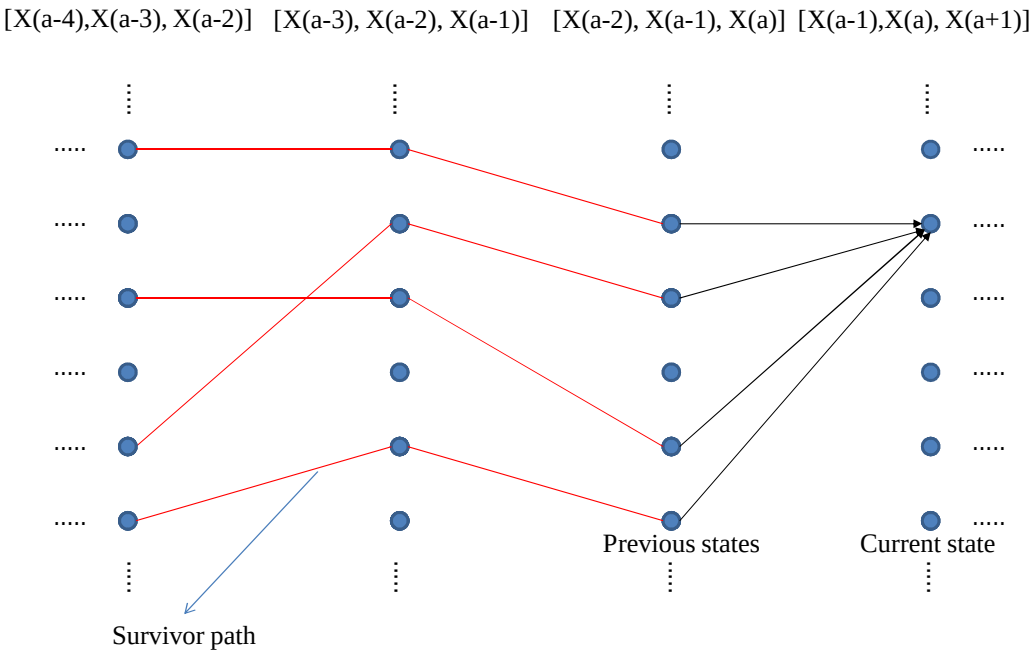

Figure 2.6: A section of the equalizer trellis in [73].

Motivated by the potential performance of trellis-based equalizers, in Chapters IV and V, we will propose improved trellis-based techniques that can take into account all the ICI energy with practical complexity.

2.3.3 Pilot Based Channel Estimation

The main challenge for channel estimation with insufficient CP systems is the corruption of pilots due to ISI and ICI. As discussed in Section 2.3.1, one of the most

effective strategies for data detection in such systems is iterative channel estimation and data detection where the channel and data estimates are refined over each iteration. However, for the iterative process to converge, it is important to acquire a good initial channel estimate. However, this is difficult because at this stage, the interference is still fully present. To overcome this, a common technique is to utilize a specially constructed pilot in the form of a TD *symmetric sequence (SS)*, which is an OFDM symbol with two equal halves [2, 19–22]. Assuming that the channel delay spread is less than half an OFDM symbol length, this SS mostly absorbs ISI and ICI in the first half, which is discarded, leaving the second half clean from interference. The channel estimation can be done with only the second half. In the case of the IJEP algorithm in [22], the interference is mitigated from the first half of the SS after the first iteration. This allows the whole SS to be used to improve the channel estimate from the second iteration onward. Figure 2.7 illustrates the estimation process of the *iterative joint estimation procedure (IJEP)* algorithm [22]. This reference will be the performance reference point to compare with the proposed channel estimation method.

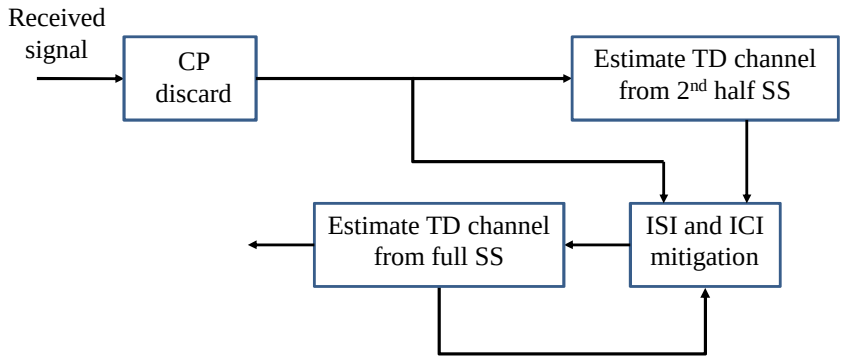

Figure 2.7: IJEP algorithm flow chart.

The SS is obtained with the transmission of the pilot sequence on the even sub-carriers, whereas zeros are used on the odd sub-carriers [2, 20]. This means that the bandwidth of a whole OFDM symbol would be used for the pilot. In the context of LTE, there needs to be at least one pilot per three data OFDM symbols [6]. So the total temporal spectral efficiency reduces significantly as a pilot OFDM symbol is transmitted 25% of the time, which is impractical. On the other hand, LTE

currently does not support such pilot arrangement so the method is not compatible with LTE systems. The main advantages of the proposed method over these designs are that our proposed method is compatible with LTE and requires fewer pilots to achieve the same estimation accuracy.

2.4 Summary

The preceding sections have outlined the communication system considered in this thesis. This includes the OFDM baseband transmission and reception models as well as the channel model used for simulation. SIMO-OFDM and MIMO-OFDM with QAM as sub-carrier modulation are the systems of interest here. The number of available pilot sub-carriers are limited and are arranged so that pilots from one transmit antenna do not interfere with other pilots or data sub-carriers from other antennas for sufficient CP. It was also shown that the transmission channel can be modelled by a Rayleigh distributed, frequency selective slow fading channel with AWGN. Finally, an overview of iterative receiver design for insufficient CP OFDM systems is given.

In the next chapter, the effect of insufficient CP on OFDM transmission and reception will be discussed in detail, leading to novel receiver designs for such conditions.

Chapter 3

Insufficient Cyclic Prefix Induced Interference

OFDM communications using a CP duration shorter than the channel delay spread is distorted by ISI and ICI as mentioned in the previous chapters. As a result, the received signal will often be very different to the transmitted signal. To reliably obtain the transmitted information, it is important to understand the characteristics of ISI and ICI. In this chapter, the interference and its effect on the transmission quality is analyzed. The chapter begins with a derivation of the received signal in the FD and the interference. We then compute the *signal to interference and noise ratio (SINR)* for analyzing the interference effect on OFDM transmissions. The interference is then analyzed leading to novel receiver designs in Chapters IV and V.

3.1 Interference Formulation

We consider OFDM systems with insufficient CP, which means $\tau_{L-1} > G$. Let $D < L$ be the number of paths with delay lower than (or equal) to the CP. The cause of ISI and ICI from a single path l among the $L - D$ paths lying outside the CP length of a channel can be shown in Fig. 3.1.

Let us consider the transmission between the v^{th} (transmit) and u^{th} (receive) antenna. From the multipath channel model in (2.4), the n^{th} TD sample of the

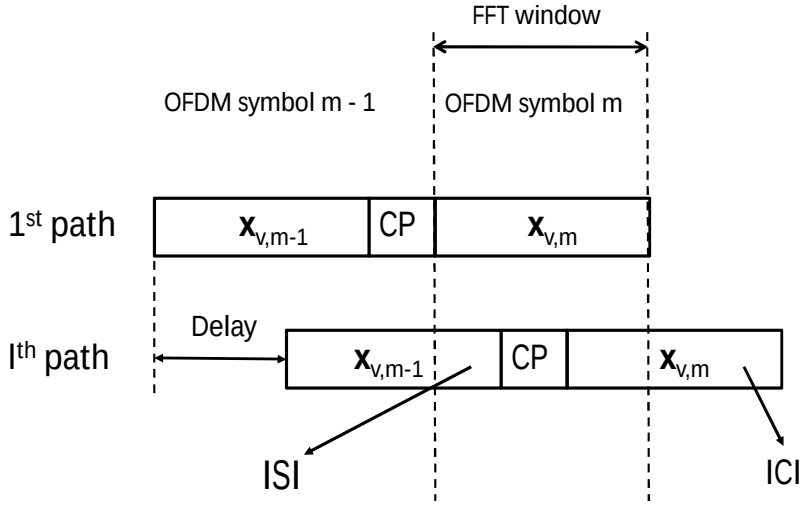

Figure 3.1: ICI and ISI caused by insufficient CP.

received signal after CP removal can be expressed as

$$\begin{aligned} r_{u,v}(n) &= \sum_{l=0}^{L-1} h_{u,v,l,m} x_{v,m}([n-\tau_l]_N)\mu(n-\tau_l+G) \\ &+ \sum_{l=D}^{L-1} h_{u,v,l,m-1} x_{v,m-1}([n-\tau_l+G]_N) \\ &\times (1-\mu(n-\tau_l+G)) + n_u(n), \end{aligned} \tag{3.1}$$

where $[n]_N$ is the residue of n modulo N, $h_{u,v,l,m}$ indicates the channel realization when the m^{th} OFDM symbol is transmitted and $n_u(n)$ represents the noise component at the u^{th} antenna. Applying the FFT to (3.1), the FD sample at the a^{th} sub-carrier is

$$\begin{aligned} R_{u,v}(a) &= X_{v,m}(a)\sum_{l=0}^{D-1} h_{u,v,l,m} e^{-j2\pi a\tau_l/N} + \sum_{l=D}^{L-1} \frac{N-\tau_l+G}{N} h_{u,v,l,m} e^{-j2\pi a\tau_l/N} \\ &+ \sum_{l=D}^{L-1} h_{u,v,l,m} \sum_{k=0,k\neq a}^{N-1} \frac{X_{v,m}(k)}{N} e^{-j2\pi k\tau_l/N} \sum_{n=\tau_l-G}^{N-1} e^{j2\pi n(k-a)/N} \\ &+ \sum_{l=D}^{L-1} h_{u,v,l,m-1} \sum_{k=0}^{N-1} \frac{X_{v,m-1}(k)}{N} e^{-j2\pi k(\tau_l-G)/N} \sum_{n=0}^{\tau_l-G-1} e^{j2\pi n(k-a)/N} + \tilde{n}_u(a), \end{aligned} \tag{3.2}$$

where $\tilde{n}_u(a)$ represents the noise component at the a^{th} sub-carrier. By applying the

geometric series formula [103], for $k \neq a$, the inner most summations of the ICI and ISI terms can be simplified to

$$\begin{aligned}\sum_{n=\tau_l-G}^{N-1} e^{j2\pi n(k-a)/N} &= \sum_{n=\tau_l-G}^{N-1} (e^{j2\pi(k-a)/N})^n = \frac{(e^{j2\pi(k-a)/N})^{\tau_l-G} - (e^{j2\pi(k-a)/N})^N}{1-e^{j2\pi(k-a)/N}} \\ &= \frac{(e^{j2\pi(k-a)/N})^{\tau_l-G} - 1}{1-e^{j2\pi(k-a)/N}} \end{aligned} \tag{3.3}$$

and

$$\begin{aligned}\sum_{n=0}^{\tau_l-G-1} e^{j2\pi n(k-a)/N} &= \sum_{n=0}^{\tau_l-G-1} (e^{j2\pi(k-a)/N})^n = \frac{(e^{j2\pi(k-a)/N})^{0} - (e^{j2\pi(k-a)/N})^{\tau_l-G}}{1-e^{j2\pi(k-a)/N}} \\ &= \frac{1-(e^{j2\pi(k-a)/N})^{\tau_l-G}}{1-e^{j2\pi(k-a)/N}}. \end{aligned} \tag{3.4}$$

Let us define $\rho_k = e^{j2\pi k/N}$, so

$$\sum_{n=\tau_l-G}^{N-1} e^{j2\pi n(k-a)/N} = \frac{\rho_{k-a}^{\tau_l-G}-1}{1-\rho_{k-a}} \text{ and } \sum_{n=0}^{\tau_l-G-1} e^{j2\pi n(k-a)/N} = \frac{1-\rho_{k-a}^{\tau_l-G}}{1-\rho_{k-a}}. \tag{3.5}$$

Hence,

$$\begin{aligned} R_{u,v}(a) &= X_{v,m}(a)\sum_{l=0}^{L-1} f(l)h_{u,v,l,m}e^{\frac{-j2\pi a\tau_l}{N}} \\ &+ \sum_{l=D}^{L-1} h_{u,v,l,m} \sum_{k=0,k\neq a}^{N-1} \frac{X_{v,m}(k)}{N} e^{\frac{-j2\pi k\tau_l}{N}} \frac{\rho_{k-a}^{\tau_l-G}-1}{1-\rho_{k-a}} \\ &+ \sum_{l=D}^{L-1} h_{u,v,l,m-1} \Bigg(\frac{X_{v,m-1}(a)(\tau_l-G)}{N} e^{\frac{-j2\pi a(\tau_l-G)}{N}} \\ &+ \sum_{k=0,k\neq a}^{N-1} \frac{X_{v,m-1}(k)}{N} e^{\frac{-j2\pi k(\tau_l-G)}{N}} \frac{1-\rho_{k-a}^{\tau_l-G}}{1-\rho_{k-a}} \Bigg) + \tilde{n}_u(a), \end{aligned} \tag{3.6}$$

where the function $f(l)$ is defined as

$$f(l) = \begin{cases} 1 & \text{if } l < D, \\ (N-\tau_l+G)/N & \text{if } l \geq D. \end{cases} \tag{3.7}$$

In (3.6), the 1^{st} term represents the desired signal and the 2^{nd} and 3^{rd} terms represent the ICI and ISI, respectively.

Equation (3.6) only considers the transmission between one transmit and one receive antenna. Since we assume that there are N_T transmit and N_R receive antennas ($N_R \geq N_T$) in our MIMO system, the overall received signal at the u^{th} antenna is

$$R_u(a) = \sum_{v=1}^{N_T} R_{u,v}(a). \tag{3.8}$$

Substituting (3.6) into (3.8), we have [81]

$$\begin{aligned} R_u(a) &= \sum_{v=1}^{N_T} X_{v,m}(a) \sum_{l=0}^{L-1} f(l) h_{u,v,l,m} e^{\frac{-j2\pi a\tau_l}{N}} \\ &+ \sum_{v=1}^{N_T}\sum_{l=D}^{L-1} h_{u,v,l,m} \sum_{k=0,k\neq a}^{N-1} \frac{X_{v,m}(k)}{N} e^{\frac{-j2\pi k\tau_l}{N}} \frac{\rho_{k-a}^{\tau_l-G}-1}{1-\rho_{k-a}} \\ &+ \sum_{v=1}^{N_T}\sum_{l=D}^{L-1} h_{u,v,l,m-1} \left(\frac{X_{v,m-1}(a)}{N} e^{\frac{-j2\pi a(\tau_l-G)}{N}} (\tau_l - G) \right. \\ &+ \left. \sum_{k=0,k\neq a}^{N-1} \frac{X_{v,m-1}(k)}{N} e^{\frac{-j2\pi k(\tau_l-G)}{N}} \frac{1-\rho_{k-a}^{\tau_l-G}}{1-\rho_{k-a}} \right) + \tilde{n}_u(a). \end{aligned} \tag{3.9}$$

Let $R_{d,u}(a)$, $R_{ici,u}(a)$ and $R_{isi,u}(a)$ be the parts of the received FD signal corresponding to the useful transmission, ICI and ISI, respectively. From (3.9), we have

$$R_{d,u}(a) = \sum_{v=1}^{N_T} X_{v,m}(a) \sum_{l=0}^{L-1} f(l) h_{u,v,l,m} e^{\frac{-j2\pi a\tau_l}{N}}, \tag{3.10}$$

$$R_{ici,u}(a) = \sum_{v=1}^{N_T}\sum_{l=D}^{L-1} h_{u,v,l,m} \sum_{k=0,k\neq a}^{N-1} \frac{X_{v,m}(k)}{N} e^{\frac{-j2\pi k\tau_l}{N}} \frac{\rho_{k-a}^{\tau_l-G}-1}{1-\rho_{k-a}}, \tag{3.11}$$

$$\begin{aligned} R_{isi,u}(a) &= \sum_{v=1}^{N_T}\sum_{l=D}^{L-1} h_{u,v,l,m-1} \left(\frac{X_{v,m-1}(a)}{N} e^{\frac{-j2\pi a(\tau_l-G)}{N}} (\tau_l - G) \right. \\ &+ \left. \sum_{k=0,k\neq a}^{N-1} \frac{X_{v,m-1}(k)}{N} e^{\frac{-j2\pi k(\tau_l-G)}{N}} \frac{1-\rho_{k-a}^{\tau_l-G}}{1-\rho_{k-a}} \right). \end{aligned} \tag{3.12}$$

3.2 Signal to Interference and Noise Ratio

SINR is often used in wireless transmission as a way to measure the quality of wireless connections. It is the ratio of useful signal energy that arrives at a particular receiver

over the energy of unwanted factors such as the background noise, and interference from other simultaneous transmissions [104]. Here, SINR is used to investigate the performance of OFDM transmissions with insufficient CP. In this case, the SINR at antenna u is defined as the desired signal power over the total power of noise and interference and is given by

$$SINR(u) = \frac{E\left\{|R_{d,u}(a)|^2\right\}}{E\left\{|R_{ici,u}(a)|^2\right\} + E\left\{|R_{isi,u}(a)|^2\right\} + \eta_0}, \tag{3.13}$$

where η_0 is the noise power and the expectation is taken over different channels and sub-carrier transmitted symbols. As the channel paths are assumed to be spatially uncorrelated and the sub-carrier symbols are also independent and un-correlated from each other, the desired signal power can be calculated as

$$\begin{aligned} E\left\{|R_{d,u}(a)|^2\right\} &= E\left\{\left|\sum_{v=1}^{N_T} X_{v,m}(a) \sum_{l=0}^{L-1} f(l) h_{u,v,l,m} e^{-j2\pi a \tau_l/N}\right|^2\right\} \\ &= \sum_{v=1}^{N_T} E\left\{|X_{v,m}(a)|^2\right\} \sum_{l=0}^{L-1} E\left\{|f(l)h_{u,v,l,m}|^2\right\} \\ &= \sum_{v=1}^{N_T} \sigma_X^2 \sum_{l=0}^{L-1} (f(l))^2 \sigma_l^2 \\ &= N_T \sigma_X^2 \sum_{l=0}^{L-1} (f(l))^2 \sigma_l^2, \end{aligned} \tag{3.14}$$

where σ_X^2 denotes the average sub-carrier power and σ_l^2 is the channel path power. Using the same assumptions and derivation steps, we can obtain the ICI and ISI power as

$$\begin{aligned} E\left\{|R_{ici,u}(a)|^2\right\} &= E\left\{\left|\sum_{v=1}^{N_T}\sum_{l=D}^{L-1} h_{u,v,l,m} \sum_{k=0,k\neq a}^{N-1} \frac{X_{v,m}(k)}{N} e^{\frac{-j2\pi k\tau_l}{N}} \frac{\rho_{k-a}^{\tau_l - G} - 1}{1-\rho_{k-a}}\right|^2\right\} \\ &= \sum_{v=1}^{N_T}\sum_{l=D}^{L-1} E\left\{|h_{u,v,l,m}|^2\right\} \sum_{k=0,k\neq a}^{N-1} E\left\{\left|\frac{X_{v,m}(k)}{N} e^{\frac{-j2\pi k\tau_l}{N}} \frac{\rho_{k-a}^{\tau_l - G} - 1}{1-\rho_{k-a}}\right|^2\right\} \\ &= \sum_{v=1}^{N_T}\sum_{l=D}^{L-1} \sigma_l^2 \sum_{k=0,k\neq a}^{N-1} \frac{\sigma_X^2}{N^2} \left|\frac{\rho_{k-a}^{\tau_l - G} - 1}{1-\rho_{k-a}}\right|^2 \\ &= \frac{N_T \sigma_X^2}{N^2} \sum_{l=D}^{L-1} \sigma_l^2 \sum_{k=0,k\neq a}^{N-1} \left|\frac{\rho_{k-a}^{\tau_l - G} - 1}{1-\rho_{k-a}}\right|^2, \end{aligned} \tag{3.15}$$

and

$$
\begin{aligned}
E\left\{|R_{isi,u}(a)|^2\right\} &= E\Bigg\{\Bigg|\sum_{v=1}^{N_T}\sum_{l=D}^{L-1} h_{u,v,l,m-1}\Bigg(\frac{X_{v,m-1}(a)}{N}e^{\frac{-j2\pi a(\tau_l-G)}{N}}(\tau_l-G) \\
&+ \sum_{k=0,k\neq a}^{N-1}\frac{X_{v,m-1}(k)}{N}e^{\frac{-j2\pi k(\tau_l-G)}{N}}\frac{1-\rho_{k-a}^{\tau_l-G}}{1-\rho_{k-a}}\Bigg)\Bigg|^2\Bigg\} \\
&= \sum_{v=1}^{N_T}\sum_{l=D}^{L-1} E\left\{\left|h_{u,v,l,m-1}\right|^2\right\}\Bigg(E\left\{\left|\frac{X_{v,m-1}(a)}{N}e^{\frac{-j2\pi a(\tau_l-G)}{N}}(\tau_l-G)\right|^2\right\} \\
&+ E\left\{\left|\sum_{k=0,k\neq a}^{N-1}\frac{X_{v,m-1}(k)}{N}e^{\frac{-j2\pi k(\tau_l-G)}{N}}\frac{1-\rho_{k-a}^{\tau_l-G}}{1-\rho_{k-a}}\right|^2\right\}\Bigg) \\
&= \sum_{v=1}^{N_T}\sum_{l=D}^{L-1}\sigma_l^2\Bigg(\frac{\sigma_X^2}{N^2}(\tau_l-G)^2+\sum_{k=0,k\neq a}^{N-1}E\Bigg\{\Bigg|\frac{X_{v,m-1}(k)}{N} \\
&\times\ e^{\frac{-j2\pi k(\tau_l-G)}{N}}\frac{1-\rho_{k-a}^{\tau_l-G}}{1-\rho_{k-a}}\Bigg|^2\Bigg\}\Bigg) \\
&= \sum_{v=1}^{N_T}\sum_{l=D}^{L-1}\sigma_l^2\left(\frac{\sigma_X^2}{N^2}(\tau_l-G)^2+\sum_{k=0,k\neq a}^{N-1}\frac{\sigma_X^2}{N^2}\left|\frac{1-\rho_{k-a}^{\tau_l-G}}{1-\rho_{k-a}}\right|^2\right) \\
&= \frac{N_T\sigma_X^2}{N^2}\sum_{l=D}^{L-1}\sigma_l^2\left((\tau_l-G)^2+\sum_{k=0,k\neq a}^{N-1}\left|\frac{\rho_{k-a}^{\tau_l-G}-1}{1-\rho_{k-a}}\right|^2\right). \qquad (3.16)
\end{aligned}
$$

From (3.15) and (3.16), it can be seen that ISI contributes more interference energy than ICI because of the extra terms of $\sigma_l^2(\tau_l-G)^2$ in the summation. From (3.15) and (3.16), we have

$$
\begin{aligned}
&E\left\{|R_{ici,u}(a)|^2\right\}+E\left\{|R_{isi,u}(a)|^2\right\} \\
&= \frac{N_T\sigma_X^2}{N^2}\sum_{l=D}^{L-1}\sigma_l^2\sum_{k=0,k\neq a}^{N-1}\left|\frac{\rho_{k-a}^{\tau_l-G}-1}{1-\rho_{k-a}}\right|^2 \\
&+ \frac{N_T\sigma_X^2}{N^2}\sum_{l=D}^{L-1}\sigma_l^2\left((\tau_l-G)^2+\sum_{k=0,k\neq a}^{N-1}\left|\frac{\rho_{k-a}^{\tau_l-G}-1}{1-\rho_{k-a}}\right|^2\right) \\
&= \frac{N_T\sigma_X^2}{N^2}\sum_{l=D}^{L-1}\sigma_l^2\left((\tau_l-G)^2+2\sum_{k=0,k\neq a}^{N-1}\left|\frac{\rho_{k-a}^{\tau_l-G}-1}{1-\rho_{k-a}}\right|^2\right). \qquad (3.17)
\end{aligned}
$$

The expression in (3.17) can be further simplified if we consider the following property of its inner most summation,

$$\sum_{k=0,k\neq a}^{N-1}\left|\frac{\rho_{k-a}^{\tau_l-G}-1}{1-\rho_{k-a}}\right|^2=\frac{|e^{j\pi(\tau_l-G)}-1|^2}{4}+2\sum_{k=1}^{N/2-1}\left|\frac{\rho_k^{\tau_l-G}-1}{1-\rho_k}\right|^2. \tag{3.18}$$

The above property will be proven in Appendix A. With (3.18), the total interference energy in (3.17) becomes

$$\begin{aligned}&E\left\{|R_{ici,u}(a)|^2\right\}+E\left\{|R_{isi,u}(a)|^2\right\}\\ =\;&\frac{N_T\sigma_X^2}{N^2}\sum_{l=D}^{L-1}\sigma_l^2\left((\tau_l-G)^2+\frac{|e^{j\pi(\tau_l-G)}-1|^2}{2}+4\sum_{k=1}^{N/2-1}\left|\frac{\rho_k^{\tau_l-G}-1}{1-\rho_k}\right|^2\right)\end{aligned} \tag{3.19}$$

The expression in (3.19) does not contain the factor a (which represents the index of the current sub-carrier of interest). This means that on average, the interference power is the same across all N sub-carriers.

Substituting (3.14) and (3.19) into (3.13), we have

$$SINR(u)=\frac{N_T\sigma_X^2\sum_{l=0}^{L-1}(f(l))^2\sigma_l^2}{\frac{N_T\sigma_X^2}{N^2}\sum_{l=D}^{L-1}\sigma_l^2\left((\tau_l-G)^2+\frac{|e^{j\pi(\tau_l-G)}-1|^2}{2}+4\sum_{k=1}^{N/2-1}\left|\frac{\rho_k^{\tau_l-G}-1}{1-\rho_k}\right|^2\right)+\eta_0}. \tag{3.20}$$

The expression in (3.20) can be simplified to

$$SINR(u)=\frac{N^2\sum_{l=0}^{L-1}(f(l))^2\sigma_l^2}{\sum_{l=D}^{L-1}\sigma_l^2\left((\tau_l-G)^2+\frac{|e^{j\pi(\tau_l-G)}-1|^2}{2}+4\sum_{k=1}^{N/2-1}\left|\frac{\rho_k^{\tau_l-G}-1}{1-\rho_k}\right|^2\right)+\bar{\eta}_0}, \tag{3.21}$$

where $\bar{\eta}_0=\frac{N^2\eta_0}{N_T\sigma_X^2}$. It can be seen from (3.21) that on average the SINR value is the same across all sub-carriers and is dependent on N and τ_l-G, the degree that the CP is exceeded for each path. On the other hand, the factor N_T (number of transmit antennas) only has an effect on the noise component of SINR.

3.3 SINR Comparison Between Different Channel Models

The SINR expression in (3.21) is formulated for a generic channel. Here, it is applied to evaluate the SINR for 2 different channel models; the two dominant path channel

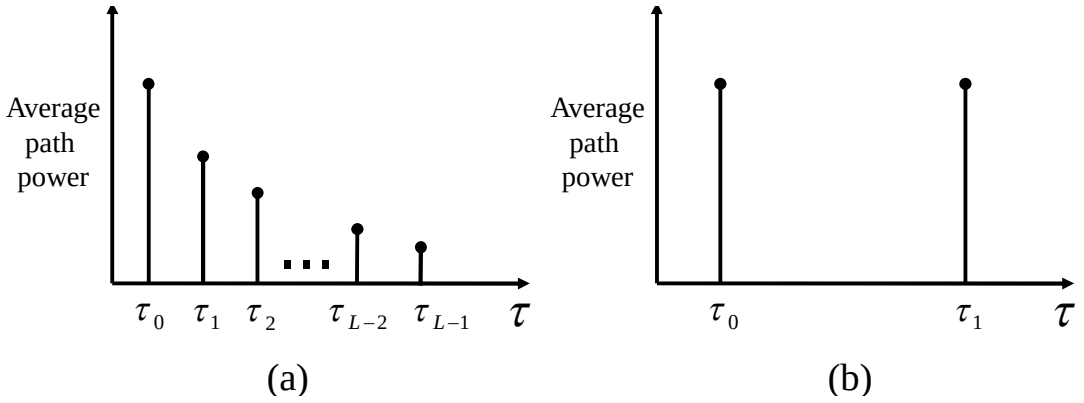

Figure 3.2: Transmission channel PDPs: (a) Exponential power decay, (b) Two equal power path.

model and the exponential decay multipath channel model. The PDPs of these channel models are illustrated in Fig. 3.2. The two dominant path channel model illustrates a wireless environment in which there is a single strong delayed version of the transmitted signal such as the case of two nearby base stations doing broadcasts or in the case of a relay system with direct and relayed paths. For this particular channel, the SINR in (3.21) becomes

$$SINR(u) = \frac{N^2 \sum_{l=0}^{1} (f(l))^2 \sigma_l^2}{\sigma_1^2 \left((\tau_1 - G)^2 + \frac{|e^{j\pi(\tau_1 - G)} - 1|^2}{2} + 4 \sum_{k=1}^{N/2-1} \left| \frac{\rho_k^{\tau_1 - G} - 1}{1 - \rho_k} \right|^2 \right) + \bar{\eta}_0}, \quad (3.22)$$

Assume the worst interference scenario in which both channel paths have equal power, $\sigma_0^2 = \sigma_1^2$, (3.22) can be simplified to

$$SINR(u) = \frac{N^2 + N(N - \tau_1 + G)}{(\tau_1 - G)^2 + \frac{|e^{j\pi(\tau_1 - G)} - 1|^2}{2} + 4 \sum_{k=1}^{N/2-1} \left| \frac{\rho_k^{\tau_1 - G} - 1}{1 - \rho_k} \right|^2 + \frac{\bar{\eta}_0}{\sigma_1^2}}. \quad (3.23)$$

From (3.23), it can be seen that the SINR value heavily depends on the delay of the second path, τ_1.

The exponential decay multipath channel model represents a less severe interference channel. Here, the powers of the delayed paths decay exponentially. So the longest delayed paths have weakest powers. We assume that the number of channel

paths is $L = 6$. Recalling from (2.6) that the power of the l^{th} path is given by $\sigma_l^2 = \alpha_l e^{-\tau_l/\tau_{rms}}$, the SINR expression for this particular channel is

$$SINR(u) = \frac{N^2 \sum_{l=0}^{5} (f(l))^2 \alpha_l e^{-\tau_l/\tau_{rms}}}{\sum_{l=D}^{5} \alpha_l e^{-\tau_l/\tau_{rms}} \left((\tau_l - G)^2 + \frac{|e^{j\pi(\tau_l - G)} - 1|^2}{2} + 4 \sum_{k=1}^{N/2-1} \left| \frac{\rho_k^{\tau_l - G} - 1}{1 - \rho_k} \right|^2 \right) + \bar{\eta}_0}. \tag{3.24}$$

From (3.24), we can see that the interference would cause an error floor, which cannot be compensated by increasing the transmission power, on the BER performance of OFDM receivers. This is because the SINR expression in (3.24) does not involve any factors related to the transmitted signal energy.

To verify this, we consider an LTE OFDM system with $N_T = 2$, $N = 128$ and $G = 9$. The channel RMS delay spread is assumed to be half the maximum channel delay, $\tau_{rms} = \tau_{L-1}/2$, for both the considered channel models. Figure 3.3 illustrates the SINR curves computed with respect to channel delay for such system parameters, where the label '2-path eqp' indicates the 2 path channel and '6-path exp' indicates the exponential decay channel with 6 paths. The *dB* values in the legend indicate the *signal to noise (SNR)*.

It can be seen that the 6 path exponential power decay channel has a better SINR for all considered SNR conditions. This is expected because of the power decay property of the exponential channel model. Due to the exponential decay PDP, the channel paths lying outside the CP have smaller power than those within the CP on average. Therefore, the overall interference resulting from these paths is smaller than that of the two equal power path channel with the same RMS and maximum delay. On the other hand, for the two equal power path channel, the second path (which is also the most delayed one) has the same energy as that of the first path, thus resulting in a higher interference channel. It is also indicated in the figure that for both types of channel, there is a fast degradation in SINR when the channel delay increases. Increasing the transmission power, and hence SNR, has little effect in compensating for such decrement. Therefore, in order to establish a reliable transmission for insufficient CP OFDM systems, the receiver must have an effective interference mitigation/equalization process.

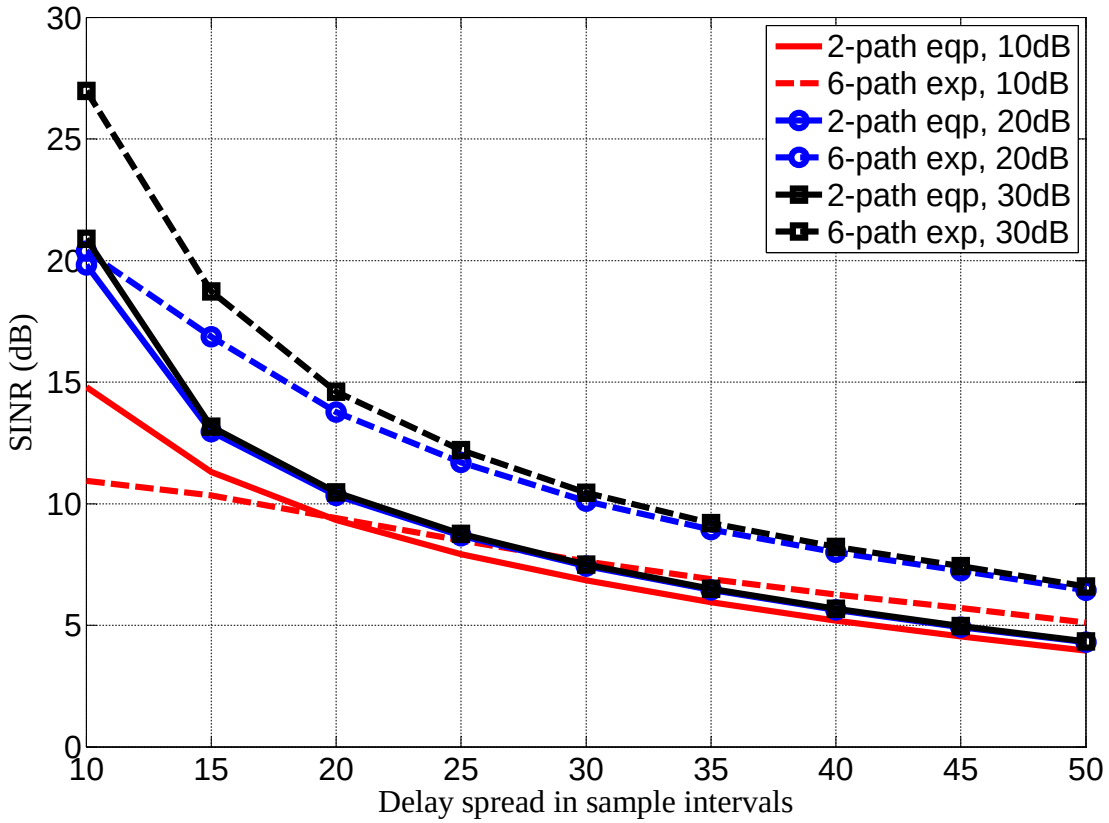

Figure 3.3: Maximum channel delay spread effect on SINR of OFDM transmission, CP length $G = 9$.

3.4 Interference Analysis

This section analyzes the properties of the insufficient CP induced interference across different sub-carriers.

3.4.1 ISI and ICI Relationship

The first property of the interference is described in Property 1:

Property 1 *For insufficient CP OFDM, on average, the ISI power contributed from sub-carrier k of the previous OFDM symbol to sub-carrier a of the current OFDM symbol is the same as the ICI power contributed from sub-carrier k of the current*

OFDM symbol for $k \neq a$.

This leads to Property 2:

Property 2 *Consider sub-carrier a of an OFDM symbol with insufficient CP transmission. On average, the total ICI power is equal to the total ISI power neglecting the ISI contributed from sub-carrier a of the previous OFDM symbol.*

Property 1 and 2 can be easily shown by considering (3.15) and (3.16). The ISI and ICI power originated from sub-carrier $k \neq a$ of the previous and current OFDM symbols are equal because they can both be expressed as

$$\frac{N_T \sigma_X^2}{N^2} \sum_{l=D}^{L-1} \sigma_l^2 \left| \frac{\rho_{k-a}^{\tau_l - G} - 1}{1 - \rho_{k-a}} \right|^2 . \tag{3.25}$$

On the other hand, from (3.16), the ISI power neglecting the ISI part contributed from sub-carrier a of the previous OFDM symbol is

$$\frac{N_T \sigma_X^2}{N^2} \sum_{l=D}^{L-1} \sigma_l^2 \sum_{k=0, k\neq a}^{N-1} \left| \frac{\rho_{k-a}^{\tau_l - G} - 1}{1 - \rho_{k-a}} \right|^2 , \tag{3.26}$$

which is equal to the total ICI power as shown in (3.15).

The two properties mean that, on average, ISI contributes more energy to the total interference than ICI due to the presence of the ISI from sub-carrier a of the previous OFDM symbol (while sub-carrier a of the current OFDM symbol is the desired signal). However, the ICI energy is still a major SINR degradation factor. This is confirmed in Fig. 3.4, which shows the ratios of the total ISI and ICI energy over the desired signal energy for a SNR of 20 dB using the same system parameters as Fig. 3.3. In addition, ISI can be effectively eliminated by a decision feedback loop from the previous detected OFDM symbol in cases when the detection is accurate as shown in [2]. Thus, ICI compensation is a crucial task for insufficient CP OFDM receivers as it not only reduces the ICI level, but also affects the ISI cancellation process of the following OFDM symbol.

3.4.2 Interference Contribution from Different Sub-carriers

Here, we investigate how different sub-carriers contribute to the total ISI and ICI energy as well as the effect of channel path delay on these contributions. Figure

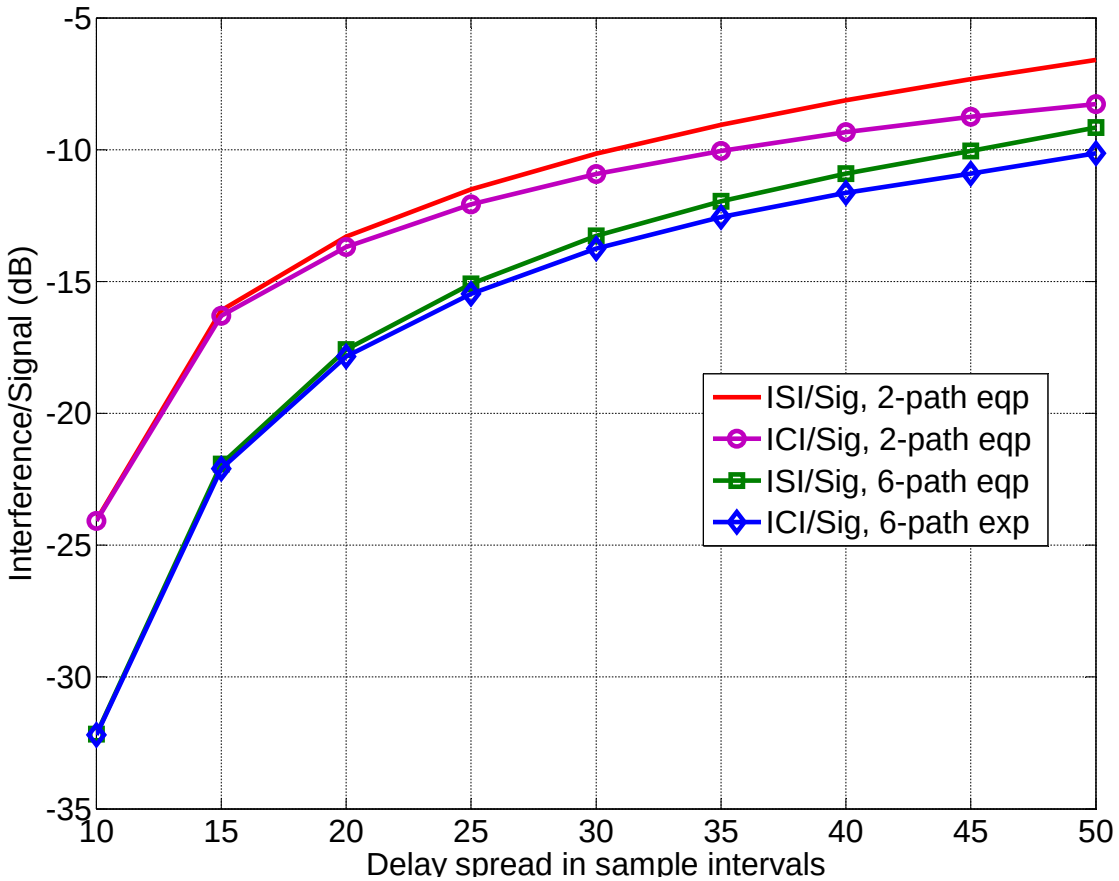

Figure 3.4: ISI and ICI over signal energy ratios with respect to maximum channel delay spread, 20 dB SNR and CP length $G = 9$.

3.5 shows the desired signal energy at sub-carrier $a = 60$ and the ICI energy contribution from various sub-carriers due to insufficient CP with a 6 path exponential power decay channel. It can be observed that the major ICI contributions are from the sub-carriers close to sub-carrier $a = 60$. From the relation between ISI and ICI, the previous block sub-carriers behave the same for ISI energy contribution. The described interference character is now summarized in property 3.

Property 3 *The ISI or ICI energy contributed from sub-carrier $k_1 = a \pm b_1$ of the previous or current OFDM symbol to the current sub-carrier a due to a number of channel paths lying outside the CP is to be greater than the one contributed from $k_2 = a \pm b_2$ for most values of $b_1 < b_2$.*

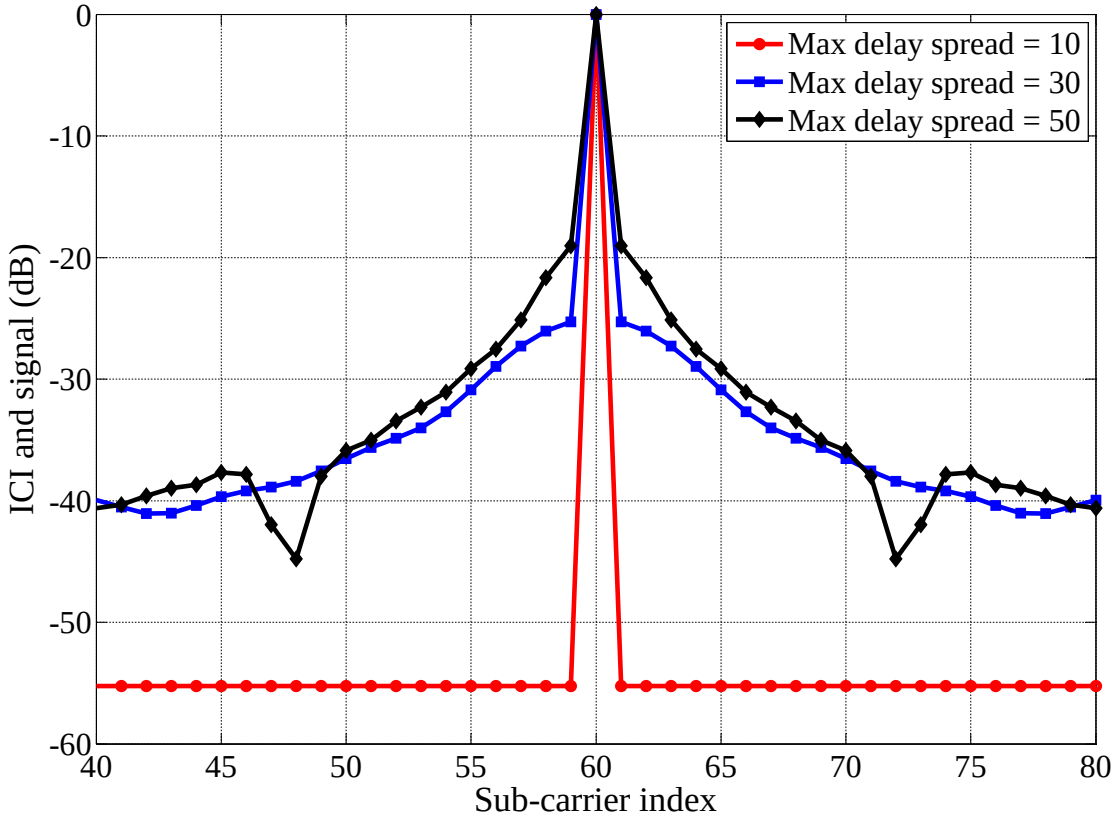

Figure 3.5: Signal at sub-carrier $a = 60$ and ICI from different sub-carriers, $G = 9$, $N = 128$ and $N_T = 2$.

According to (3.15) and (3.16), property 3 can be mathematically expressed as

$$\frac{N_T\sigma_X^2}{N^2}\sum_{l=D}^{L-1}\sigma_l^2\left|\frac{\rho_{k_1-a}^{\tau_l-G}-1}{1-\rho_{k_1-a}}\right|^2 > \frac{N_T\sigma_X^2}{N^2}\sum_{l=D}^{L-1}\sigma_l^2\left|\frac{\rho_{k_2-a}^{\tau_l-G}-1}{1-\rho_{k_2-a}}\right|^2. \tag{3.27}$$

The inequality in (3.27) is equivalent to

$$\begin{aligned}&\left|\frac{\rho_{b_1}^{\tau_l-G}-1}{1-\rho_{b_1}}\right|^2 > \left|\frac{\rho_{b_2}^{\tau_l-G}-1}{1-\rho_{b_2}}\right|^2\\ \iff &\left|\sum_{n=\tau_l-G}^{N-1}e^{j2\pi nb_1/N}\right|^2 > \left|\sum_{n=\tau_l-G}^{N-1}e^{j2\pi nb_2/N}\right|^2.\end{aligned} \tag{3.28}$$

By expanding the complex exponential functions on both sides of (3.28), we have

$$\left|\sum_{k=\tau_l-G}^{N-1}\cos(2\pi kb_1/N)\right|^2+\left|\sum_{k=\tau_l-G}^{N-1}\sin(2\pi kb_1/N)\right|^2$$
$$>\left|\sum_{k=\tau_l-G}^{N-1}\cos(2\pi kb_2/N)\right|^2+\left|\sum_{k=\tau_l-G}^{N-1}\sin(2\pi kb_2/N)\right|^2. \quad (3.29)$$

We will show that the inequality in (3.29) holds for most cases of $b_1 < b_2$, leading to an explanation for property 3.

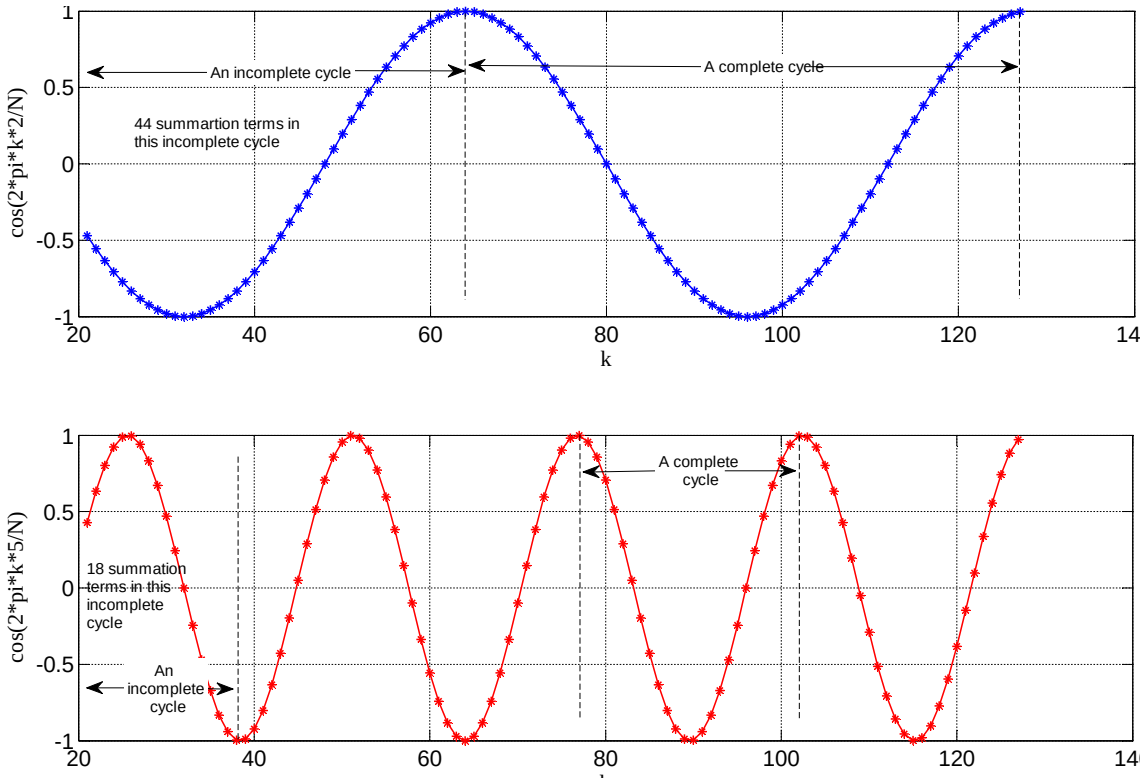

Figure 3.6: Plot of $\cos(2\pi kb/N)$ with respect to $\tau_l - G \leq k \leq N-1$, $G = 9$, $N = 128$, $\tau_l = 30$, $b = 2$ for the first plot and $b = 5$ for the second plot.

First, it is observed that for $k = 0$ to $k = N-1$, there are b complete sinusoidal cycles for the functions $\cos(2\pi kb/N)$ and $\sin(2\pi kb/N)$, where b is a positive integer and $b < N$. Since the limits of the summations in (3.29) are from $k = \tau_l - G$ to $k = N-1$, each of them is taken over $q \leq b$ cycles. Depending on the value of

$\tau_l - G$, the first cycle among those q cycles can be incomplete because of losing samples at the beginning of the sinusoidal waveform as illustrated in Fig. 3.6. Due to the symmetrical shapes of cos() and sin(), the terms for the later $q-1$ complete cycles within each sum cancel each other resulting in zero. Thus, the value of each summation in (3.29) depends on the samples of the first/incomplete cycle. Since $b_1 < b_2$, for each sinusoidal cycle, there would be more summation terms in $\left|\sum_{k=\tau_l-G}^{N-1} \cos(2\pi k b_1/N)\right|^2$ than in $\left|\sum_{k=\tau_l-G}^{N-1} \cos(2\pi k b_2/N)\right|^2$. Hence, there are likely more terms within the incomplete cycles corresponding to b_1. As the number of terms within an incomplete cycle increases, the better the chance those terms can add up to form a higher absolute value. So, for most scenarios, we have

$$\left|\sum_{k=\tau_l-G}^{N-1} \cos(2\pi k b_1/N)\right|^2 > \left|\sum_{k=\tau_l-G}^{N-1} \cos(2\pi k b_2/N)\right|^2. \tag{3.30}$$

Similarly,

$$\left|\sum_{k=\tau_l-G}^{N-1} \sin(2\pi k b_1/N)\right|^2 > \left|\sum_{k=\tau_l-G}^{N-1} \sin(2\pi k b_2/N)\right|^2. \tag{3.31}$$

Since both (3.30) and (3.31) are true most of the time, (3.29) also holds for most cases leading to property 3.

Property 3 has shown us that the closer a sub-carrier is to the sub-carrier of interest, the higher the ICI energy it causes when the CP is insufficient. This means that a major part of the ICI energy can be caused by a small number of sub-carriers close to the desired one. Table 3.1 illustrates the ratios between the ICI energy caused by different numbers of sub-carriers that are closest to the desired one and the total ICI energy. The values are calculated with different delay spread values for the two considered channel models. It can be seen that across all the considered scenarios, the majority of ICI energy is found in the closest 6 to 8 sub-carriers and it would take a significant number of additional sub-carriers to have meaningful increments over such values.

3.4.3 Interference Distribution

Here, we investigate the distribution of the insufficient CP induced interference. From (3.9), it can be seen that ICI and ISI are the sums of NN_T scaled independent and identically distributed variables drawn from a finite constellation. According to

Number of nearby sub-carriers (both sides)	2 eqp path channel			6 exp path channel		
	20	$\tau_1 = 40$	$\tau_1 = 60$	$\tau_5 = 20$	$\tau_5 = 40$	$\tau_5 = 60$
2	0.1835	0.5251	0.7624	0.1244	0.3241	0.4687
4	0.3541	0.8007	0.8375	0.2425	0.5506	0.6657
6	0.5048	0.8711	0.8687	0.3510	0.6801	0.7503
8	0.6306	0.8718	0.9172	0.4473	0.7502	0.8028
10	0.7293	0.8886	0.9305	0.5299	0.7957	0.8339
20	0.8961	0.9493	0.9588	0.7581	0.9046	0.8954
40	0.9486	0.9757	0.9807	0.8884	0.9532	0.9537

Table 3.1: The ratio of the sum of the ICI energy in the closest sub-carriers to the total ICI energy from all sub-carriers within an OFDM symbol. The values are calculated with $N_T = 2$, $N = 128$ and $G = 9$.

the central limit theorem, if NN_T is large enough, the interference is approximately Gaussian distributed with a zero mean (due to the QAM constellation points having a mean of zero). The approximation is supported by the histograms shown in Fig. 3.7, which includes both the sample distribution and the normal distribution fitted on the sample vectors. This is also supported by its measured auto-correlation that is approximately a delta function as shown in Fig. 3.8. Similar results are found for the imaginary parts. For further investigation, a Chi-Square goodness of fit test on the sample vectors of the real and imaginary part of ISI and ICI is conducted to identify if the samples come from a normal distribution. Matlab simulations have shown that the interference distribution passes the test with a significance level of 1.5%. This indicates that the interference distribution weakly approximates the Gaussian distribution. Note: It is trivial to see that the variances of ISI and ICI distributions would be $\sigma^2_{ISI} = E\{|R_{isi,u}(a)|^2\}$ and $\sigma^2_{ICI} = E\{|R_{ici,u}(a)|^2\}$.

3.5 Summary

In this chapter, insufficient CP interference is mathematically formulated and its characteristics are analyzed. It can be seen that the interference has a negative effect on the transmission quality in the form of reduction in SINR, which cannot be mitigated by increasing the signal strength. So, interference mitigation and equalization are required for data detection. It was shown that ICI is a major

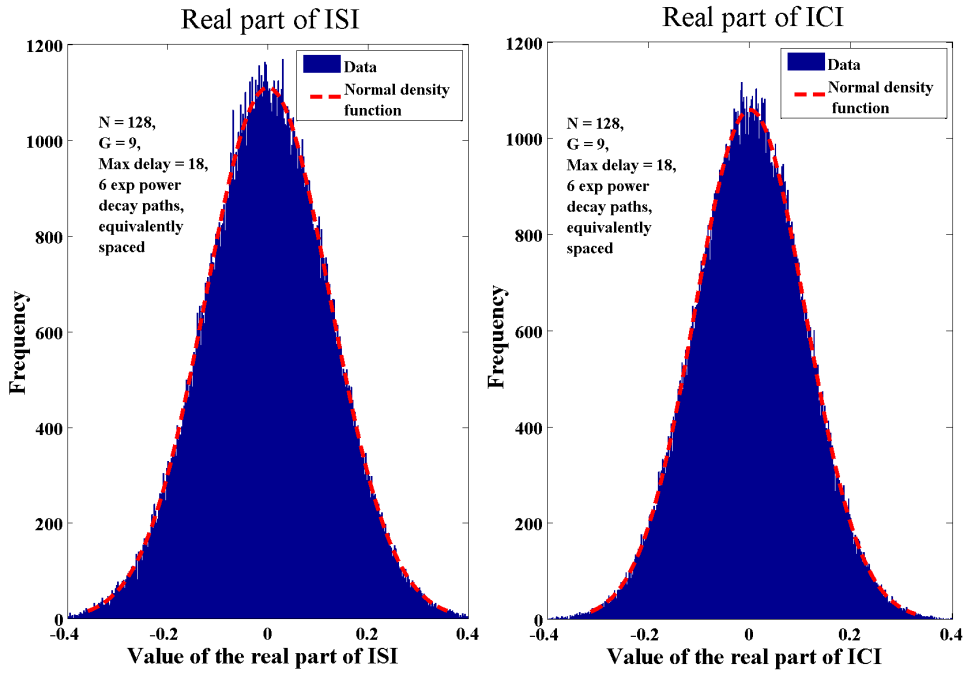

Figure 3.7: Histogram of the real part of ISI and ICI for 4 QAM sub-carriers. Number of data points is 152000 and there are 400 intervals.

degradation factor (almost as severe as ISI) and most ICI energy comes from sub-carriers, which are close to the sub-carrier of interest. This important property will be utilized by the proposed receivers for interference cancellation. In the next chapter, based on the obtained interference analysis, different receiver designs will be proposed for accurate data detection in insufficient CP SIMO-OFDM systems.

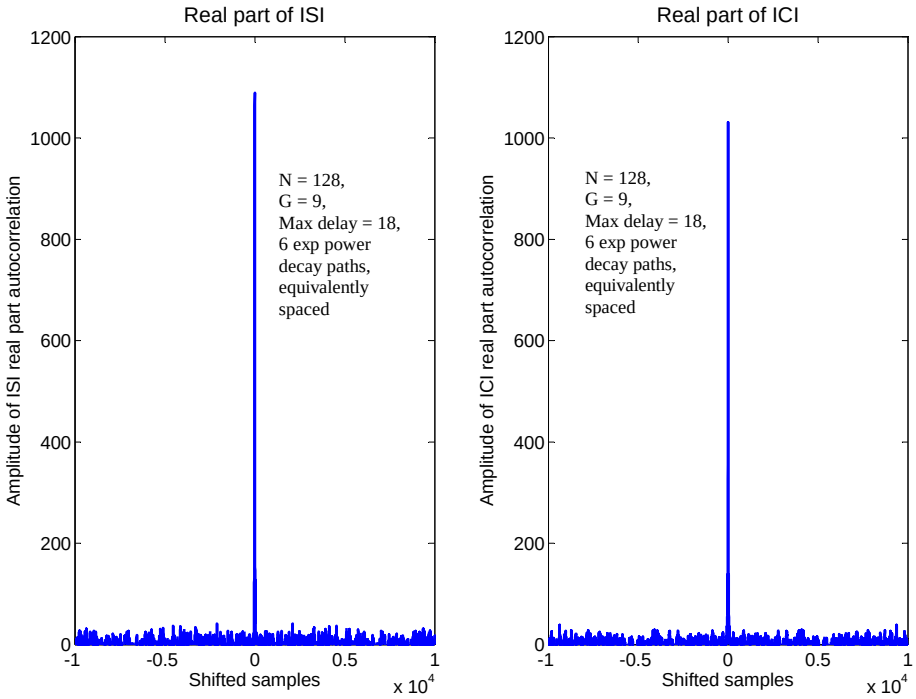

Figure 3.8: Autocorrelation of the real part of ISI and ICI for 4 QAM as modulation on the sub-carriers.

Chapter 4

Receiver Design for SIMO-OFDM Systems with Insufficient CP

In this chapter, we propose effective receiver designs for insufficient CP SIMO-OFDM systems based on the interference derivation and analysis in Chapter 3. In the context of insufficient CP OFDM transmission, the received OFDM signal will often be very different from the transmitted signal due to ISI and ICI. The receiver must identify the most likely transmitted data according to some criteria of optimality based on the noisy and distorted received signal. In order to do this, the receiver needs to have knowledge about the transmission channel, which can be estimated with pilot sub-carriers. However, due to the presence of interference, the pilot sub-carriers are also corrupted leading to inaccuracy in channel estimations. This can result in an overall degradation in the detection process. Here, by utilizing the spatial diversity available in SIMO systems, we are able to construct effective channel estimation and data detection methods for insufficient CP OFDM transmissions. These methods will be used as building blocks to the receiver designs for the full multi-antenna (MIMO) OFDM systems with insufficient CP.

We begin with the design of an iterative receiver consisting of channel estimation, interference mitigation and trellis based equalization. The design can be applied to different channel conditions without restrictions on the number of receive antennas. Following it, the derivation of the sub-carrier pilot based channel estimation process is given. The construction of the equalizer trellis and the equalization algorithm are then described. We then introduce two additional data detection methods based on

ZF and MMSE criterion with lower complexity than the trellis equalizer. However, these reduced complexity approaches have restrictions on the number of receive antennas and transmission channels they can handle. The complexity analysis of these proposed methods is also included here. The final section compares and discusses the performances of the proposed designs.

4.1 Receiver Design for a Generic Channel Model

Figure 4.1 shows the baseband system model of our proposed receiver design for insufficient-CP SIMO-OFDM systems. Here, we assume perfect synchronization.

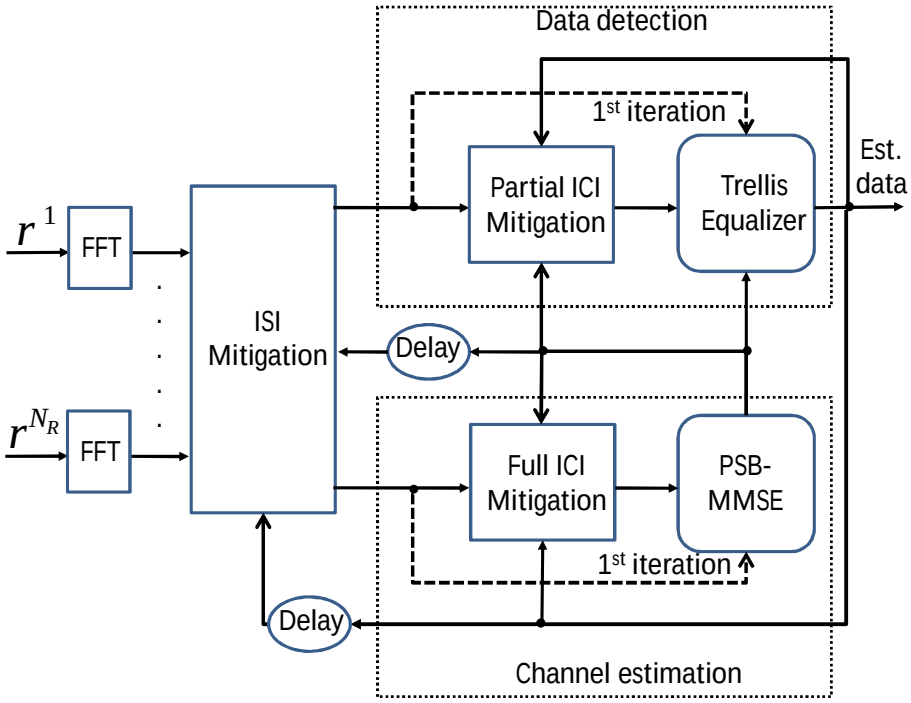

Figure 4.1: Simplified receiver block diagram with N_R receive antennas.

In this design, detected data from previous OFDM symbols and iterations is used to approximate the ISI and ICI in the current OFDM symbol for interference mitigation. There are 2 types of ICI mitigation: Full and partial. Full ICI mitigation is utilized for channel estimation while the process of partial ICI mitigation supports the equalization procedure. In full ICI mitigation, the receiver attempts

to remove all ICI so that the input signal to the channel estimator can be as clean as possible. On the other hand, the process of partial ICI mitigation is to remove ICI components caused by sub-carriers far from the desired sub-carriers. The remaining (major) ICI would be dealt with by the trellis equalizer to enable accurate data detection. In the first iteration, the processes for ICI mitigation are neglected. The interference mitigation is described as follows while the processes of channel estimation and trellis-based equalization are described in Sections 4.2 and 4.3. In comparison to the iterative receiver in Fig. 2.5, this design also does TD channel estimation, FD interference cancellation and FD data detection. However, our iterative design differentiates from the receiver in Fig. 2.5 by: 1) Our design does not have a channel prediction process as the pilot sub-carriers (in LTE systems) are distributed across a transmission frame such that the variation in wireless channel can be accounted for; 2) The ICI cancellation process in our design is modified to support the trellis based equalizer; 3) The detection process does not require the MRC combiner.

Since we consider SIMO systems, the desired signal, ISI and ICI expressions in (3.10), (3.11) and (3.12) can be simplified to

$$R_{d,u}(a) = X_m(a) \sum_{l=0}^{L-1} f(l) h_{u,l,m} e^{\frac{-j2\pi a \tau_l}{N}}, \tag{4.1}$$

$$R_{ici,u}(a) = \sum_{l=D}^{L-1} h_{u,l,m} \sum_{k=0,k\neq a}^{N-1} \frac{X_m(k)}{N} e^{\frac{-j2\pi k \tau_l}{N}} \frac{\rho_{k-a}^{\tau_l - G} - 1}{1 - \rho_{k-a}}, \tag{4.2}$$

$$\begin{aligned} R_{isi,u}(a) \;=\; & \sum_{l=D}^{L-1} h_{u,l,m-1} \left(\frac{X_{m-1}(a)}{N} e^{\frac{-j2\pi a(\tau_l - G)}{N}} (\tau_l - G) \right. \\ & \left. + \sum_{k=0,k\neq a}^{N-1} \frac{X_{m-1}(k)}{N} e^{\frac{-j2\pi k(\tau_l - G)}{N}} \frac{1 - \rho_{k-a}^{\tau_l - G}}{1 - \rho_{k-a}} \right). \end{aligned} \tag{4.3}$$

The sub-script notation v corresponding to the transmit antenna index is also suppressed in the above expressions. Interference mitigation is performed by feeding back the hard data decisions ($\widehat{X}_m(k)$) obtained from the trellis equalizer's output and the corresponding channel estimates in order to approximate the current ISI and ICI. From (4.2) and (4.3), the interference estimates can be expressed as

$$\widehat{R}_{ici,u}(a) = \sum_{l=D}^{L-1} \widehat{h}_{u,l,m} \sum_{k=0,k\neq a}^{N-1} \frac{\widehat{X}_m(k)}{N} e^{\frac{-j2\pi k \tau_l}{N}} \frac{\rho_{k-a}^{\tau_l - G} - 1}{1 - \rho_{k-a}}, \tag{4.4}$$

$$\widehat{R}_{isi,u}(a) = \sum_{l=D}^{L-1} \widehat{h}_{u,l,m-1} \left(\frac{\widehat{X}_{m-1}(a)}{N} e^{\frac{-j2\pi a(\tau_l - G)}{N}} (\tau_l - G) + \sum_{k=0,k\neq a}^{N-1} \frac{\widehat{X}_{m-1}(k)}{N} e^{\frac{-j2\pi k(\tau_l - G)}{N}} \frac{1-\rho_{k-a}^{\tau_l - G}}{1-\rho_{k-a}} \right). \quad (4.5)$$

The ISI and full ICI cancellation are carried out by

$$\breve{R}_u(a) = R_u(a) - \widehat{R}_{isi,u}(a), \quad (4.6)$$

$$\dot{Y}_u(a) = \breve{R}_u(a) - \widehat{R}_{ici,u}(a). \quad (4.7)$$

The resulting signal $\dot{Y}_{u,m}(a)$ is used for channel estimation.

As shown in Table 3.1, most of the ICI energy comes from the $d = d_1 + d_2$ sub-carriers close to the desired sub-carrier, where d, d_1, and d_2 are small positive integers. This major part of ICI, labeled $R_{ici1,u}(a)$, would be dealt with by the subsequent equalization process. In partial ICI mitigation, the minor part of ICI, labeled $R_{ici2,u}(a)$, is cancelled. This can be done by estimating $R_{ici2,u}(a)$ from the current channel estimate and OFDM symbol hard decisions obtained from the previous iteration using just the components from sub-carriers outside the interval $[a - d_1, a + d_2]$,

$$R_{ici2,u}(a) = \sum_{l=D}^{L-1} \widehat{h}_{u,l,m} \sum_{k=0,k\notin[a-d_1,a+d_2]}^{N-1} \frac{\widehat{X}_m(k)}{N} e^{\frac{-j2\pi k\tau_l}{N}} \left(\frac{\rho_k^{\tau_l - G} - 1}{1-\rho_k} \right), \quad (4.8)$$

and subtracting it from the signal $\breve{R}_u(a)$ to give

$$Y_u(a) = \breve{R}_u(a) - \widehat{R}_{ici2,u}(a). \quad (4.9)$$

The equalizer extracts transmitted data from the resulting signal $Y_{u,m}(a)$.

4.2 Channel Estimation

In the context of insufficient CP, it is difficult to acquire an accurate channel estimate because the unknown data sub-carriers contaminate the pilot sub-carriers. In addition, it becomes more difficult when the channel statistics (in the form of the channel PDP) are not available at the receiver side. To overcome these issues,

we propose an accurate *pilot sub-carrier based - MMSE (PSB-MMSE)* channel estimator for insufficient-CP SIMO-OFDM systems using a limited number of pilot sub-carriers. This consists of 2 steps: Estimating the channel PDP and identifying the channel coefficients. The main advantage of the proposed method over [32] is that the iterative process in our method directly updates the estimates of the channel PDP and channel coefficients while [32] relies on the pilots and the expectation of transmitted signals (obtained from the last iteration) to train the RLS estimation process. Since the detected signal can still contain errors in the early iterations, it can take more iterations for the iterative estimation process in [32] to convert in comparison to the proposed method.

4.2.1 Channel PDP Estimation

Let the vector of the pilot sub-carriers of the current OFDM symbol be $\boldsymbol{X}_{m,p} = [X_m(p_0), X_m(p_1), \ldots, X_m(p_{N_p-1})]$. Using *least square (LS)* estimation, the channel FD estimate corresponding to the u^{th} receive antenna, $\widehat{H}_u(p_i)$, at a pilot sub-carrier of the m^{th} OFDM symbol is

$$\widehat{H}_{u,m}(p_i) = \frac{\dot{Y}_{u,m}(p_i)}{X_m(p_i)}, \tag{4.10}$$

where $\dot{Y}_{u,m}(p_i)$ is the received signal at pilot sub-carrier p_i after interference mitigation. The channel estimates of the pilot sub-carriers in the TD are given by

$$\tilde{h}_{u,m,n} = \frac{1}{N_p} \sum_{k=0}^{N_p-1} \widehat{H}_{u,m}(p_k) e^{j2\pi nk/N_p}, n = 0, 1, \ldots, \tau_{L-1}. \tag{4.11}$$

We assume the maximum channel delay (in sample intervals) τ_{L-1} is known and $\tau_{L-1} < N_p$. Let the vector $\tilde{\boldsymbol{h}}_{u,m} = [\tilde{h}_{u,m,0}, \ldots, \tilde{h}_{u,m,L-1}]^T$ denote the TD channel estimate corresponding to the u^{th} antenna. We assume that the channel PDP is the same for all received antennas. Let $\boldsymbol{C}_m$ be the PDP matrix when the m^{th} OFDM symbol is transmitted. It can be estimated as

$$\tilde{\boldsymbol{C}}_m = \frac{1}{N_R} \sum_{u=1}^{u=N_R} \tilde{\boldsymbol{h}}_{u,m} \tilde{\boldsymbol{h}}_{u,m}^{\dagger}. \tag{4.12}$$

By considering the magnitude of the diagonal of $\tilde{\boldsymbol{C}}_m$, we propose a simple method to identify the number of channel paths. This is based on the fact that the power

vectors of the TD channels would have L peaks assuming that the channel paths are at least 2 sample intervals apart. This is often the case when the channel has few paths and the delay spread is high. Our proposed method for estimating the number of paths is summarized as follows:

- Identify the peaks in the magnitude of the diagonal of $\tilde{\boldsymbol{C}}_m$.
- Discard a peak if its magnitude is less than 5% of the magnitude of the first peak (13 dB less power than the first path), which corresponds to the first arrived path. This is to eliminate false peaks caused by noise or interference. It was observed from simulation that a value of 5% provides good performance [1].
- The number of remaining peaks provides a value for $\widehat{L}$.

The positions of these peaks on the diagonal provide the estimated values for the path delays τ_l. The other elements are discarded and the $\tau_{L-1} \times \tau_{L-1}$ matrix $\tilde{\boldsymbol{C}}_m$ shrinks to a $L \times L$ matrix $\widehat{\boldsymbol{C}}_m$. In the first iteration, the estimates are still affected by ICI; however, these are improved in later iterations as the ICI is mitigated.

4.2.2 Path Coefficient Estimation

We now propose a MMSE procedure for estimating the path coefficients. Many pilot sub-carrier based channel estimators tend to estimate the channel frequency response samples at the pilots and then interpolate these samples to obtain the full channel response [105]. In contrast, our method directly estimates the TD channel taps. This helps in avoiding the errors caused by interpolation. From (3.9) and (4.7), the received sample corresponding to a pilot tone can be written as (dropping the subscript m for simplicity)

$$\dot{Y}_u(p_i) = X(p_i) \sum_{l=0}^{L-1} f(l) h_{u,l} e^{\frac{-j2\pi p_i \tau_l}{N}} + z_{p_i}, \tag{4.13}$$

where z_{p_i} is a combination of noise and residual interference. Let the notation diag denote a diagonal matrix. We define

$$\dot{\boldsymbol{Y}}_{p,u} = \left[\dot{Y}_u(p_0), \dot{Y}_u(p_1), \ldots, \dot{Y}_u(p_{N_p-1})\right]^T, \tag{4.14}$$

[1] Simulations were run for 1000 OFDM symbols with threshold values of 1%, 5% and 10%. It was found that 5% gave the best performance. However, further optimization may result in small performance gains.

$$\boldsymbol{h}_u = \left[h_{u,0}, h_{u,1}, \ldots, h_{u,L-1}\right]^T, \tag{4.15}$$

$$\boldsymbol{\Gamma} = \mathrm{diag}\left(\left[X_{p_0}, X_{p_1}, \ldots, X_{p_{N_p-1}}\right]\right), \tag{4.16}$$

$$\tilde{\boldsymbol{F}} = \mathrm{diag}\left([f(0), f(1), \ldots, f(L-1)]\right), \tag{4.17}$$

$$\boldsymbol{z}_p = \left[z_{p_0}, z_{p_1}, \ldots, z_{p_{P-1}}\right]^T, \tag{4.18}$$

$$\boldsymbol{\mathcal{F}}_p = \begin{bmatrix} e^{\frac{-j2\pi p_0 \tau_0}{N}} & e^{\frac{-j2\pi p_0 \tau_1}{N}} & \ldots & e^{\frac{-j2\pi p_0 \tau_{L-1}}{N}} \\ e^{\frac{-j2\pi p_1 \tau_0}{N}} & e^{\frac{-j2\pi p_1 \tau_1}{N}} & \ldots & e^{\frac{-j2\pi p_1 \tau_{L-1}}{N}} \\ \vdots & \vdots & \ddots & \vdots \\ e^{\frac{-j2\pi p_{N_p-1} \tau_0}{N}} & e^{\frac{-j2\pi p_{N_p-1} \tau_1}{N}} & \ldots & e^{\frac{-j2\pi p_{N_p-1} \tau_{L-1}}{N}} \end{bmatrix}, \tag{4.19}$$

where $\dot{\boldsymbol{Y}}_{p,u}$ is the received sample vector, $\boldsymbol{h}_u$ is the vector containing the channel path coefficients corresponding to the u^{th} receive antenna, $\boldsymbol{\Gamma}$ contains the pilot symbols, $\tilde{\boldsymbol{F}}$ contains the scaling factors for different channel paths, $\boldsymbol{z}_p$ is the noise-residual interference vector and $\boldsymbol{\mathcal{F}}_p$ is the FFT matrix. From (4.13), the received sample vector at the pilot sub-carriers can be expressed as

$$\dot{\boldsymbol{Y}}_{p,u} = \boldsymbol{\Gamma}\boldsymbol{\mathcal{F}}_p\tilde{\boldsymbol{F}}\boldsymbol{h}_u + \boldsymbol{z}_p = \boldsymbol{S}_p\boldsymbol{h}_u + \boldsymbol{z}_p. \tag{4.20}$$

From (4.20), we can formulate the PSB-MMSE channel estimator. Let $\boldsymbol{W}$ be our weight matrix, our goal here is to find $\boldsymbol{W}$ so that the MSE $E\left\{\left|\boldsymbol{W}^\dagger\dot{\boldsymbol{Y}}_{p,u} - \boldsymbol{h}_u\right|^2\right\}$ is minimized. The MMSE criteria is achieved by the Wiener-Hopf solution

$$\boldsymbol{W}^\dagger = \boldsymbol{C}\boldsymbol{S}_p^\dagger(\boldsymbol{S}_p\boldsymbol{C}\boldsymbol{S}_p^\dagger + \eta_z\boldsymbol{I})^{-1}, \tag{4.21}$$

where $\boldsymbol{I}$ is the identity matrix, η_z is the variance of z_{p_i} and $\dagger$ is the conjugate transpose operator. Since the actual values of $\tilde{\boldsymbol{F}}$, $\boldsymbol{\mathcal{F}}_p$ and $\boldsymbol{C}$ are not known, these matrices are replaced by their estimates in the $\boldsymbol{W}^\dagger$ calculation. These estimates can be computed from $\widehat{L}$ and $\widehat{\tau_l}$ obtained in Section 4.2.1.

4.3 Trellis-based Equalization

In order to achieve fast convergence of the proposed iterative reception process, we propose a high performance trellis equalizer. The design here differentiates itself from [73] by using past decisions (from the survivor paths) to capture more ICI energy without increasing the trellis size. Let $\boldsymbol{Y}_u = [Y_u(0), Y_u(1), \ldots, Y_u(N-1)]$ and $\boldsymbol{X} = [X(0), \ldots, X(a), \ldots, X(N-1)]$ (dropping the subscript m for simplicity).

The reception process is carried out by choosing the sequence that maximizes the likelihood

$$p(\boldsymbol{Y}_1, \ldots, \boldsymbol{Y}_{N_R}, \boldsymbol{X}) = p(\boldsymbol{Y}_1, \boldsymbol{X})p(\boldsymbol{Y}_2, \boldsymbol{X}) \ldots p(\boldsymbol{Y}_{N_R}, \boldsymbol{X}). \tag{4.22}$$

Applying the natural log to both sides of (4.22), we have

$$\ln(p(\boldsymbol{Y}_1, \ldots, \boldsymbol{Y}_{N_R}, \boldsymbol{X})) = \sum_{u=1}^{N_R-1} \ln(p(\boldsymbol{Y}_u, \boldsymbol{X})). \tag{4.23}$$

Let us define $\boldsymbol{Y}_u([n_1, n_2]) = [Y_u(n_1), \ldots, Y_u(n_2)]$, where $n_1 < n_2$ and they are both positive integer. By applying the probability chain rule, we have

$$\begin{aligned} p(\boldsymbol{Y}_u, \boldsymbol{X}) &= p(Y_u(N-1)|\boldsymbol{Y}_u([0, N-2], \boldsymbol{X})p(Y_u(N-2)|\boldsymbol{Y}_u([0, N-3], \boldsymbol{X}) \times \ldots \\ &\quad \times p(Y_u(0)|\boldsymbol{X})p(\boldsymbol{X}). \end{aligned} \tag{4.24}$$

Since $p(\boldsymbol{X} = p(X(0))p(X(1)) \ldots p(X(N-1))$, (4.24) becomes

$$\begin{aligned} p(\boldsymbol{Y}_u, \boldsymbol{X}) &= p(Y_u(N-1)|\boldsymbol{Y}_u([0, N-2], \boldsymbol{X})p(X(N-1))) \\ &\quad \times p(Y_u(N-2)|\boldsymbol{Y}_u([0, N-3], \boldsymbol{X})p(X(N-2))) \times \ldots \\ &\quad \times p(Y_u(0)|\boldsymbol{X})p(X(0)). \end{aligned} \tag{4.25}$$

This is equivalent to

$$\ln(p(\boldsymbol{Y}_u, \boldsymbol{X})) = \sum_{a=0}^{N-1} \ln(p(Y_u(a)|\boldsymbol{Y}_u([0, a-1], \boldsymbol{X}))) + \ln(p(X_a)). \tag{4.26}$$

Substituting (4.26) into (4.23), we have

$$\ln(p(\boldsymbol{Y}_1, \ldots, \boldsymbol{Y}_{N_R}, \boldsymbol{X})) = \sum_{a=0}^{N-1} \sum_{u=1}^{N_R-1} \ln(p(Y_u(a)|\boldsymbol{Y}_u([0, a-1], \boldsymbol{X}))) + \ln(p(X_a)). \tag{4.27}$$

Equation (4.27) means that the metric for the whole sequence is a sum of the metrics at successive symbol times and each symbol time metric is a sum of the metrics from different receive antennas.

Since the OFDM tones are independent from each other, the dependence between $Y_u(a)$ and $\boldsymbol{Y}_u([0, a-1]$ is due to the ICI. To simplify the detection process, we use the approximation $p(Y_u(a)|\boldsymbol{Y}_u([0, a-1], \boldsymbol{X}) \approx p(Y_u(a)|\boldsymbol{X})$. Simulation results will show us accurate data detection can be achieved with such approximation.

As the channel response is assumed to be deterministic and the ICI distribution is approximately Gaussian as shown in Section 3.4.3, we can assume that each element in $\boldsymbol{Y}_u$ is Gaussian when conditioned on the data sequence $\boldsymbol{X}$. Hence,

$$p(Y_u(a)|\boldsymbol{X}) = \frac{1}{\pi\eta_{In}} \exp\left(\frac{-|Y_u(a) - \tilde{Y}_u(a)|^2}{2\eta_{In}}\right), \tag{4.28}$$

where $\tilde{Y}_u(a)$ is the mean of $Y_u(a)$ conditioned on $\boldsymbol{X}$ and η_{In} is the noise plus residual interference power. As the majority of the ICI energy comes from a few tones on each side of the considered sub-carrier, ICI can be estimated from these. Therefore, $\tilde{Y}_u(a) = R_{d,u}(a) + R_{ici1,u}(a)$. The sub-branch metric corresponding to the u^{th} received antenna, denoted as $\mu_u(a)$, is given by

$$\begin{aligned} \mu_u(a) &= -\ln(p(Y_u(a)|\boldsymbol{X})) - \ln(p(X_a)) \\ &= \left|Y_u(a) - \tilde{Y}_u(a)\right|^2 - \ln(p(X_a)). \end{aligned} \tag{4.29}$$

The term $\ln(p(X_a))$ indicates the prior knowledge regarding the transmission of symbol X_a. In the case of iterative detection-decoding, $\ln(p(X_a))$ can be substituted by the soft information computed from a channel decoder for enhancing the equalization process. However, since turbo channel estimation-detection-decoding can become very computationally demanding without effective complexity reduction methods, we only consider iterative channel estimation and data detection in this thesis. So, the $\ln(p(X_a))$ value is determined by the transmission symbol probability. Here, we assume equal probability of transmission so $\ln(p(X_a))$ becomes a constant and can be neglected in (4.29). Hence, from (4.27), the overall sequence metric, which is minimized by the right choice of $\boldsymbol{X}$, is the sum of the branch metrics

$$\Omega(\boldsymbol{X}) = \sum_{a=0}^{N-1} \sum_{u=1}^{N_R-1} \mu_u(a). \tag{4.30}$$

To reduce complexity, we define the trellis state as $[X(a), X(a+1)]$, instead of the $[X(a-1), X(a), X(a+1)]$ used in [73]. This decreases the number of different trellis states from A^3 to A^2 with little effect on performance as the missing symbol, $X(a-1)$, can be retrieved during the equalizer's operation. With this definition, $d_2 = 1$ so $\widehat{R}_u^{ici1}(a)$ can be expressed as

$$R_{ici1,u}(a) = \sum_{l=D}^{L-1} h_{u,l,m} \sum_{k=0, k\in[a-d_1, a+1]}^{N-1} \frac{X_m(k)}{N} e^{\frac{-j2\pi k\tau_l}{N}} \left(\frac{\rho_k^{\tau_l - G} - 1}{1 - \rho_k}\right). \tag{4.31}$$

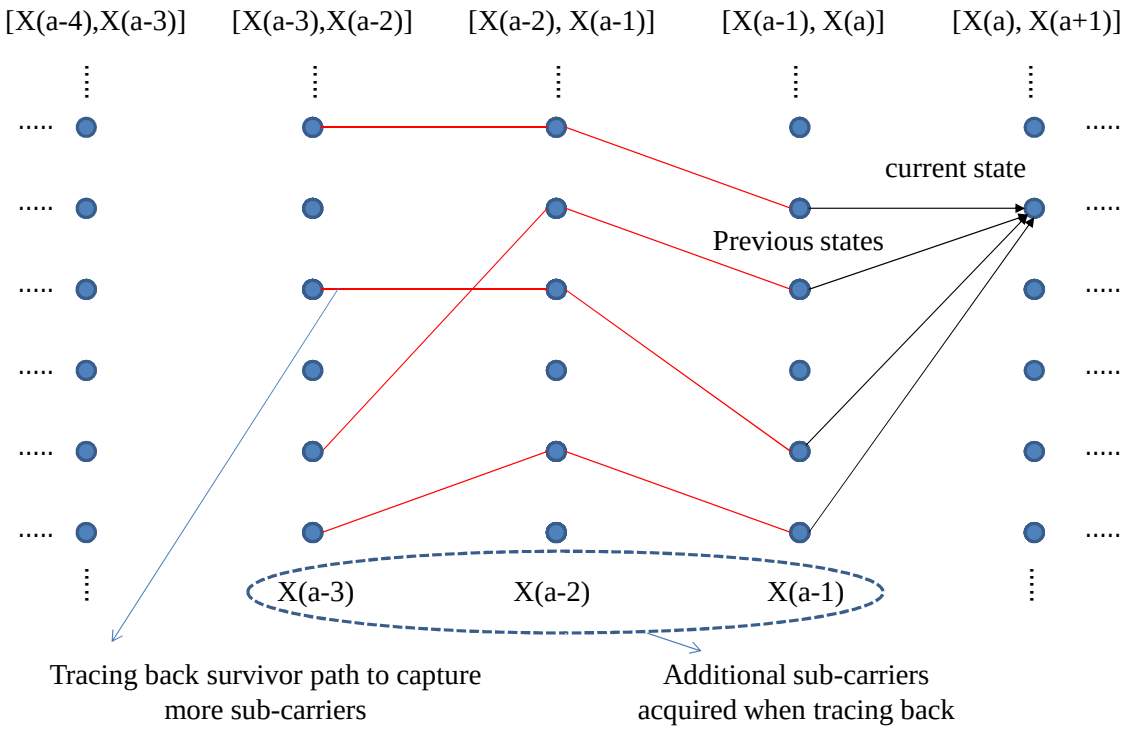

Figure 4.2: Trellis for equalization of SIMO-OFDM transmission with insufficient CP, $d_1 = 3$.

Hence, there needs to be d_1+2 sub-carriers involved in a branch metric computation. As a single trellis state of the trellis can only represent 2 sub-carriers among these, the equalization process acquires the remaining d_1 sub-carriers (including the missing symbol $X_m(a-1)$) by tracking back along the survivor path. An example of such a trellis is shown in Fig. 4.2 for $d_1 = 3$.

4.4 Zero Forcing and MMSE Detectors

In this section, we propose two additional data detection methods based on the ZF and MMSE criteria for insufficient CP SIMO-OFDM transmission. Here, it is assumed that the number of channel paths outside the CP is lower than the number of receive antennas, $L - D < N_R$. The two methods have lower complexity in comparison to the proposed trellis-equalizer. However, they have a restriction regarding the number of channel paths and the number of receive antennas due

to the stated assumption. Hence, they are not as generalized as the trellis-based method. The ZF and MMSE detectors are incorporated with the proposed channel estimator in an iterative manner as shown in Fig. 4.3.

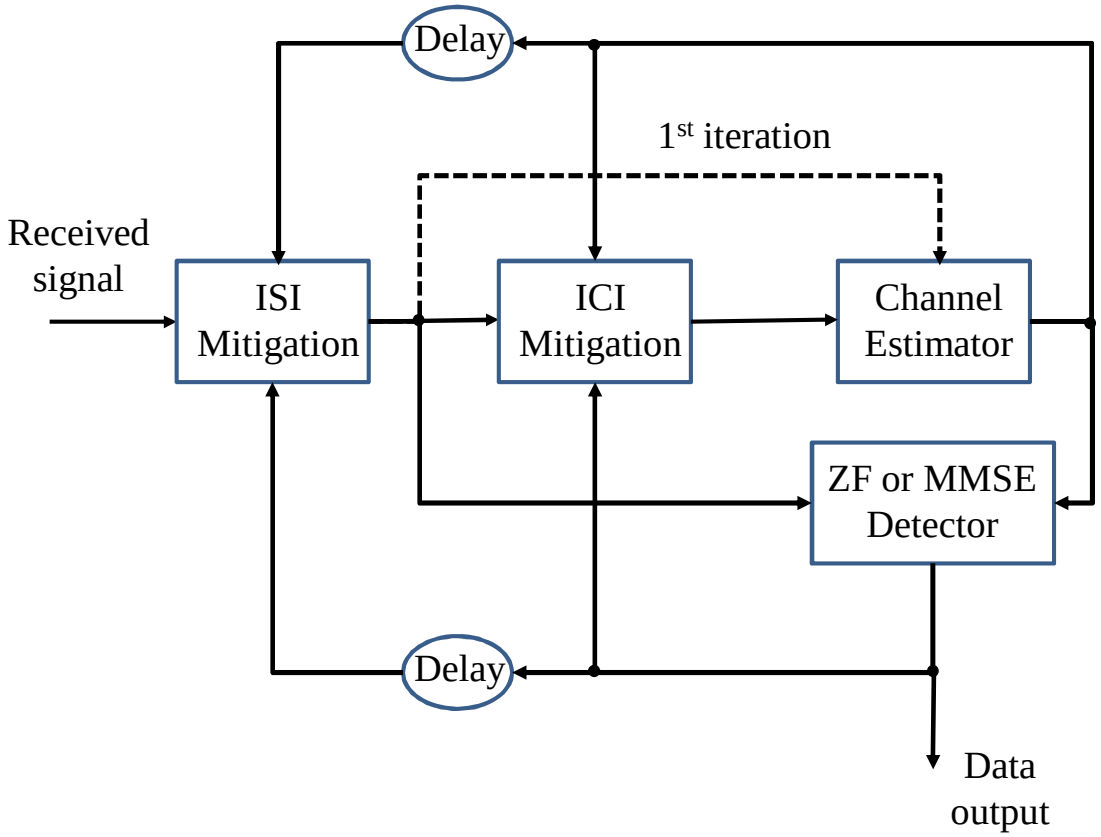

Figure 4.3: Iterative data reception with ZF or MMSE detector.

4.4.1 ZF-based Estimator

From (4.6), after ISI mitigation, the resulting signals can be written as

$$\breve{R}_u(a) = X(a)\sum_{l=0}^{L-1} f(l)h_{u,l}e^{\frac{-j2\pi a\tau_l}{N}} + \sum_{l=D}^{L-1} h_{u,l}\sum_{k=0,k\neq a}^{N-1}\frac{X(k)}{N}e^{\frac{-j2\pi k\tau_l}{N}}\frac{\rho_{k-a}^{\tau_l-G}-1}{1-\rho_{k-a}} + \tilde{n}_u(a), \quad (4.32)$$

where $\tilde{n}_u(a)$ now contains both the Gaussian noise and the residual ISI interference. Let us denote

$$\gamma_l(a) = \sum_{k=0,k\neq a}^{N-1} \frac{X(k)}{N} e^{\frac{-j2\pi k\tau_l}{N}} \frac{\rho_{k-a}^{\tau_l - G} - 1}{1 - \rho_{k-a}}, \tag{4.33}$$

$$\beta_u(a) = \sum_{l=0}^{L-1} f(l) h_{u,l} e^{\frac{-j2\pi a\tau_l}{N}}. \tag{4.34}$$

The expression in (4.32) becomes

$$\breve{R}_u(a) = \beta_u(a)X(a) + h_{u,D}\gamma_D(a) + \ldots + h_{u,L-1}\gamma_{L-1}(a) + \tilde{n}_u(a). \tag{4.35}$$

To ease the description of the ZF detection process, we consider the case of $N_R = L - D + 1$ (in the case of $N_R > L - D + 1$, we can simply select the $L - D + 1$ received signals with highest signal strength). Let us define

$$\breve{\boldsymbol{r}} = \left[\breve{R}_1(a), \breve{R}_2(a), \ldots, \breve{R}_{N_R}(a)\right]^T, \boldsymbol{s} = \left[X(a), \gamma_D(a), \ldots, \gamma_{L-1}(a)\right]^T, \tag{4.36}$$

$$\tilde{\boldsymbol{n}} = \left[\tilde{n}_1(a), \tilde{n}_2(a), \ldots, \tilde{n}_{N_R}(a)\right]^T, \boldsymbol{T} = \begin{bmatrix} \beta_1(a) & h_{1,D} & \ldots & h_{1,L-1} \\ \beta_2(a) & h_{2,D} & \ldots & h_{2,L-1} \\ \vdots & \vdots & \ddots & \vdots \\ \beta_{N_R}(a) & h_{N_R,D} & \ldots & h_{N_R,L-1} \end{bmatrix}. \tag{4.37}$$

From (4.35), we have

$$\breve{\boldsymbol{r}} = \boldsymbol{T}\boldsymbol{s} + \tilde{\boldsymbol{n}}. \tag{4.38}$$

To recover the transmitted data $X(a)$ from $\breve{\boldsymbol{r}}$, the vector $\boldsymbol{s}$ needs to be estimated. This can be carried out by $\widehat{\boldsymbol{s}} = \widehat{\boldsymbol{T}}^{-1}\breve{\boldsymbol{r}}$, where $\widehat{\boldsymbol{T}}$ is an estimate of $\boldsymbol{T}$ based on the channel estimates provided by the proposed channel estimator. Note: Since $\boldsymbol{s}$ is a $L - D + 1$ vector and $\boldsymbol{T}$ is a $(L - D + 1) \times (L - D + 1)$ square matrix, it is possible to find its inversion.

4.4.2 MMSE-based Estimator

Although the ZF method can provide complete ICI cancelation, it suffers from noise enhancement when the interference is still small. This can become worse when the noise level increases. Here, an alternative MMSE method to replace ZF is introduced. Let $\boldsymbol{W}_s$ be our weight matrix, our goal here is to find $\boldsymbol{W}_s$ so that the

MSE of $E\left\{ \left| \boldsymbol{W}_s^{\dagger}\breve{\boldsymbol{r}} - \boldsymbol{s} \right|^2 \right\}$ is minimized. The solution found to achieve the MMSE criterion is the Wiener-Hopf solution [106],

$$\boldsymbol{W}^{\dagger} = \boldsymbol{S}\boldsymbol{T}^{\dagger}(\boldsymbol{T}\boldsymbol{S}\boldsymbol{T}^{\dagger} + \eta_0 \boldsymbol{I})^{-1}, \tag{4.39}$$

where $\boldsymbol{S} = \boldsymbol{s}\boldsymbol{s}^{\dagger}$ is the signal-interference power matrix. Since $E\{\boldsymbol{s}\} = \boldsymbol{0}$ due to $E\{X(a)\} = E\{\gamma_l(a)\} = 0$, we have

$$\boldsymbol{S} = \begin{bmatrix} E\left\{|X_a|^2\right\} & 0 & \dots & 0 \\ 0 & E\left\{|\gamma_D(a)|^2\right\} & \dots & 0 \\ \vdots & \vdots & \ddots & \vdots \\ 0 & 0 & \dots & E\left\{|\gamma_{L-1}(a)|^2\right\} \end{bmatrix}. \tag{4.40}$$

For the same reason as above,

$$\begin{aligned} E\left\{|\gamma_l(a)|^2\right\} &= E\left\{ \left| \sum_{k=0,k\neq a}^{N-1} \frac{X(k)}{N} e^{\frac{-j2\pi k\tau_l}{N}} \frac{\rho_{k-a}^{\tau_l - G} - 1}{1 - \rho_{k-a}} \right|^2 \right\} \\ &= \frac{\sigma_X^2}{N^2} \sum_{k=0,k\neq a}^{N-1} E\left\{ \left| \frac{\rho_{k-a}^{\tau_l - G} - 1}{1 - \rho_{k-a}} \right|^2 \right\}. \end{aligned} \tag{4.41}$$

Substituting (3.18) into (4.41), we have

$$E\left\{|\gamma_l(a)|^2\right\} = \frac{\sigma_X^2}{N^2} \left(\frac{|e^{j\pi(\tau_l - G)} - 1|^2}{4} + 2 \sum_{k=1}^{N/2-1} \left| \frac{\rho_k^{\tau_l - G} - 1}{1 - \rho_k} \right|^2 \right). \tag{4.42}$$

The MMSE method is more complex than ZF. However, its performance is significantly better as will be shown in Section 4.6.

4.5 Complexity Analysis

In this section, we consider the computational complexity in terms of the number of complex multiplications involved in the processes of channel estimation, interference mitigation and data detection for an OFDM symbol with insufficient CP. Here, a real multiplication operation is considered as a quarter of its complex equivalence. Table 4.1 shows the approximate complexities of different processes within the developed PSB-MMSE process. The complexity of the standard MMSE method is

also included in Table 4.1 for comparison.

Using $N_p = 21$, $L = 6$, and $\tau_{L-1} = 20$, it can be seen that the complexity of our proposed algorithm is approximately 75% that of the conventional MMSE algorithm. This is because without the channel path identification process, the standard MMSE channel estimator needs to calculate the full TD channel response coefficients while the proposed PSB-MMSE method only needs to estimate the channel path coefficients, which are considerably fewer in numbers. Although the difference in complexity between the PSB-MMSE method and the standard MMSE method is modest, it will be shown that the developed method can provide a significantly more accurate channel estimate for insufficient CP SIMO-OFDM systems.

	PSB-MMSE	Standard MMSE
Channel estimation process	No complex multiplications	No complex multiplications
FD channel estimate at pilot	$2N_p$	$2N_p$
Covariance matrix estimate	$2N_p(2N_p+1)$	–
Computing $\boldsymbol{W}^\dagger$	$3N_p^3 + 2N_p^2(L+2)$ $+N_p(4L+11)$	$3N_p^3 + 2N_p^2(\tau_{L-1}+2)$ $+N_p(4\tau_{L-1}+11)$
TD channel coefficient estimate	$2N_pL$	$2N_p\tau_{L-1}$
Total	$37,674$	$49,980$

Table 4.1: Algorithm complexity comparison for PSB-MMSE and standard MMSE. The total values were calculated with $N_p = 21$, $L = 6$, and $\tau_{L-1} = 20$.

We now compare the complexities of the proposed data detection techniques. The computational cost takes into account the number of complex multiplications involved in the developed interference mitigation and data detection processes. Let I represent the number of iterations. Table 4.2 illustrates the approximate complexities of different processes within the developed algorithms. The complexity of the RISIC algorithm [2] is also included in Table 4.2 for comparison.

The total number of complex multiplication values are calculated for a SIMO-OFDM system with $N_R = 2$, $N = 128$ and 4-QAM sub-carrier modulation. We consider a transmission channel having 6 discrete paths ($L = 6$), half the number of paths is within the CP ($D = 3$) and 2 iterations of data reception ($I = 2$). With these parameters, it can be seen that the RISIC algorithm is approximately 2 and 1.5 times more complex than the proposed ZF and MMSE detectors respectively. On the other hand, the proposed trellis equalizer is approximately 1.5 times more complex than the RISIC algorithm. However, it will be shown in Section 4.6 that the trellis equalizer provides the best BER performance. It should be noted that the ICI and ISI mitigation processes in the RISIC algorithm are more complex than those of our proposed methods. This is because there is an extra process of data transformation from the FD to TD in the RISIC algorithm while the mitigation processes in the proposed methods are entirely in the FD.

Process	ZF detector	MMSE detector	Trellis equalizer	RISIC [2]
ISI mitigate	$2N_R(L-D)$ $\times N^2$	$2N_R(L-D)$ $\times N^2$	$2N_R(L-D)$ $\times N^2$	$2N_R(L-D)N^2$ $+N^2$
ICI mitigate	–	–	$2N_R(L-D)$ $\times N^2(I-1)$	$(2N_R(L-D)$ $\times N^2+N^2)(I-1)$
Signal equalize/ data detect	$((L-D+1)^3$ $+(L-D+1)^2$ $+N_RL)N$ $\times(I-1)$	$(3(L-D+1)^3$ $+(L-D+1)^2$ $+N_RL+(N+4)$ $\times(L-D+1))$ $\times N(I-1)$	NA^3 $\times N_R(d_1+2)$ $\times(L-D)I$	$5N_RA^2NI$
Total	$208,384$	$292,352$	$638,976$	$446,464$

Table 4.2: Algorithm complexity comparison for SIMO-OFDM system using ZF detector, MMSE detector, trellis equalizer and RISIC [2] with parameters $N_R = 2$, $N = 128$, $A = 4$ (modulation level), $L = 6$, $D = 3$, $d_1 = 3$ and $I = 2$.

4.6 Results and Discussion

Our simulations consider un-coded 1×2 SIMO-OFDM system with LTE-OFDM parameters, $N = 128$, $G = 9$ (standard LTE CP length) and 4-QAM for sub-carrier modulation. The pilot sub-carrier arrangement also follows the LTE standard [1] so there is 1 pilot sub-carrier for every 5 data sub-carriers in a reference OFDM symbol (defined as an OFDM symbol containing pilot sub-carriers). The pilot OFDM symbols are evenly distributed along a transmission frame and there is 1 reference OFDM symbol for every 3 data OFDM symbols. The channel path coefficients are assumed to stay static for a duration of $K = 4$ OFDM symbols and then vary independently from one static period to another. The main sub-channel model considered in our simulations consists of $L = 6$ equivalently spaced Rayleigh fading paths with exponential power decay profile and a RMS delay spread of $\tau_{rms} = \tau_{L-1}/2$. We also consider the two paths with equal power channel for simulations. In all simulations, the proposed design considers $d_1 = 3$ (recall that $d_2 = 1$ due to the definition of the trellis).

4.6.1 MSE Results

Here, the channel estimate MSE is utilized as the metric to compare the developed channel estimator with other schemes. The MSE is defined as

$$MSE = \sum_{u=1}^{N_R} ||\boldsymbol{h}_{f,u} - \widehat{\boldsymbol{h}}_{f,u}||^2, \tag{4.43}$$

where $\boldsymbol{h}_{f,u}$ is the full TD channel response of the channel corresponding to the u^{th} receive antenna.

Figures 4.4 shows the simulated MSE of the channel estimation process (supported by the proposed trellis-equalizer as shown in Fig. 4.1) with respect to the variation of signal strength. The considered channel has 6 paths with exponential decay power and the maximum channel delay spread is kept at $\tau_{L-1} = 20$, which is more than twice the CP length ($G = 9$). The notation 'PM' indicates the proposed method, 'Trel' indicates the trellis equalizer being used for detection and 'Ite' indicates the number of iterations. Here, our proposed scheme is also compared with a reception process consisting of a LS or a standard MMSE channel estimator connected with the SIMO-OFDM receiver shown in Fig. 2.3. The standard MMSE

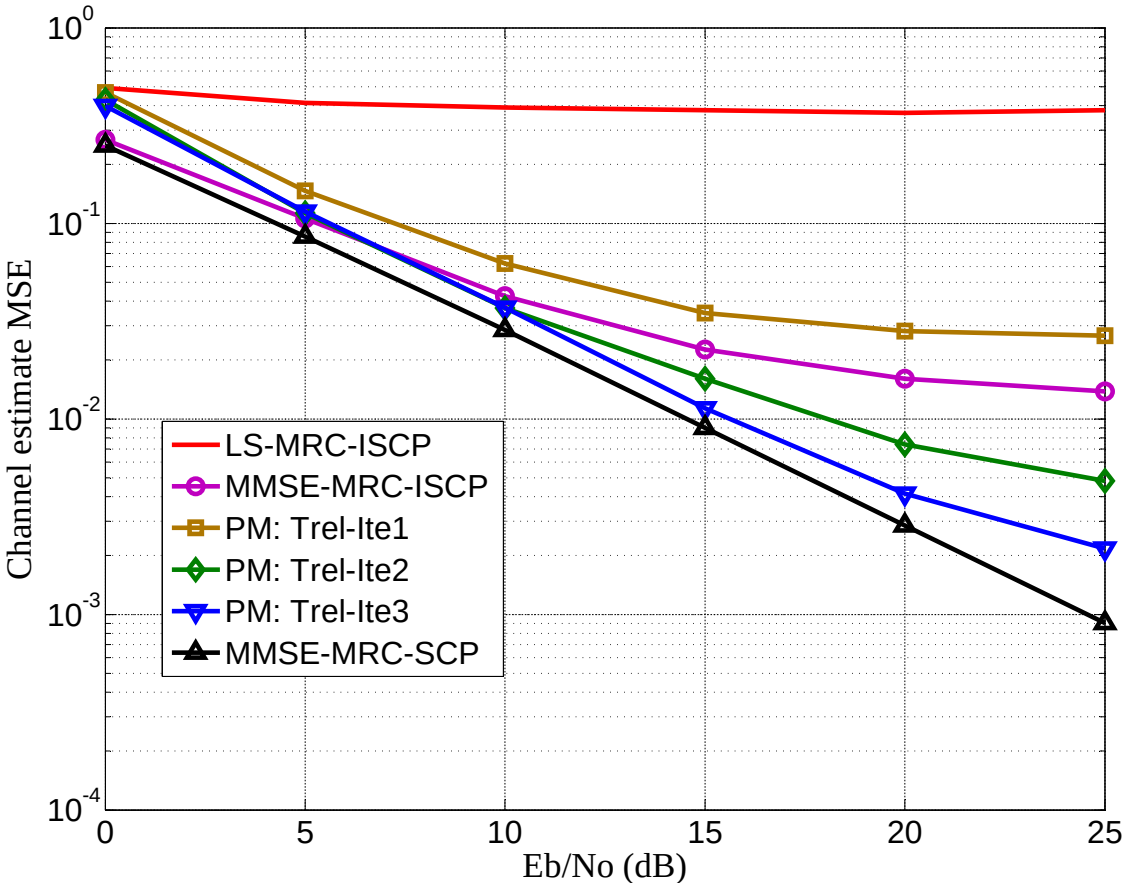

Figure 4.4: Channel estimate MSE with maximum delay of $\tau_{L-1} = 20$, 6 path exponential power decay channel.

estimator only needs to estimate the path coefficients as the channel covariance matrix is assumed available for its operation. The MSE and BER results of the comparison schemes are obtained for both scenarios of insufficient CP ('ISCP') and sufficient CP ('SCP'). In the first case, the CP is kept at $G = 9$ while it is extended to the maximum delay spread for the latter.

It can be seen that at sufficiently high SNRs, the proposed method out performs both LS-MRC and MMSE-MRC with only 2 iterations. With 3 iterations, the corresponding MSE curve approaches that of the MMSE-MRC-SCP curve. This means that the developed algorithm is also able to achieve near interference-free MMSE estimation accuracy for high delay spread channel. Hence, the proposed iterative

PSB-MMSE scheme is an effective channel estimation strategy for insufficient CP SIMO-OFDM systems. It should be noted that with 1 iteration, the proposed PSB-MMSE (PM) performance is worse than that of the standard MMSE method because the path delay estimates can be inaccurate at this initial estimation stage while the standard MMSE technique only calculates the channel path coefficients.

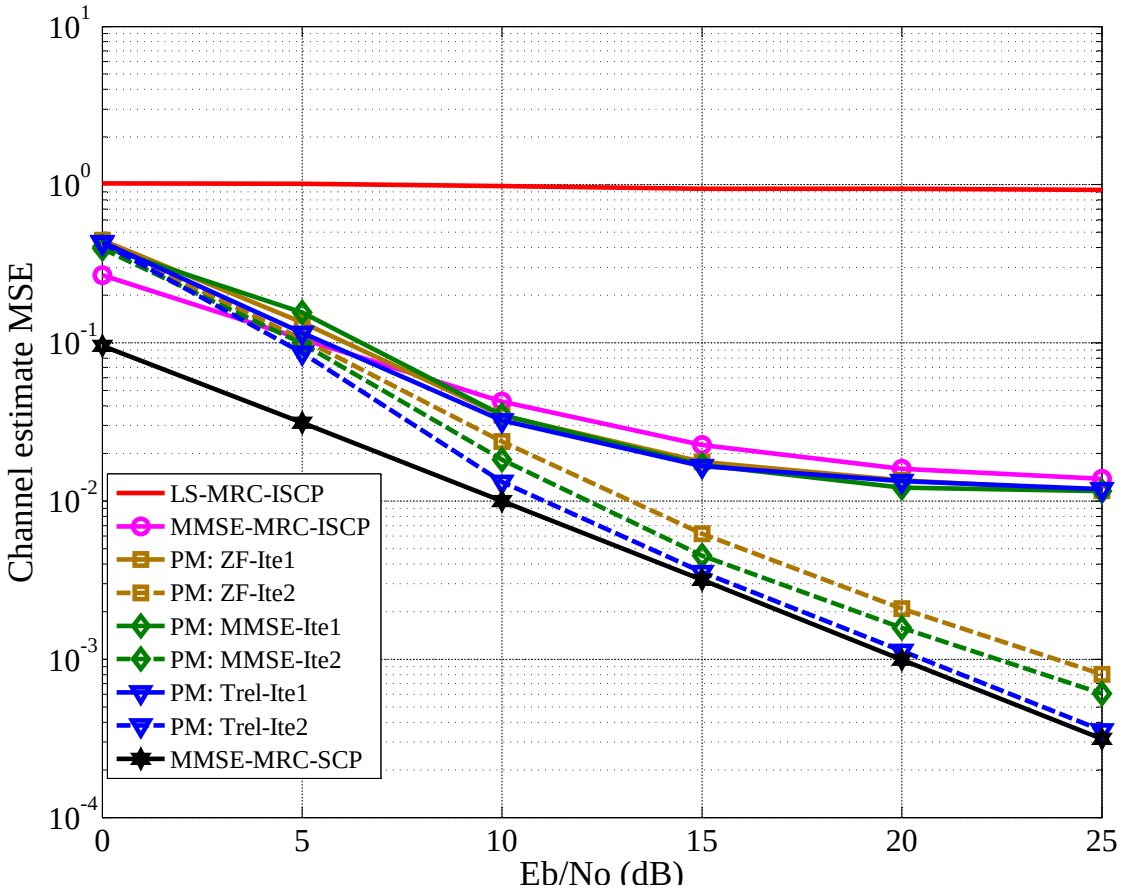

Figure 4.5: Channel estimate MSE with maximum delay of $\tau_{L-1} = 20$, 2 equal power path channel.

Figures 4.5 shows the MSE vs E_b/N_0 performances of the proposed channel estimation scheme when a 2 equal power path channel is considered. The maximum channel delay spread is also kept at $\tau_{L-1} = 20$. Here, apart from comparing with the standard methods, we investigate the effect of different proposed data detectors on the iterative channel estimation process, which is shown in Fig. 4.1 and 4.3.

The notations 'ZF' and 'MMSE' on the curve labels indicate the presence of the ZF and MMSE detectors, respectively. In general, the performance of the PSB-MMSE channel estimator is better for this channel than the 6 path channel. Here, the proposed method (PM) MSE curves after 1 iteration are lower than the MSE curve corresponding to the standard MMSE estimator with insufficient CP. After 2 iterations, the MSE curve for the trellis based method approaches the sufficient CP MSE curve while it is within 3 dB and 4 dB for MMSE and ZF methods, respectively. It requires 3 iterations to achieve such results in the 6 path channel with the trellis based method. This is because the two discrete paths of this channel are well separated and both paths have significant power. These two factors allow the PSB-MMSE estimator to obtain accurate channel PDP matrix and path delay leading to a better full TD channel estimate. It should be noted that this type of channel introduces more ISI and ICI than the 6 path channel since on average, 50% of the transmission power is outside the CP (while 35% of the transmission power is outside the CP for the considered 6 path channel with $\tau_{L-1} = 20$). However, the above advantages are more than enough to compensate for such increase in interference power. We can also see in Fig. 4.5 that the trellis-equalizer allows the PSB-MMSE estimator to achieve the lowest MSE results. For 2 iterations, they almost reach the sufficient CP MSE results. The PSB-MMSE estimator is less accurate with the MMSE detector and it is least accurate with the ZF detector.

Figures 4.6 illustrates the performance of the proposed channel estimator with respect to different channel delay spreads. The results were obtained with a SNR of 20 dB. It can be seen that the increment in channel delay spread has a significant effect on the proposed channel estimation method for both considered channel types. This is not only because of the increasing ISI and ICI power, but is also due to the limited number of pilot sub-carriers. As shown in Section 4.2.1, it is necessary to have a sufficient number of pilot sub-carriers so that $N_p > \tau_{L-1}$ and the PSB-MMSE process can provide good estimates of the number of channel paths and path delays. In the case of $N_p < \tau_{L-1}$, any paths whose τ_l are higher than N_p are neglected by the estimation process, thus leading to a large estimation error. This can be observed in Fig. 4.6 (especially part (b)) as there is a severe performance degradation in the proposed method when the channel delay spread exceeds 20 sample intervals. This is because the number of pilot sub-carriers for the simulated OFDM system is limited to $N_p = 21$. The degradation rate in Fig. 4.6 part (b) is worse than that

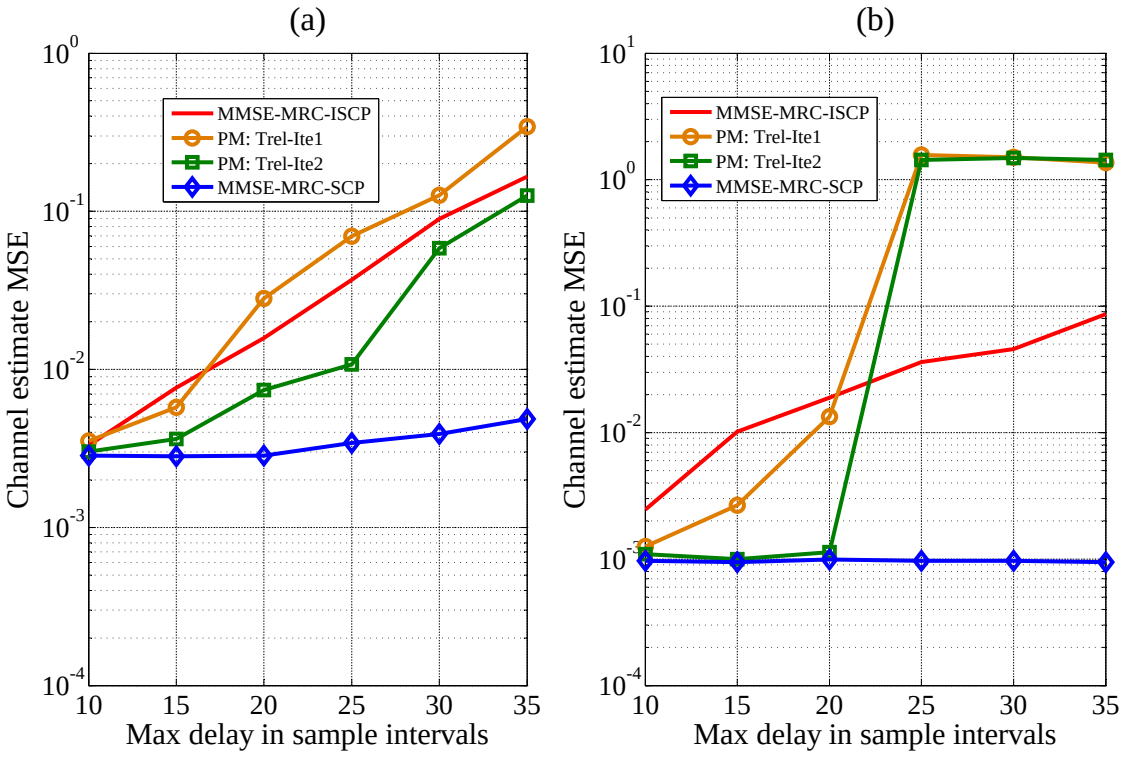

Figure 4.6: Channel estimate MSE with SNR of 20 dB. Figure (a) considers 6 path channel with exponential decay power and figure (b) considers 2 path channel with equal power.

of Fig. 4.6 part (a) because as soon as the channel delay spread exceeds this value, 50% of the channel power (on average) is not included in the channel estimation process. For this particular system, the proposed PSB-MMSE method can provide accurate channel estimation for channel delay spread up to twice the CP length.

4.6.2 BER Results

Figure 4.7 illustrates the BER vs delay spread performances of the proposed receivers for the 2 path channel. Here, to investigate the capabilities of the proposed detection methods, we assume ideal channel knowledge available at receivers. Hence, there is no need for having more than 1 iteration for the ZF and MMSE detectors as the iteration process shown in Fig. 4.3 is to improve the channel estimates. On

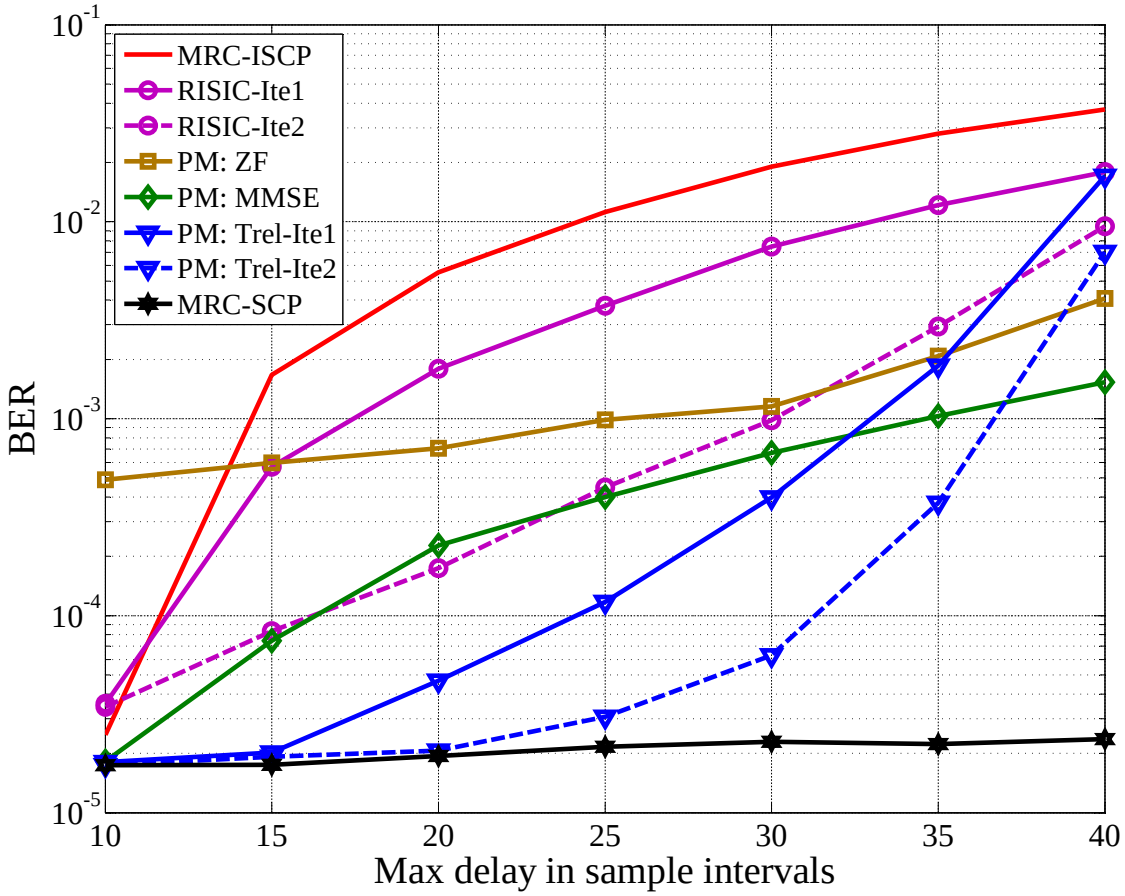

Figure 4.7: BER vs delay spread with SNR of 20 dB and 2 path channel with equal power is considered. Assuming ideal channel knowledge is available at receivers.

the other hand, due to the ICI mitigation process, the trellis equalization can iterate to enhance its performance. It can be observed that all the proposed detection methods (ZF, MMSE and trellis) provide significantly better performance than the standard MRC detector (described in Section 2.2.1). However, the detection accuracy of these methods degrade quickly as the channel delay spread increases due to the increment in interference power.

The ZF performance is worst among the proposed methods and its BER is worse than that of the standard MRC receiver when the channel delay spread is just above the CP ($\tau_{L-1} = 10$). This is due to the noise enhancement effect in its operation.

The MMSE detector has better performance as it includes the noise power in the weight matrix calculation. The trellis equalization provides the best performance. With 2 iterations, it is able to achieve a BER close to that of sufficient CP systems when $\tau_{L-1} = 25$ (about 3 times the CP length). This can mean a 70% reduction in the bandwidth reserved for CP transmission. However, when the channel delay spread increases beyond this point, the trellis equalizer performance degrades quickly. This happens because the trellis operation is not able to capture the major sub-carriers in the direction $(a + 2) \rightarrow (N - 1)$.

In comparison to the RISIC algorithm [2], all three proposed techniques outperform the scheme with 1 iteration. With 2 iterations, RISIC provides better performance than the ZF detector and comes close to the MMSE detector (recalling that the two proposed methods are less complex than RISIC). However, it is still outperformed by the trellis equalizer with the same number of iterations.

Figure 4.8 shows the BER performance of the iterative reception process of the PSB-MMSE channel estimator and the trellis equalizer. It can be seen that with 3 iterations, the proposed method is able to achieve accuracy close to that of the sufficient CP case, while it only required 2 iterations for a maximum delay of 20 sample intervals for the 2 path channel considered in Fig. 4.7. This is due to the channel estimation process requiring 1 extra iteration to reach the estimate accuracy that allows the sub-sequent trellis equalizer to provide such BER values. The performance of the proposed channel estimator with ZF and MMSE detectors are not included here again because their detection processes would require twice the number of available receive antennas for this channel.

The BER performances of all proposed receiver designs for SIMO systems are shown in Fig. 4.9. The simulations were carried out with the 2 equal power path channel. We can see that the proposed designs outperform the standard methods with only 2 iterations, especially the trellis based design. The trellis based design provides the best performance and its corresponding BER curve for 2 iterations follows the sufficient CP BER curve closely. The MMSE based design is second while the ZF based design gives the worst BER performance among the proposed methods. These results are expected as they agree with the previous obtained results in Fig. 4.5.

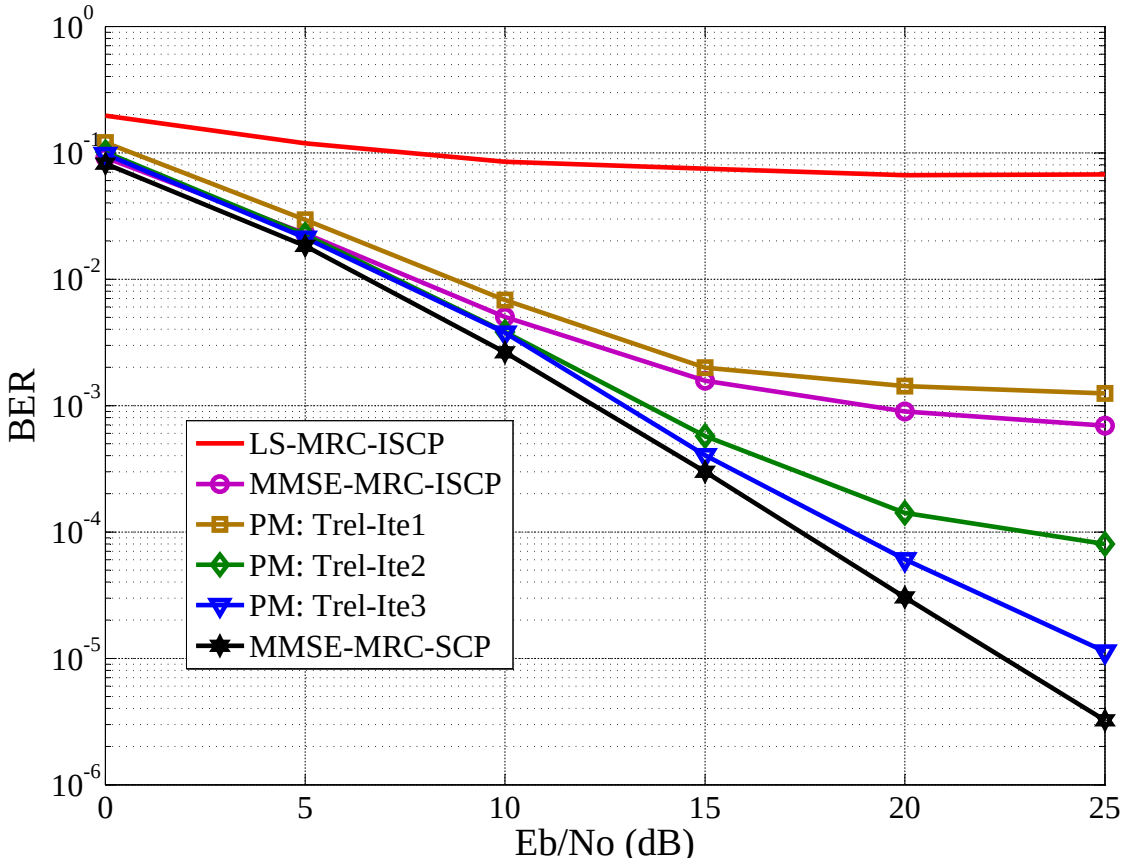

Figure 4.8: BER vs SNR with maximum delay spread of $\tau_{L-1} = 20$, 6 path exponential power decay channel.

The simulation results in Fig. 4.10 display the trellis based design performance with respect to variations in maximum channel delay spread. It can be seen that the proposed method performance degrades considerably with the increment of channel delay spread. This is because of the increased ISI and ICI power affecting both the channel estimation and equalization processes.

Due to the insufficient number of pilot sub-carriers (21 pilots in this simulation), the PSB-MMSE channel estimator is unable to provide accurate channel estimates to the trellis equalizer leading to a big increase in BER when the channel delay spread changes from $\tau_{L-1} = 20$ to $\tau_{L-1} = 25$ for both considered channel types.

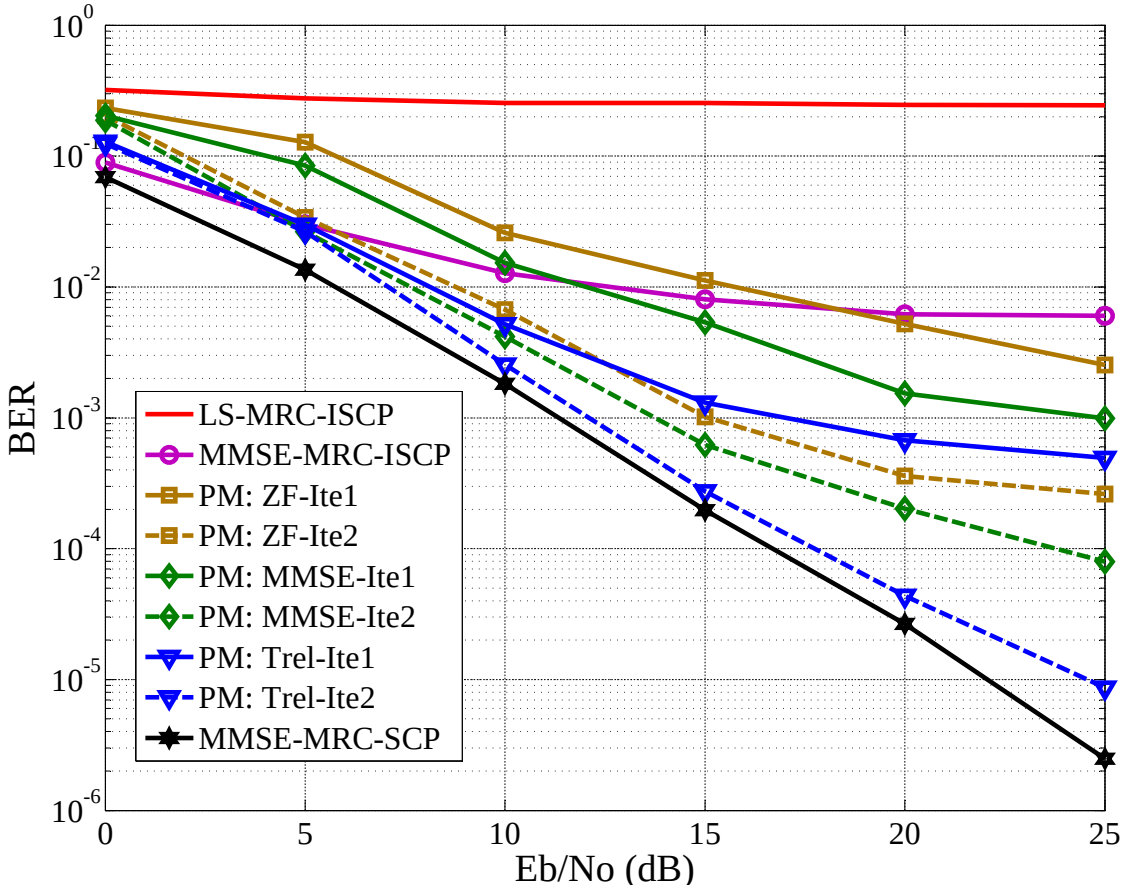

Figure 4.9: BER vs SNR with maximum delay spread of $\tau_{L-1} = 20$, 2 path channel with equal power.

These results agree with the previous MSE results in Fig. 4.6.

4.7 Summary

In this chapter, we have proposed various iterative receiver designs for channel estimation and data detection in insufficient CP SIMO-OFDM transmission. Simulated MSE results have indicated that the proposed PSB-MMSE channel estimator is an effective estimation technique as it is able to provide accurate channel estimate for a channel delay spread up to twice the CP length. However, the method is limited by the number of pilot sub-carriers available to estimate long delay spread channel.

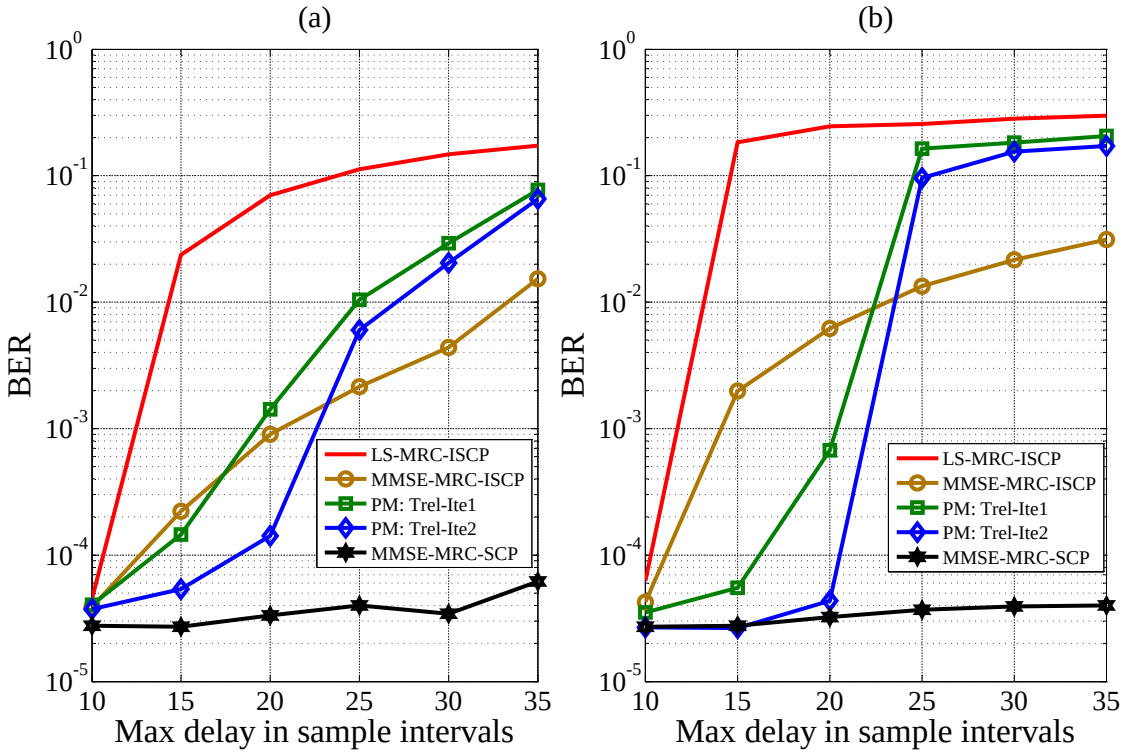

Figure 4.10: BER with SNR of 20 dB. Figure (a) considers 6 path channel with exponential decay power and figure (b) considers 2 path channel with equal power.

On the other hand, the proposed data detectors outperform the standard detection methods, especially the trellis equalizer. It is able to achieve detection accuracy close to that of sufficient CP transmission with only a few iterations. However, the trellis equalizer performance degrades significantly as the channel delay spread exceeds 3 times the CP length due to the exclusion of the major ICI contributed sub-carriers in the forward direction.

In the next chapter, both the channel estimator and the trellis equalizer will be extended to MIMO systems. The channel estimation will be modified so that it can still estimate long channel delay spread with a limited number of pilot sub-carriers. The trellis equalizer will also be redesigned so that it can take into account the major ICI contributed sub-carriers in the forward direction as well as reducing its

complexity for practical MIMO reception.

Chapter 5

Receiver Design for MIMO-OFDM Systems with Insufficient CP

As discussed in Chapter 4, although the proposed channel estimator and trellis equalizer provide good data reception performance for insufficient CP SIMO-OFDM transmissions, performance is still limited in high delay spread channels. The channel estimation process is restricted by the number of available pilot sub-carriers while the trellis equalizer is not able to include enough sub-carriers in its detection process. In this chapter, both of these methods are re-formulated so that they are not only extended to MIMO systems, but their limitations are removed resulting in performance enhancements.

This chapter begins with the description of the iterative system of channel estimation, interference mitigation and trellis based equalization for insufficient CP MIMO-OFDM transmissions. The channel estimation process is then formulated into an optimization process and the derivation of an effective search algorithm to reduce the complexity of the estimator is given. We then describe the design of the improved trellis equalizer for MIMO-OFDM systems with insufficient CP. The CRB is then derived as a reference for investigating the performance of the channel estimation. The complexity analysis of these proposed methods is also included here. The final section illustrates the obtained simulation results as well as discussing the performance of the proposed designs.

5.1 Iterative Receiver Design

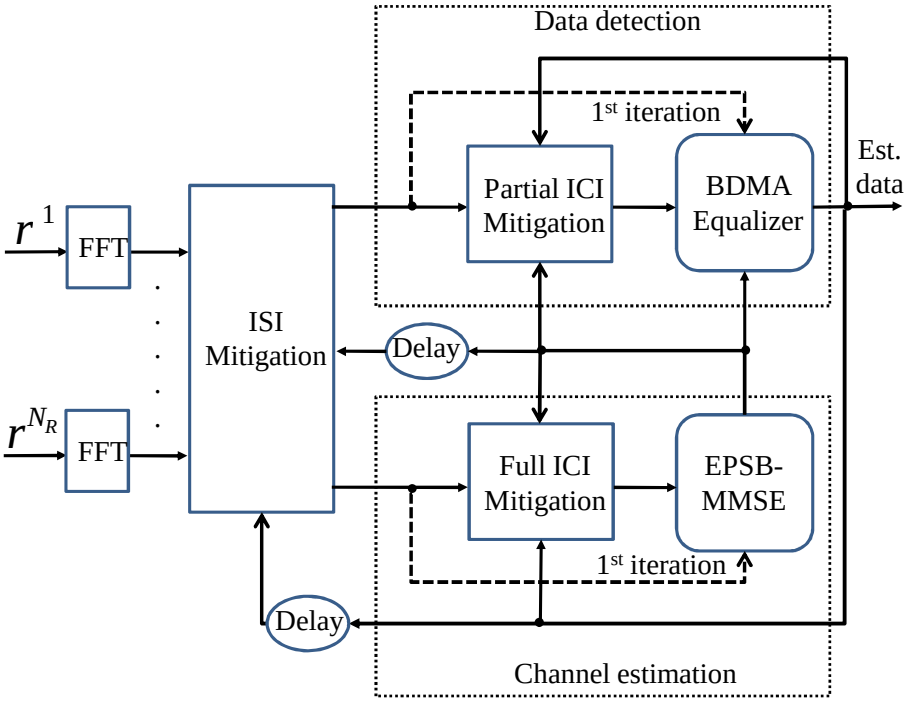

Figure 5.1: Block diagram of the proposed design for insufficient CP MIMO-OFDM systems.

Figure 5.1 shows our proposed receiver design for insufficient CP MIMO-OFDM systems. The general design is similar to the receiver design for insufficient CP SIMO-OFDM systems in Fig. 4.1. However, the previous channel estimation and equalization processing blocks are replaced by their new counterparts for MIMO systems. In a similar manner, detected data from previous OFDM symbols and iterations is used to approximate the ISI and ICI in the current OFDM symbol for interference mitigation. Both full and partial ICI mitigation are considered. In full ICI mitigation, the receiver tries to remove all ICI so that the input signal to the channel estimator can be as good as possible. On the other hand, the process of partial ICI mitigation is to remove the ICI caused by sub-carriers, which are far away from the desired sub-carriers (minor contributors to the overall ICI). The remaining (major) ICI is equalized by the trellis based process for accurate data detection. In the first iteration, the processes of ICI mitigation are not carried out as information

about the current OFDM symbol is not yet available. The processes of interference mitigation are described here, while the developed channel estimator and equalizer will be described in the next two sections.

ISI and full ICI cancellation are performed by feeding back the hard decisions of the equalizer and the corresponding channel estimates to approximate the current ISI and ICI using (3.11) and (3.12) as

$$\begin{aligned}\widehat{R}_{isi,u}(a) &= \sum_{v=1}^{N_T}\sum_{l=D}^{L-1}\widehat{h}_{u,v,l,m-1}\left(\frac{\widehat{X}_{v,m-1}(a)}{N}e^{\frac{-j2\pi a(\tau_l-G)}{N}}(\tau_l-G)\right.\\ &\quad\left.+\sum_{k=0,k\neq a}^{N-1}\frac{\widehat{X}_{v,m-1}(k)}{N}e^{\frac{-j2\pi k(\tau_l-G)}{N}}\frac{1-\rho_{k-a}^{\tau_l-G}}{1-\rho_{k-a}}\right),\end{aligned} \tag{5.1}$$

$$\widehat{R}_{ici,u}(a)=\sum_{v=1}^{N_T}\sum_{l=D}^{L-1}\widehat{h}_{u,v,l,m}\sum_{k=0,k\neq a}^{N-1}\frac{\widehat{X}_{v,m}(k)}{N}e^{\frac{-j2\pi k\tau_l}{N}}\frac{\rho_{k-a}^{\tau_l-G}-1}{1-\rho_{k-a}}. \tag{5.2}$$

The interference mitigation processes are carried out by subtracting the interference estimates from the received signal to give

$$\breve{R}_u(a)=R_u(a)-\widehat{R}_{isi,u}(a), \tag{5.3}$$

$$\dot{Y}_u(a)=\breve{R}_u(a)-\widehat{R}_{ici,u}(a). \tag{5.4}$$

The resulting signal $\dot{Y}_u(a)$ is used for channel estimation. In general, the above procedures of ISI and full ICI cancellation is similar to those in Chapter 4. The only difference is that the ISI and ICI estimation in (5.1) and (5.2) are for MIMO received signal.

The analysis in Table 3.1 illustrates that most of the ICI energy comes from the $2d$ sub-carriers immediately adjacent on either side of the desired sub-carrier, where d is a small positive integer. Here, the minor part of ICI is approximated as

$$\widehat{R}_{ici2,u}(a)=\sum_{v=1}^{N_T}\sum_{l=D}^{L-1}\widehat{h}_{u,v,l,m}\sum_{k=0,k\notin[a-d,a+d]}^{N-1}\frac{\widehat{X}_{v,m}(k)}{N}e^{\frac{-j2\pi k\tau_l}{N}}\frac{\rho_{k-a}^{\tau_l-G}-1}{1-\rho_{k-a}}. \tag{5.5}$$

In partial ICI mitigation, the minor part of ICI is cancelled by subtracting it from the signal $\breve{R}_u(a)$ to give

$$Y_u(a)=\breve{R}_u(a)-\widehat{R}_{ici2,u}(a). \tag{5.6}$$

The remaining part of ICI, $R_{ici1,u}(a)$, will be equalized by the subsequent equalization process. The equalizer extracts transmitted data from the resulting signal $Y_u(a)$. In the first iteration, $\widehat{R}_{ici,u}(a)$ and $\widehat{R}_{ici2,u}(a)$ are assigned zero values. It should be noted that the expression for $\widehat{R}_{ici2,u}(a)$ here excludes all the sub-carriers in $[a-d, a+d]$ while its expression in Chapter 4 excludes the sub-carriers in $[a-d_1, a+d_2]$. This is because the equalization process proposed in this chapter is able to include an equal number of sub-carriers from both sides of the desired sub-carrier. This enhances the detection accuracy.

5.2 Enhanced PSB-MMSE Channel Estimator

In this section, taking some elements of the previously proposed PSB-MMSE channel estimator in Section 4.2, we introduce an *enhanced PSB-MMSE (EPSB-MMSE)* channel estimation strategy for the considered systems. The new channel estimator is able to provide accurate channel estimates with a limited number of pilot sub-carriers when the channel delay spread is much longer than the CP length. To this end, we first formulate the estimation process into a ML form. Let the vector of the pilot sub-carriers of the current OFDM symbol transmitted from antenna v be $\boldsymbol{X}_{p,v} = [X_v(p_0^v), X_v(p_1^v), \ldots, X_v(p_{N_p-1}^v)]$ (dropping the subscript m for simplicity), where p_i^v is a pilot sub-carrier index. Due to the pilot arrangement that a pilot reserves an OFDM tone across all transmit antennas (i.e there is no data sub-carrier or other pilot interference if the CP is sufficient), we have

$$\dot{Y}_u(p_i^v) = H_{u,v}(p_i^v)X_v(p_i^v) + I_u(p_i^v) + n_u(p_i^v), \tag{5.7}$$

where $H_{u,v}(p_i^v)$ is the FD channel sample at pilot p_i^v and $I_u(p_i^v)$ is the residual interference term after full ICI cancellation. The channel FD estimate can be given as

$$\widehat{H}_{u,v}(p_i^v) = \frac{\dot{Y}_u(p_i^v)}{X_v(p_i^v)} = H_{u,v}(p_i^v) + \frac{I_u(p_i^v) + n_u(p_i^v)}{X_v(p_i^v)}. \tag{5.8}$$

According to the interference analysis in Chapter 3, $I_u(p_i^v)$ is approximately Gaussian distributed with zero mean. Hence, the sum of $I_u(p_i^v)$ and $n_u(p_i^v)$, $n_{I,u}(p_i^v)$, is also Gaussian distributed with zero mean.

Recalling that $\widehat{H}_{u,v}(p_i^v)$ is the FD channel estimate at sub-carrier p for the channel between the v^{th} transmit and u^{th} receive antenna. Let $\widehat{\boldsymbol{H}}_{p,u,v}$, $\boldsymbol{H}_{p,u,v}$ and $\boldsymbol{n}_{s,I,u}$

be the $1 \times N_p$ vector of $\widehat{H}_{u,v}(p_i^v)$, $H_{u,v}(p_i^v)$ and the scaled noise-interference term, respectively. From (5.8), we have

$$\widehat{\boldsymbol{H}}_{p,u,v} = \boldsymbol{H}_{p,u,v} + \boldsymbol{n}_{s,I,u}. \tag{5.9}$$

Let $\boldsymbol{H}_{p,u,v}^{hy}$ represent a hypothesized value of $\boldsymbol{H}_{p,u,v}$. Due to $\boldsymbol{n}_{s,I,u}$ having an approximately Gaussian distribution, for a given hypothesis, we have the joint probability density function

$$p(\widehat{\boldsymbol{H}}_{p,u,v})|\boldsymbol{H}_{p,u,v}^{hy}) = \frac{1}{(\pi\sigma_{s,nI}^2)^{N_p}} e^{-\frac{1}{2\sigma_{s,nI}^2}|\widehat{\boldsymbol{H}}_{p,u,v} - \boldsymbol{H}_{p,u,v}^{hy}|^2}, \tag{5.10}$$

where $\sigma_{s,nI}$ is the standard deviation of $\boldsymbol{n}_{s,I,u}$. The log-likelihood function for a hypothesis can then be defined as

$$\mathscr{L}_{u,v}(\boldsymbol{H}_{p,u,v}^{hy}) = |\widehat{\boldsymbol{H}}_{p,u,v} - \boldsymbol{H}_{p,u,v}^{hy}|^2. \tag{5.11}$$

On the other hand, the vector $\boldsymbol{H}_{p,u,v}$ can be expressed as

$$\boldsymbol{H}_{p,u,v} = \boldsymbol{\mathcal{F}}_{p,v}\boldsymbol{h}_{u,v}, \tag{5.12}$$

where $\boldsymbol{\mathcal{F}}_{p,v}$ is the $N_p \times L$ transformation matrix given by

$$\boldsymbol{\mathcal{F}}_{p,v} = \begin{bmatrix} e^{\frac{-j2\pi p_0^v \tau_0}{N}} & e^{\frac{-j2\pi p_0^v \tau_1}{N}} & \dots & e^{\frac{-j2\pi p_0^v \tau_{L-1}}{N}} \\ e^{\frac{-j2\pi p_1^v \tau_0}{N}} & e^{\frac{-j2\pi p_1^v \tau_1}{N}} & \dots & e^{\frac{-j2\pi p_1^v \tau_{L-1}}{N}} \\ \vdots & \vdots & \ddots & \vdots \\ e^{\frac{-j2\pi p_{N_p-1}^v \tau_0}{N}} & e^{\frac{-j2\pi p_{N_p-1}^v \tau_1}{N}} & \dots & e^{\frac{-j2\pi p_{N_p-1}^v \tau_{L-1}}{N}} \end{bmatrix} \tag{5.13}$$

and $\boldsymbol{h}_{u,v}$ is the $L \times 1$ vector containing the TD path coefficients such that

$$\boldsymbol{h}_{u,v} = [h_{u,v,0}, h_{u,v,1}, \dots, h_{u,v,L-1}]^T. \tag{5.14}$$

So, the likelihood function in (5.11) is equivalent to

$$\mathscr{L}_{u,v}(\boldsymbol{\mathcal{F}}_{p,v}^{hy}, \boldsymbol{h}_{u,v}^{hy}) = |\widehat{\boldsymbol{H}}_{p,u,v} - \boldsymbol{\mathcal{F}}_{p,v}^{hy}\boldsymbol{h}_{u,v}^{hy}|^2. \tag{5.15}$$

Since $\boldsymbol{\mathcal{F}}_{p,v}$ is a function of $[L, \tau_0, \dots, \tau_{L-1}]$, the hypothesis $\boldsymbol{\mathcal{F}}_{p,v}^{hy}$ is also dependent on $[L, \tau_0, \dots, \tau_{L-1}]$. In addition, it will be shown in the following that the approximation of $\boldsymbol{h}_{u,v}$ is also a function of $[L, \tau_0, \dots, \tau_{L-1}]$. Hence, the likelihood function in (5.15) can be written as

$$\mathscr{L}_{u,v}(L, \tau_0, \dots, \tau_{L-1}) = |\widehat{\boldsymbol{H}}_{p,u,v} - \boldsymbol{\mathcal{F}}_{p,v}^{hy}(L, \tau_0, \dots, \tau_{L-1})\widehat{\boldsymbol{h}}_{u,v}^{hy}(L, \tau_0, \dots, \tau_{L-1})|^2. \tag{5.16}$$

This likelihood function is for a single sub-channel between the v^{th} transmit and u^{th} receive antennas in the MIMO system. As all the sub-channels share the same delay profile and fading statistic, we can define the overall likelihood function as the mean of individual likelihood functions of each sub-channel to reduce the effect of noise and interference, resulting in

$$\mathscr{L}(L, \tau_0, \ldots, \tau_{L-1}) = \frac{1}{N_T \times N_R} \sum_{u=1}^{N_R} \sum_{v=1}^{N_T} \mathscr{L}_{u,v}(L, \tau_0, \ldots, \tau_{L-1}). \tag{5.17}$$

From (5.17), the channel estimation process is equivalent to the following optimization process,

$$\begin{aligned} \min_{L,\tau_0,\ldots,\tau_{L-1}} \quad & \mathscr{L}(L, \tau_0, \ldots, \tau_{L-1}) \\ \text{subject to} \quad & L \in \mathscr{Z}^+, \tau_0 = 0, \\ & \tau_0 < \tau_1 < \cdots < \tau_{L-1} \leq \tau_{_{PD}} \in \mathscr{Z}^+, \end{aligned} \tag{5.18}$$

where $\tau_{_{PD}}$ is the pre-defined maximum channel delay for our receiver and $\mathscr{Z}^+$ is the positive integer set.

The optimization problem in (5.18) is difficult to solve because the unknown variable L affects the number of τ_l variables. On the other hand, for high delay spread channels, the number of possible values for the variable vector $[L, \tau_0, \ldots, \tau_{L-1}]$ can become too high for a brute force ML method. Here, in order to solve (5.18), we propose a multi-step procedure: First, the channel PDP matrix, $\boldsymbol{C}$, and the number of channel paths, L, are estimated. The result is then used to estimate individual path delays and acquire the initial path coefficient values. The estimates are finally refined with detected data sub-carriers. Figure 5.2 illustrates the channel estimation procedure.

5.2.1 Estimate of Channel PDP Matrix and Number of Channel Paths

In a similar manner to the previously proposed PSB-MMSE estimator in Section 4.2, the channel PDP matrix is estimated by considering the power of the estimated TD channel. The TD channel estimate is computed using pilot sub-carriers only (to avoid interpolation error), and is given by

$$\widetilde{h}_{u,v,z} = \frac{1}{N_p} \sum_{i=0}^{N_p-1} \widehat{H}_{u,v}(p_{i+1}^v) e^{j2\pi iz/N_p}, z = 0, 1, \ldots, N_p - 1. \tag{5.19}$$

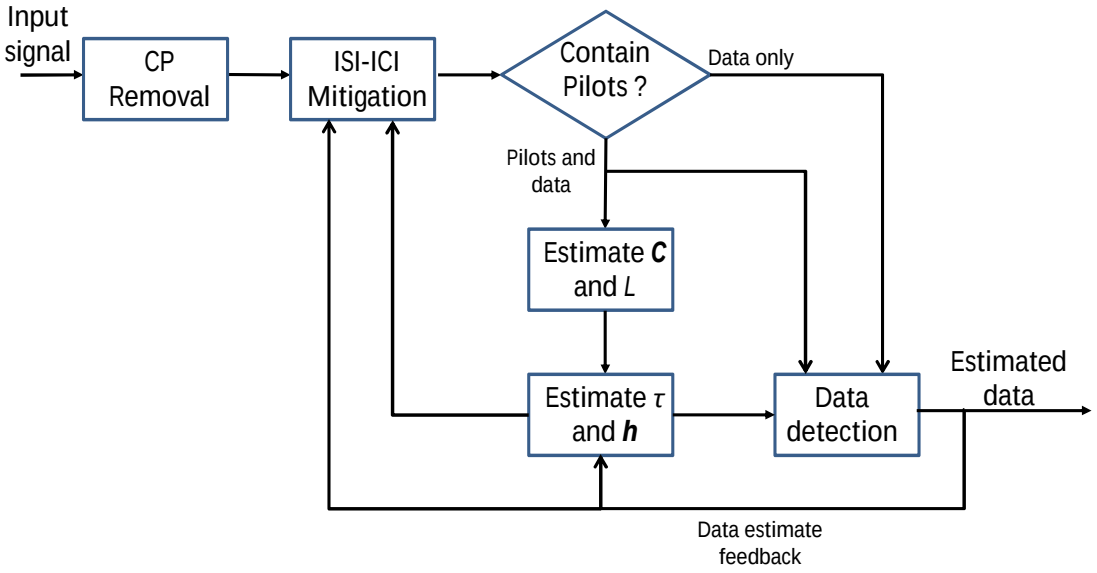

Figure 5.2: Block diagram of the EPSB-MMSE channel estimation process for insufficient CP MIMO-OFDM systems.

Let the vector $\tilde{\boldsymbol{h}}_{u,v} = [\tilde{h}_{u,m,0}, \ldots, \tilde{h}_{u,m,N_p-1}]^T$. Assuming that the channel covariance matrix $\boldsymbol{C}$ is the same for all sub-channels, it can be estimated as

$$\tilde{\boldsymbol{C}} = \frac{1}{N_T \times N_R} \sum_{u=1}^{N_R} \sum_{v=1}^{N_T} \tilde{\boldsymbol{h}}_{u,v} \tilde{\boldsymbol{h}}_{u,v}^{\dagger}. \tag{5.20}$$

By considering the magnitude of the diagonal of $\tilde{\boldsymbol{C}}$, we can apply the most significant taps algorithm of [107,108] to identify and reserve the most significant elements, which can provide an estimate of the number of channel paths L. An example of the magnitude of matrix $\tilde{\boldsymbol{C}}$ diagonal for an instant of the MIMO channel is illustrated in Fig. 5.3.

We propose a simple method to identify the number of channel paths by considering the number of peaks within the diagonal of $\tilde{\boldsymbol{C}}$. This is based on the fact that the power vectors of the TD channels would have L magnitude peaks assuming that the channel paths are at least 2 sample intervals apart. This is often the case when the channel has few paths and the delay spread is high. However, since N_p can be smaller than τ_{L-1}, some of the peaks can be next to each other making it difficult to distinguish them. To partially compensate for this effect, we consider

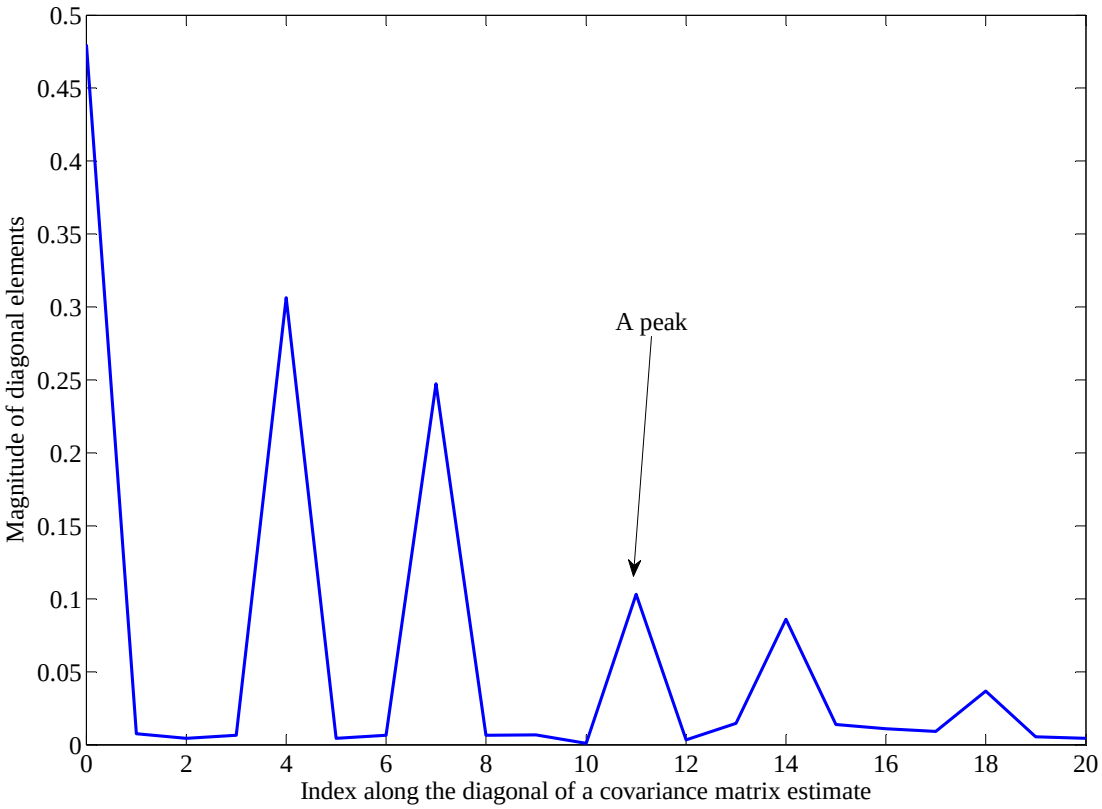

Figure 5.3: Magnitude of the diagonal of $\tilde{\boldsymbol{C}}$ for a channel instant. Channel has 6 exponentially decay paths that are equally spaced, $\tau_5 = 18$, $G = 9$ and $N_p = 21$.

the neighbouring elements of each significant peak within the diagonal of $\tilde{\boldsymbol{C}}$. Our proposed method for estimating the number of paths is summarized as follows:

- Identify the peaks in the diagonal of $\tilde{\boldsymbol{C}}$.
- Discard a peak if its magnitude is less than 5% of the magnitude of the first peak, which corresponds to the first arrival path. This is to eliminate false peaks caused by noise or interference. It is observed from simulation that 5% provided good performance.
- The number of remaining peaks provides a value for $\widehat{L}$.
- For each peak at $\tilde{\boldsymbol{C}}(z, z)$, investigate if the magnitudes of $\tilde{\boldsymbol{C}}(z-1, z-1)$ or

$\tilde{\boldsymbol{C}}(z+1, z+1)$ are more than 5% of the magnitude of the first peak. If yes, $\widehat{L} = \widehat{L} + 1$.

All the other elements, which are not associated with the chosen peaks, are discarded and the $N_p \times N_p$ matrix $\tilde{\boldsymbol{C}}$ shrinks to a $\widehat{L} \times \widehat{L}$ diagonal matrix $\widehat{\boldsymbol{C}}$. In the first iteration, the estimates are still affected by ICI; however, these are improved in later iterations as the ICI is mitigated.

5.2.2 Channel Path Coefficients Estimation

We will now describe the process of estimating the path coefficients for a given delay profile $[\tau_0, \tau_1, \ldots, \tau_{L-1}]$ and an estimated number of channel paths $\widehat{L}$. For the first iteration, the estimation process can only rely on the available pilot sub-carriers like the PSB-MMSE method. However, on the sub-sequent iterations, hard decisions on the transmitted data are available to enhance the estimation. The main advantage of this method, in comparison to other available channel estimation methods in literature, is that it utilizes a limited number of sub-carriers and estimated data sub-carriers for insufficient CP MIMO-OFDM channel estimation while other channel estimation methods require pilot OFDM symbols.

5.2.2.1 First Iteration

From (5.3) and (5.4), in the first iteration, we have

$$\begin{aligned}\dot{Y}_u(a) &= \sum_{v=1}^{N_T} X_{v,m}(a) \sum_{l=0}^{L-1} f(l) h_{u,v,l,m} e^{\frac{-j2\pi a \tau_l}{N}} \\ &\quad + \sum_{v=1}^{N_T} \sum_{l=D}^{L-1} h_{u,v,l} \sum_{k=0, k\neq a}^{N-1} \frac{X_v(k)}{N} e^{-j2\pi k \tau_l / N} \frac{\rho_k^{\tau_l - G} - 1}{1 - \rho_k} + n_u(a). \quad (5.21)\end{aligned}$$

Recalling that a pilot reserves an OFDM tone across all transmit antennas, so

$$\begin{aligned}\dot{Y}_u(p_i^v) &= X_v(p_i^v) \sum_{l=0}^{L-1} f(l) h_{u,v,l} e^{-j2\pi p_i^v \tau_l / N} \\ &\quad + \sum_{v=1}^{N_T} \sum_{l=D}^{L-1} h_{u,v,l} \sum_{k=0, k\neq p_i^v}^{N-1} \frac{X_v(k)}{N} e^{-j2\pi k \tau_l / N} \frac{\rho_k^{\tau_l - G} - 1}{1 - \rho_k} + n_u(p_i^v) \\ &= X_v(p_i^v) \sum_{l=0}^{L-1} f(l) h_{u,v,l} e^{-j2\pi p_i^v \tau_l / N} + n_{I,u}(p_i^v). \quad (5.22)\end{aligned}$$

Let us define

$$\dot{\boldsymbol{Y}}_{p,u,v} = \left[\dot{Y}_u(p_1^v), \dot{Y}_u(p_2^v), \ldots, \dot{Y}_u(p_{N_p}^v)\right]^T, \tag{5.23}$$

$$\boldsymbol{\Gamma}_{p,v} = \text{diag}\left(\left[X_v(p_1^v), X_v(p_2^v), \ldots, X_v(p_{N_p}^v)\right]\right), \tag{5.24}$$

$$\boldsymbol{h}_{u,v} = [h_{u,v,0}, h_{u,v,1} \ldots, h_{u,v,L-1}]^T, \tag{5.25}$$

and

$$\boldsymbol{n}_{I,u} = \left[n_{I,u}(p_1^v), n_{I,u}(p_2^v), \ldots, n_{I,u}(p_{N_p}^v)\right]^T. \tag{5.26}$$

From (5.22), the received sample vector at pilot sub-carriers can be expressed as

$$\dot{\boldsymbol{Y}}_{p,u,v} = \boldsymbol{\Gamma}_{p,v}\boldsymbol{\mathcal{F}}_{p,v}\tilde{\boldsymbol{F}}\boldsymbol{h}_{u,v} + \boldsymbol{n}_{I,u} = \boldsymbol{S}_{p,v}\boldsymbol{h}_{u,v} + \boldsymbol{n}_{I,u}, \tag{5.27}$$

where $\boldsymbol{S}_{p,v} = \boldsymbol{\Gamma}_{p,v}\boldsymbol{\mathcal{F}}_{p,v}\tilde{\boldsymbol{F}}$. From (5.27), a MMSE estimator can be formulated for estimating the channel coefficients. Let $\boldsymbol{W}_{p,u,v}$ be the weight matrix, the goal here is to find $\boldsymbol{W}_{p,u,v}$ so that

$$E\left\{\left|\boldsymbol{W}_{p,u,v}^{\dagger}\dot{\boldsymbol{Y}}_{p,u,v} - \boldsymbol{h}_{u,v}\right|^2\right\} \tag{5.28}$$

is minimized.

The MMSE criteria is satisfied by the Wiener-Hopf solution,

$$\boldsymbol{W}_{p,u,v}^{\dagger} = \boldsymbol{C}_{u,v}\boldsymbol{S}_{p,v}^{\dagger}(\boldsymbol{S}_{p,v}\boldsymbol{C}_{u,v}\boldsymbol{S}_{p,v}^{\dagger} + \eta_{In}\boldsymbol{I})^{-1}, \tag{5.29}$$

where $\eta_{In} = E\{|R_{ici,u}(a)|^2\} + \eta_0$ is the variance of the combined interference-noise factor, $\boldsymbol{I}$ is the identity matrix, and $\boldsymbol{C}_{u,v} = E\{\boldsymbol{h}_{u,v}\boldsymbol{h}_{u,v}^{\dagger}\}$ is the channel PDP matrix for the sub-channel between the v^{th} transmit and u^{th} receive antenna. Note that: $\boldsymbol{C}_{u,v} \equiv \boldsymbol{C}$ as we have assumed that the channel PDP matrix is the same for all sub-channels. Since $\boldsymbol{C}$ is not available, it is replaced by $\widehat{\boldsymbol{C}}$ in the calculation of $\boldsymbol{W}_{p,u,v}^{\dagger}$, so

$$\boldsymbol{W}_{p,u,v}^{\dagger} = \widehat{\boldsymbol{C}}\boldsymbol{S}_{p,v}^{\dagger}(\boldsymbol{S}_{p,v}\widehat{\boldsymbol{C}}\boldsymbol{S}_{p,v}^{\dagger} + \eta_{In}\boldsymbol{I})^{-1}. \tag{5.30}$$

The channel path coefficient vector denoted $\widehat{\boldsymbol{h}}_{u,v}$ is computed by

$$\widehat{\boldsymbol{h}}_{u,v} = \boldsymbol{W}_{p,u,v}^{\dagger}\dot{\boldsymbol{Y}}_{p,u,v}. \tag{5.31}$$

The result is utilized for computing $\mathscr{L}_{u,v}(\widehat{L}, \tau_0, \ldots, \tau_{L-1})$ and $\mathscr{L}(\widehat{L}, \tau_0, \ldots, \tau_{L-1})$ subsequently for the optimization process in (5.18).

5.2.2.2 Later Iterations

To improve the estimation accuracy, the design utilizes both hard data decisions from the previous iteration and pilots to estimate the channel path coefficients. Due to the ICI cancellation process taking place before the channel estimation in these iterations, we have

$$\dot{Y}_u(a) = \sum_{v=1}^{N_T} X_v(a) \sum_{l=0}^{L-1} f(l) h_{u,v,l} e^{-j2\pi a\tau_l/N} + n(a), \tag{5.32}$$

where the residual interference is included in the noise term $n(a)$. From (5.32), it can be seen that it is difficult to separate $X_v(a)$ from other $X_{v'}(a)$ $(v \neq v')$. Hence, the channel path coefficients $h_{u,v,l}$ $\forall v, l$ have to be estimated together.

Here, we define the received sample vector, the scaling vector, the TD channel coefficient vector and the transmitted data vector as

$$\dot{\boldsymbol{Y}}_u = \left[\dot{Y}_u(0), \dot{Y}_u(1), \ldots, \dot{Y}_u(N-1)\right]^T, \tag{5.33}$$

$$\boldsymbol{F} = \mathrm{diag}\left(\left[\mathrm{diag}(\tilde{\boldsymbol{F}}), \mathrm{diag}(\tilde{\boldsymbol{F}}), \ldots, \mathrm{diag}(\tilde{\boldsymbol{F}})\right]\right), \tag{5.34}$$

$$\boldsymbol{h}_u = \left[\boldsymbol{h}_{u,1}^T, \boldsymbol{h}_{u,2}^T, \ldots, \boldsymbol{h}_{u,N_T}^T\right]^T, \tag{5.35}$$

$$\boldsymbol{X}_v = \left[X_v(0), X_v(1), \ldots, X_v(N-1)\right]. \tag{5.36}$$

From (5.32), $\dot{\boldsymbol{Y}}_u$ and $\boldsymbol{h}_u$ are related by

$$\dot{\boldsymbol{Y}}_u = \boldsymbol{S}\boldsymbol{h}_u, \tag{5.37}$$

where

$$\boldsymbol{S} = [\boldsymbol{\Gamma}_1\boldsymbol{\mathcal{F}}, \boldsymbol{\Gamma}_2\boldsymbol{\mathcal{F}}, \ldots, \boldsymbol{\Gamma}_{N_T}\boldsymbol{\mathcal{F}}] \times \boldsymbol{F}, \tag{5.38}$$

$$\boldsymbol{\Gamma}_v = \mathrm{diag}\left(\boldsymbol{X}_v\right), \tag{5.39}$$

$$\boldsymbol{\mathcal{F}} = \begin{bmatrix} 1 & 1 & \ldots & 1 \\ e^{\frac{-j2\pi\tau_0}{N}} & e^{\frac{-j2\pi\tau_1}{N}} & \ldots & e^{\frac{-j2\pi\tau_{L-1}}{N}} \\ \vdots & \vdots & \ddots & \vdots \\ e^{\frac{-j2\pi(N-1)\tau_0}{N}} & e^{\frac{-j2\pi(N-1)\tau_1}{N}} & \ldots & e^{\frac{-j2\pi(N-1)\tau_{L-1}}{N}} \end{bmatrix}. \tag{5.40}$$

In a similar manner to the first iteration, the MMSE weight matrix is calculated by

$$\boldsymbol{W}^\dagger = \boldsymbol{G}\boldsymbol{S}^\dagger(\boldsymbol{S}\boldsymbol{G}\boldsymbol{S}^\dagger + \eta_0\boldsymbol{I})^{-1}, \tag{5.41}$$

where $\boldsymbol{G}$ is a $\widehat{L}N_T \times \widehat{L}N_T$ diagonal matrix and is defined as

$$\boldsymbol{G} = \text{diag}\left(\left[\text{diag}(\widehat{\boldsymbol{C}}), \text{diag}(\widehat{\boldsymbol{C}}), \ldots, \text{diag}(\widehat{\boldsymbol{C}})\right]\right). \tag{5.42}$$

Since the transmitted data $X_v(a)$ is unknown at the receiver, but its estimates $\widehat{X}_v(a)$ (i.e hard decisions from the previous iteration) are known, the matrix $\boldsymbol{X}_v$ is constructed by a mixture of $\widehat{X}_v(a)$ and pilot sub-carriers. It should also be noted that η_0 is used in the expression (5.41) instead of η_{In} because of the prior ICI cancellation. This is due to the ICI mitigation process meaning that the ICI contamination can be significantly reduced. On the other hand, it is difficult to estimate the residual ICI energy. The estimation of $\boldsymbol{h}_u$ is obtained by

$$\widehat{\boldsymbol{h}}_u = \boldsymbol{W}^{\dagger}\dot{\boldsymbol{Y}}_u. \tag{5.43}$$

The resulting estimates can be used to perform the optimization in (5.18) for the current iteration.

5.2.3 Path Delay Profile Estimation

This subsection will investigate the path delay profile estimation process for insufficient CP MIMO-OFDM. Given the result of $\widehat{L}$ obtained in Section 5.2.1, the optimization problem in (5.18) becomes

$$\begin{aligned} \min_{\tau_0,\ldots,\tau_{\widehat{L}-1}} \quad & \mathscr{L}(\widehat{L}, \tau_0, \ldots, \tau_{\widehat{L}-1}) \\ \text{subject to} \quad & \tau_0 = 0 \text{ and } \tau_0 < \tau_1 < \cdots < \tau_{\widehat{L}-1} \leq \tau_{PD} \in \mathscr{Z}^+. \end{aligned} \tag{5.44}$$

Since it is impractical to consider all possible values for $[\tau_0, \tau_1, \ldots, \tau_{\widehat{L}-1}]$, we developed a sub-optimal search method with low complexity to identify the most likely delay values. The procedure consists of the initialization step, which is to establish a rough estimate of the path delays, and the refinement step that increases the accuracy of these estimates. The path delay profile estimation process is summarized below.

5.2.3.1 Initialization step

- Assign the maximum possible values for all path delays except the first two paths, i.e. $\tau_{\widehat{L}-1} = \tau_{PD}, \ldots, \tau_2 = \tau_{PD} - \widehat{L} + 2$. Then, compute $\mathscr{L}(\widehat{L}, \tau_0, \ldots, \tau_{\widehat{L}-1})$ for all possible values of τ_1 given that $\tau_1 \in [1, 2, \ldots, \tau_{PD} - \widehat{L} + 2]$. The value

of τ_1 that provides the lowest MSE, denoted as $\widehat{\tau}_1^i$, is selected as the initial estimate of τ_1.

- Keep the assigned values of $\tau_3, \ldots, \tau_{\widehat{L}-1}$. Compute $\mathscr{L}(\widehat{L}, \tau_0, \widehat{\tau}_1^i, \ldots, \tau_{\widehat{L}-1})$ for all possible values of τ_2 given that $\tau_2 \in [\widehat{\tau}_1^i + 1, \ldots, \tau_{PD} - \widehat{L} + 2]$. The value of τ_2 that provides the lowest MSE, denoted as $\widehat{\tau}_2^i$, is selected as the initial estimate of τ_2.

- The above step is repeated until all initial estimates of the channel paths are acquired, $[\widehat{\tau}_1^i, \ldots, \widehat{\tau}_{\widehat{L}-1}^i]$.

5.2.3.2 Refinement step

Let $[\widehat{\tau}_1(b), \ldots, \widehat{\tau}_{\widehat{L}-1}(b)]$ be the refined estimates of the channel path delays, where b indicates the iteration index.

- Given $[\widehat{\tau}_3^i, \ldots, \widehat{\tau}_{\widehat{L}-1}^i]$, $\mathscr{L}(\widehat{L}, \tau_0, \tau_1, \tau_2, \widehat{\tau}_3^i, \ldots, \tau_{\widehat{L}-1}^i)$ is computed for all possible combinations of τ_1 and τ_2, where $\tau_1 \in [1, \ldots, \widehat{\tau}_3^i - 2]$ and $\tau_2 \in [\tau_1 + 1, \ldots, \widehat{\tau}_3^i - 1]$. The values of τ_1 and τ_2 that provide the lowest MSE are selected as $\widehat{\tau}_1(0)$ and $\widehat{\tau}_2(0)$, respectively.

- Given $[\widehat{\tau}_1(0), \widehat{\tau}_4^i, \ldots, \widehat{\tau}_{\widehat{L}-1}^i]$, compute $\mathscr{L}(\widehat{L}, \tau_0, \widehat{\tau}_1(0), \tau_2, \tau_3, \widehat{\tau}_4^i, \ldots, \tau_{\widehat{L}-1}^i)$ for all possible combinations of τ_2 and τ_3, where $\tau_2 \in [\widehat{\tau}_1(0) + 1, \ldots, \widehat{\tau}_4^i - 2]$ and $\tau_3 \in [\tau_2 + 1, \ldots, \widehat{\tau}_4^i - 1]$. Let the lowest MSE obtained in the current step be A_c and the lowest MSE obtained in the previous step be A_p. If $A_c > A_p$, $\widehat{\tau}_2(1)$ and $\widehat{\tau}_3(0)$ are updated by the values corresponding to A_c. If $A_c < A_p$, only $\widehat{\tau}_3(0)$ is updated and $\widehat{\tau}_2(1) = \widehat{\tau}_2(0)$.

- The process continues until we obtain $[\widehat{\tau}_1(1), \ldots, \widehat{\tau}_{\widehat{L}-1}(1)]$, which serves as the output of the path delay estimation.

It was found that for most cases, $b = 1$ is sufficient for the estimation process with insignificant gain from further iterations. As the computation of the MSE also involves estimation of the path coefficients given a certain delay profile, the coefficient estimates corresponding to $[\widehat{\tau}_1(1), \ldots, \widehat{\tau}_{\widehat{L}-1}(1)]$ are selected. Hence, at the end of this process, the TD channel estimation is available for subsequent interference mitigation and data detection.

5.3 BDMA Trellis Equalizer

Given the iterative nature of our design in which the channel estimation would affect the equalization and vice versa, it is important to find a high performance equalization method to help the system converge. In the context of insufficient CP OFDM, trellis based equalizers can be a good choice as they have been shown to achieve good performance in Chapter 4. However, the proposed method cannot be applied to MIMO systems as the trellis size can become too high for practical purposes. For example, a small 2×2 MIMO-OFDM system with 4QAM as sub-carrier modulation would already lead to a trellis with $4^{2+2} = 256$ states. On the other hand, its performance degrades considerably with the increase in the excess delay spread (to the CP length). In this section, we present a trellis-based design with practical complexity for MIMO systems, which can tolerate very high channel delay spread conditions. In the following, we first introduce the construction of the trellis for MIMO systems. Based on the available trellis, a *bi-directional M-algorithm (BDMA)* is then designed for accurate equalization and data detection.

5.3.1 Trellis for Equalization

Since the equalization process is done in the frequency domain, the trellis state must be defined to represent a single sub-carrier symbol or a group of sub-carrier symbols. In most cases, the complexity of a trellis based operation depends entirely on the trellis size, which in turn depends on the trellis state definition. Since the transmit sub-carrier symbol from one antenna is independent to that of other antennas, the smallest possible state definition in this case must represent $[X_1(a)X_2(a)\ldots X_{N_T}(a)]$. So, the number of different trellis states is A^{N_T}. It should be noted that if the trellis structure in Chapter 4 is extended to MIMO, each state of the trellis needs to include not only a sub-carrier symbol, but also an adjacent sub-carrier symbol per antenna. Hence, the number of trellis states would be A^{2N_T}, which is much higher.

Figure 5.4 illustrates an example of our trellis given a 2×2 MIMO system with $4QAM$ as the sub-carrier modulation. The trellis states are labeled by the index of the symbols from transmit antennas 1 and 2 at sub-carrier a, $[X_1(a), X_2(a)]$. The dashed lines indicate different past transitions along a survivor path and the solid lines indicate the current state transitions. The pair of symbols along a line

represents two symbols transmitted in the same sub-carrier via the two transmit antennas.

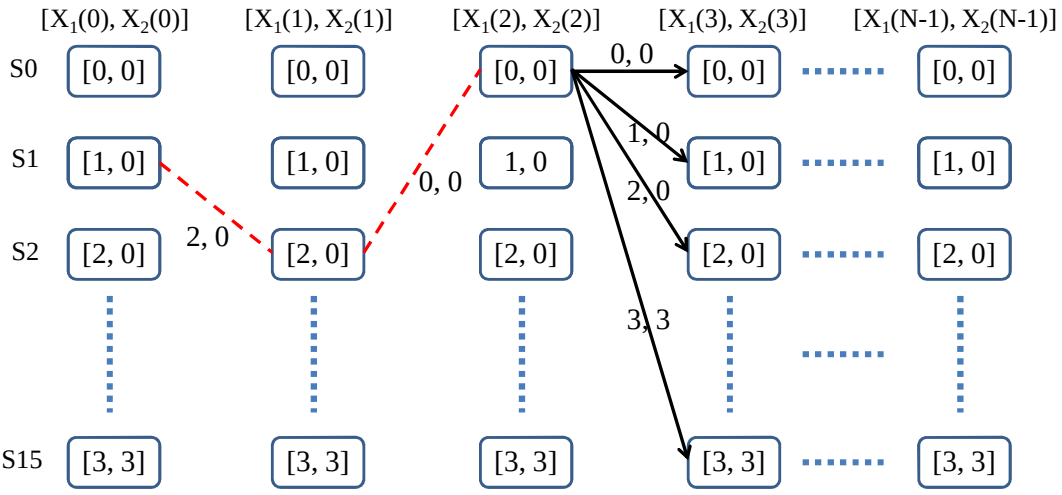

Figure 5.4: Example trellis for equalization of insufficient CP $4QAM$-2×2 MIMO-OFDM systems.

5.3.2 BDMA Equalization

Let $\boldsymbol{Y}_u = [Y_u(0), Y_u(1), \ldots, Y_u(N-1)]$ and $\boldsymbol{X}_v = [X_v(0), X_v(1), \ldots, X_v(N-1)]$. Here, the trellis equalization process in Section 4.3 is redefined for MIMO systems by choosing the sequence that maximizes the likelihood

$$p(\boldsymbol{Y}_1, \ldots, \boldsymbol{Y}_{N_R}, \boldsymbol{X}_1, \ldots, \boldsymbol{X}_{N_T}) = p(\boldsymbol{Y}_1, \boldsymbol{X}) \ldots p(\boldsymbol{Y}_{N_R}, \boldsymbol{X}), \tag{5.45}$$

where $\boldsymbol{X} = [\boldsymbol{X}_1, \boldsymbol{X}_2, \ldots, \boldsymbol{X}_{N_T}]$. Let us define $\boldsymbol{Y}_u([n_1, n_2]) = [Y_u(n_1), \ldots, Y_u(n_2)]$ where $n_1 < n_2 \in \mathscr{Z}^+$. The indices n_1 and n_2 denote end points of a subset of $\boldsymbol{Y}_u$. By applying the probability chain rule, we have

$$\begin{aligned} p(\boldsymbol{Y}_u, \boldsymbol{X}) \;=\; & p(Y_u(N-1)|\boldsymbol{Y}_u([0, N-2]), \boldsymbol{X}) p(\boldsymbol{X}(N-1)) \\ & \times p(Y_u(N-2)|\boldsymbol{Y}_u([0, N-3]), \boldsymbol{X}) p(\boldsymbol{X}(N-2)) \\ & \times \cdots \times p(Y_u(0)|\boldsymbol{X}) p(\boldsymbol{X}(0)). \end{aligned} \tag{5.46}$$

This is equivalent to

$$\ln(p(\boldsymbol{Y}_u, \boldsymbol{X})) = \sum_{a=0}^{N-1} \ln(p(Y_u(a)|\boldsymbol{Y}_u([0, a-1], \boldsymbol{X})) + \ln(p(\boldsymbol{X}(a))). \tag{5.47}$$

So, the metric for the whole sequence is a sum of the metrics at successive symbol times.

Since the OFDM tones are independent from each other, the dependence between $Y_u(a)$ and $\boldsymbol{Y}_u([0, a-1]$ is due to the ICI. To simplify the detection process, we use the approximation $p(Y_u(a)|\boldsymbol{Y}_u([0, a-1], \boldsymbol{X}) \approx p(Y_u(a)|\boldsymbol{X})$ (similar to the approximation made in Chapter 4). As the channel response is assumed to be deterministic and the ICI distribution is approximately Gaussian, we can assume that each element in $\boldsymbol{Y}_u$ is Gaussian when conditioned on the data sequence $\boldsymbol{X}$. Hence,

$$p(Y_u(a)|\boldsymbol{X}) = \frac{1}{\pi\eta_{In}} \exp\left(\frac{-|Y_u(a) - \tilde{Y}_u(a)|^2}{2\eta_{In}}\right), \tag{5.48}$$

where $\tilde{Y}_u(a)$ is the mean of $R_u(a)$ conditioned on $\boldsymbol{X}$. As the majority of the ICI energy comes from a few tones on each side of the considered sub-carrier, ICI can be estimated from these. Therefore, $\tilde{Y}_u(a) = R_{d,u}(a) + R_{ici2,u}(a)$ and recalling that

$$R_{ici2,u}(a) = \sum_{v=1}^{N_T} \sum_{l=D}^{L-1} h_{u,v,l} \sum_{k=a-d, k\neq a}^{a+d} \frac{X_v(k)}{N} e^{\frac{-j2\pi k\tau_l}{N}} \frac{\rho_k^{\tau_l - G} - 1}{1 - \rho_k}. \tag{5.49}$$

The sub-branch metric corresponding to the u^{th} received antenna, denoted as $\mu_u(a)$, is given by

$$\begin{aligned} \mu_u(a) &= -\ln(p(Y_u(a)|\boldsymbol{X})) - \ln(p(\boldsymbol{X}(a))) \\ &\equiv \left|Y_u(a) - \tilde{Y}_u(a)\right|^2 - \ln(p(\boldsymbol{X}(a))). \end{aligned} \tag{5.50}$$

Since it is assumed that all the sub-carrier symbols are transmitted with equal probability, $\ln(p(\boldsymbol{X}(a)))$ is a constant and can be neglected in the definition of $\mu_u(a)$. The overall branch metric can then be computed as

$$\mu(a) = \sum_{u=1}^{N_R} \left|Y_u(a) - \tilde{Y}_u(a)\right|^2. \tag{5.51}$$

The overall sequence metric, which is minimized by the right choice of $\boldsymbol{X}$, is the sum of the branch metrics

$$\Omega(\boldsymbol{X}) = \sum_{a=0}^{N-1} \mu(a). \tag{5.52}$$

It is trivial to see that a single state of our trellis can only provide a hypothesis for the desired sub-carrier. In order to provide the hypothesis for the ICI term, a tracking back the survivor path process is applied here. Assuming that the detection process starts from $a = 0$, by tracing back d previous states on the survivor path of the current state, we can retrieve $d \times N_T$ symbols corresponding to the sub-carriers $a - d$ to $a - 1$. This is only half of what is needed to approximate the ICI term as shown in (5.49). Therefore, we propose a bi-directional procedure in which the detection process would be able to obtain all the symbols corresponding to the sub-carriers $a - d$ to $a + d$ via equalizing the received signal twice (from a different direction each time). In addition, the M-algorithm [83] is utilized to further reduce the detection complexity by preserving only the M paths with lowest path metrics for each detection epoch instead of keeping all the paths. The overall equalization, namely the BDMA, is summarized below.

- An equalization process is carried out with the M-algorithm and decision feedback; the equalization direction is from $a = N - 1$ to $a = 0$. The survivor path with length d at each state is saved for the next detection phase. Note that only half the ICI part of $\tilde{Y}_u(a)$ can be computed.
- A 2^{nd} equalization process with the same M-algorithm and tracking back survivor path is carried out on the resultant ICI mitigated signal. This starts from $a = 0$ to $a = N - 1$. The survivor paths obtained from the previous detection phase allow a full $\tilde{Y}_u(a)$ to be calculated, leading to better detection accuracy.

5.4 Channel Estimation Performance Analysis

The performance analysis in the simulations will be assessed by the CRB [109–111] for channel estimations. Here, the bound is calculated based on the assumption that the estimated values of the channel delay profile and number of paths are correct. Furthermore, to establish the CRB, it is assumed that all data estimates used in the estimation process are correct and all interference is effectively eliminated. This allows the CRB to represent the best possible performance of the developed estimator. Let us reconsider the likelihood function of $\dot{\boldsymbol{Y}}_u$, which from (5.37), can be expressed as

$$p(\dot{\boldsymbol{Y}}_u|\boldsymbol{h}_u) = \frac{1}{(\pi\sigma_n^2)^N} \exp\left(\frac{-||\dot{\boldsymbol{Y}}_u - \boldsymbol{S}\boldsymbol{h}_u||^2}{\sigma_n^2}\right). \tag{5.53}$$

The CRB is obtained using the *Fisher Information Matrix (FIM)*, denoted as **FIM** [109]. In a similar manner to [22], the matrix can be computed from the derivative of $\ln(p(\dot{\boldsymbol{Y}}_u|\boldsymbol{h}_u))$ with respect to the vector $\boldsymbol{\theta}_u = [Re(\boldsymbol{h}_u)^T Im(\boldsymbol{h}_u)^T]^T$, which contains all the parameters to be estimated. Here, the CRB is represented by the $2N_T L \times 1$ vector $\mathbf{CRB}_u$, where each element defines a bound on the variance of the corresponding element in $\boldsymbol{\theta}_u$. The i^{th} component of $\mathbf{CRB}_u$ is found as the (i,i) element of the inverse of the FIM matrix or

$$var\{\boldsymbol{\theta}_u(i)\} \geq \mathbf{CRB}_u(i) = \mathbf{FIM}_u^{-1}(i,i), \tag{5.54}$$

where each element of $\mathbf{FIM}_u$ can be defined as

$$\mathbf{FIM}_u(i_1,i_2) = -E\left\{\frac{\partial^2 \ln(p(\dot{\boldsymbol{Y}}_u|\boldsymbol{h}_u))}{\partial\boldsymbol{\theta}_u(i_1)\partial\boldsymbol{\theta}_u(i_2)}\right\}. \tag{5.55}$$

The derivatives of the log-likelihood function $\ln(p(\dot{\boldsymbol{Y}}_u|\boldsymbol{h}_u))$ with respect to the components of the parameter vector $\boldsymbol{\theta}_u$, i.e $Re(\boldsymbol{h}_u)$ and $Im(\boldsymbol{h}_u)$, result in different sections/submatrix of the $\mathbf{FIM}_u$ matrix. Let the superscript notations $\{t,l\}$, $\{t,r\}$, $\{b,l\}$ and $\{b,r\}$ indicate the top-left, top-right, bottom-left and bottom-right quadrants of the $\mathbf{FIM}_u$ matrix. We have

$$\mathbf{FIM}_u^{t,l} = E\left\{\frac{\partial \ln(p(\dot{\boldsymbol{Y}}_u|\boldsymbol{h}_u))}{\partial \mathrm{Re}(\boldsymbol{h}_u)}\left(\frac{\partial \ln(p(\dot{\boldsymbol{Y}}_u|\boldsymbol{h}_u))}{\partial \mathrm{Re}(\boldsymbol{h}_u)}\right)^T\right\} = \frac{2}{\sigma_n^2}\mathrm{Re}(\boldsymbol{S}^\dagger\boldsymbol{S}), \tag{5.56}$$

$$\mathbf{FIM}_u^{t,r} = E\left\{\frac{\partial \ln(p(\dot{\boldsymbol{Y}}_u|\boldsymbol{h}_u))}{\partial \mathrm{Re}(\boldsymbol{h}_u)}\left(\frac{\partial \ln(p(\dot{\boldsymbol{Y}}_u|\boldsymbol{h}_u))}{\partial \mathrm{Im}(\boldsymbol{h}_u)}\right)^T\right\} = -\frac{2}{\sigma_n^2}\mathrm{Im}(\boldsymbol{S}^\dagger\boldsymbol{S}), \tag{5.57}$$

$$\mathbf{FIM}_u^{b,l} = E\left\{\frac{\partial \ln(p(\dot{\boldsymbol{Y}}_u|\boldsymbol{h}_u))}{\partial \mathrm{Im}(\boldsymbol{h}_u)}\left(\frac{\partial \ln(p(\dot{\boldsymbol{Y}}_u|\boldsymbol{h}_u))}{\partial \mathrm{Re}(\boldsymbol{h}_u)}\right)^T\right\} = \frac{2}{\sigma_n^2}\mathrm{Im}(\boldsymbol{S}^\dagger\boldsymbol{S}), \tag{5.58}$$

$$\mathbf{FIM}_u^{b,r} = E\left\{\frac{\partial \ln(p(\dot{\boldsymbol{Y}}_u|\boldsymbol{h}_u))}{\partial \mathrm{Im}(\boldsymbol{h}_u)}\left(\frac{\partial \ln(p(\dot{\boldsymbol{Y}}_u|\boldsymbol{h}_u))}{\partial \mathrm{Im}(\boldsymbol{h}_u)}\right)^T\right\} = \frac{2}{\sigma_n^2}\mathrm{Re}(\boldsymbol{S}^\dagger\boldsymbol{S}). \tag{5.59}$$

Hence, the FIM matrix is defined as

$$\mathbf{FIM}_u = \frac{2}{\sigma_n^2}\begin{bmatrix}\mathrm{Re}(\boldsymbol{S}^\dagger\boldsymbol{S}) & -\mathrm{Im}(\boldsymbol{S}^\dagger\boldsymbol{S}) \\ \mathrm{Im}(\boldsymbol{S}^\dagger\boldsymbol{S}) & \mathrm{Re}(\boldsymbol{S}^\dagger\boldsymbol{S})\end{bmatrix} \tag{5.60}$$

and the CRB can then be obtained given $\mathbf{CRB}_u = \text{diag}(\mathbf{FIM}_u^{-1})$.

There are a high number of independent channel parameters (both real and complex), which are bounded by the CRB. In the case of MIMO systems, we would need to consider $2N_R N_T L$ individual assessments of estimation accuracy. To simplify the assessment process, we define a single metric to assess the estimation quality of the overall MIMO channel as

$$\mathbf{CRB} = \sum_{u=1}^{N_R} \sum_{i=1}^{2N_T L} \mathbf{CRB}_u(i). \tag{5.61}$$

5.5 Complexity Analysis

In a similar manner to the complexity analysis in Section 4.5, the assessment of the computational cost takes into account the number of complex multiplications involved in the EPSB-MMSE and BDMA algorithms for an OFDM symbol containing pilots. Let us recall that I represents the number of iterations. Table 5.1 illustrates the approximate complexities of different processes within the developed channel estimator. The complexity of the IJEP algorithm [22] is also included in Table 5.1 for comparison. The total value indicates the total number of complex multiplications when $N_R = N_T = 2$, $N = 128$, $N_p = 12$, $L = 6$, $D = 3$, $\tau_{PD} = 12$, $M = 4$, $I = 2$, $d = 2$ and $4QAM$ modulation. With these parameters, it can be seen that our proposed system is approximately 1.9 times more complex than the IJEP algorithm. However, our method is applicable to the pilot setting used in LTE and offers better bandwidth efficiency by requiring significantly fewer pilot sub-carriers (a reduction of 70% in the number of pilot sub-carriers with the considered system parameters). On the other hand, our channel estimation method is flexible in terms of pilot arrangement so this method can be applied to a variety of OFDM systems employing pilot sub-carriers.

Table 5.2 shows the approximate complexities of the BDMA equalizer. The complexity of the RISIC algorithm [2] is also included in Table 5.2 for comparison. It can be seen that the BDMA is approximately 2.5 times more complex than the RISIC algorithm. However, it will be shown in Section 5.6 that our method provides significantly better BER and allows accurate data detection even when the channel delay spread far exceeds the CP length.

	EPSB-MMSE algorithm	IJEP algorithm [22]
	Complex multiplications	Complex multiplications
ISI mitigation	$2N_RN_T(L-D)N^2$	$(2N_RN_T(L-D)+1)\,N^2$
ICI mitigation	$2N_RN_T(L-D)(N-1)N(I-1)$	$2N_RN_T(L-D)(N-1)$ $\times N(I-1)+N^2$
Estimate $\widehat{L}$	$N_T(N_R+2N_p)(I-1)$	-
Estimate $\widehat{\boldsymbol{h}}$	$\frac{4\tau_{PD}^2}{L}\Big(NN_R^2N_T\tau_{PD}+N_p^3N_T$ $+N_p^2N_T\frac{L^2}{4}+N_pL^2N_TN_R$ $+(N^2N_T+NLN_TN_R)(I-1)\Big)$	$NN_R^3(N_T\tau_{PD})^2+\frac{N}{2}N_R^2N_T\tau_{PD}+$ $(N_RN_T\tau_{PD})^3+\Big(2NN_R^3(N_T\tau_{PD})^2$ $+(N_RN_T\tau_{PD})^3\Big)(I-1)$
Total	$5,366,784$	$2,825,216$

Table 5.1: EPSB-MMSE algorithm complexity. The total value is calculated with $N_R=N_T=2$, $N=128$, $N_p=12$, $L=6$, $D=3$, $\tau_{_{PD}}=12$, $M=4$, $I=2$, $d=2$ and $4QAM$.

5.6 Simulation Results

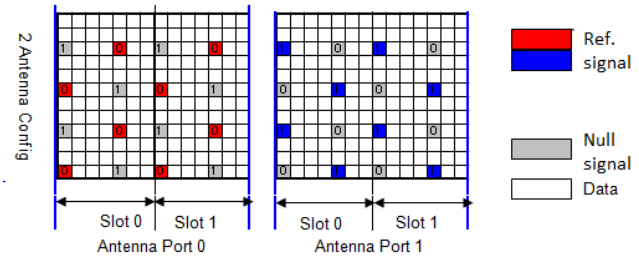

Figure 5.5: LTE pilot sub-carrier (or *reference signal (RS)*) arrangement [1].

In the following, we provide numerical results to confirm the designs developed in the previous sections. We will show that our design is applicable to LTE systems and compare it to [22] in terms of converging to the MSE-BER performance of sufficient CP systems. Our simulations consider an uncoded 2×2 MIMO-OFDM system with LTE-OFDM parameters, $N=128$, $N_s=76$ (the number of sub-carriers), $G=9$

	BDMA equalization	RISIC algorithm [2]
Process	No. complex multiplications	No. complex multiplications
ISI mitigation	$2N_RN_T \times(L-D)N^2$	$2N_RN_T (L-D)N^2+N^2$
ICI mitigation	$2N_RN_T(L-D) \times(N-1)N(I-1)$	$2N_RN_T(L-D) \times(N-1)N(I-1) +N^2$
Equalization/ Detection	$2NMA^{N_T}N_RN_T \times(L-D)(2d+1)I$	$N_RA^{N_T}(4+N_T)NI$
Total	$2,159,616$	$865,280$

Table 5.2: BDMA equalization complexity. The total value is calculated with $N_R = N_T = 2$, $N = 128$, $L = 6$, $D = 3$, $M = 4$, $I = 2$, $d = 2$ and $4QAM$.

(standard LTE CP length) and 4QAM for sub-carrier modulation. The pilot sub-carrier arrangement follows the LTE standard as shown in Fig. 5.5 (which shows the first 12 sub-carriers of a LTE sub-frame for 2 transmit antennas). The red and blue patterns show the pilot sub-carrier positions on the sub-frame with respect to the first and second transmit antennas. The grey patterns show the null sub-carriers so that pilot sub-carriers experience no interference with sufficient CP. Lastly, the white patterns show the data sub-carriers. With such pilot arrangement, there is one pilot sub-carrier for every 6 sub-carriers per transmit antenna in a reference OFDM symbol.

The channel path coefficients are assumed to stay static for a duration of 4 OFDM symbols and then they vary independently from one static period to another as described in Section 2.1. The sub-channel model considered in our simulations consists of $L = 6$ equally spaced Rayleigh fading paths with a RMS delay spread of $\tau_{rms} = \tau_{L-1}/2$. The average power of each path follows an exponential decay model. In addition, the channel model with $L = 2$ Rayleigh fading paths with equal power is also used in our simulations. In all simulations, the proposed design considers $d = 3$ as it was shown in Section 3.4 that the major part of ICI energy comes from the sub-carriers within the interval $[a-3, a+3]$.

5.6.1 MSE Results

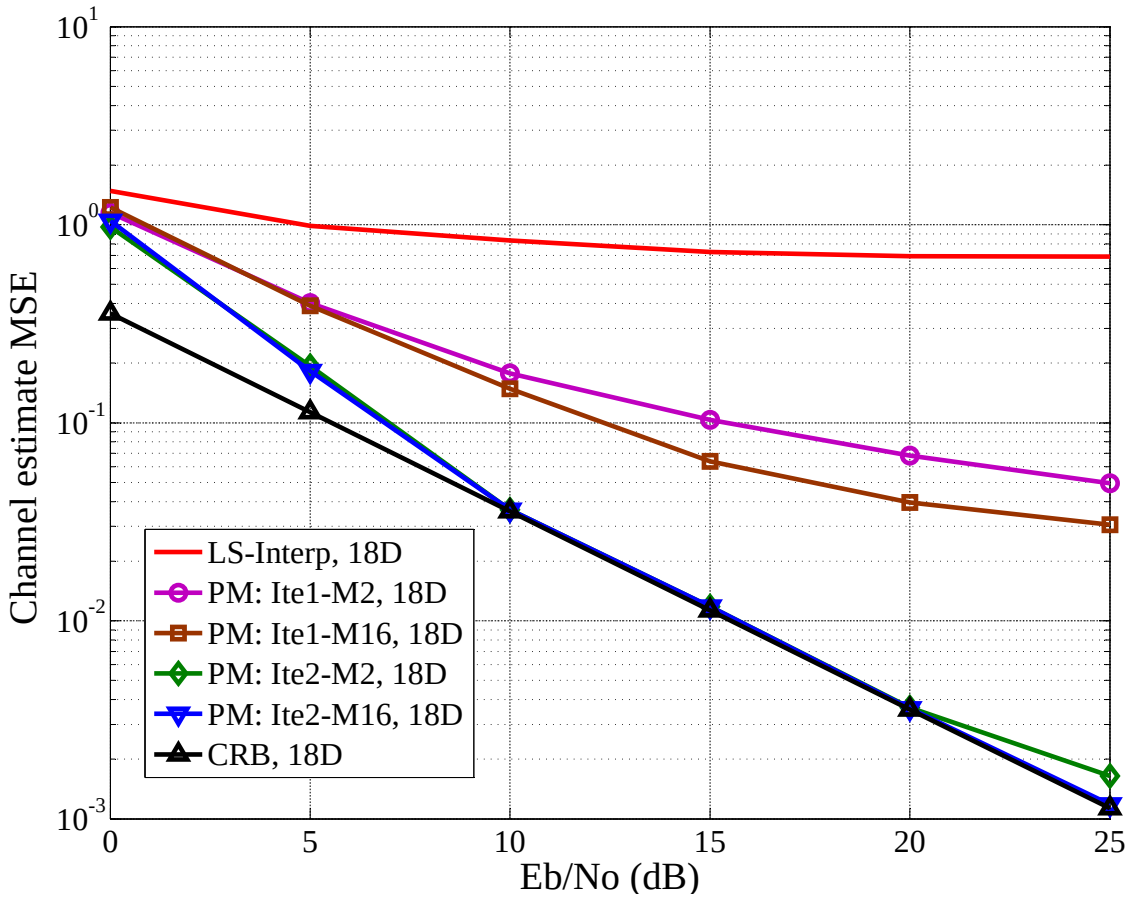

Figure 5.6: Channel estimation MSE performance with $\tau_{PD} = \tau_{L-1} = 18$, 6 path channel with exponential decay power.

Here, the MSE is utilized as the metric to compare the developed channel estimator with other schemes. Let $\boldsymbol{h}_{f,u,v}$ be the full TD channel response of the sub-channel uv. For $N_T \times N_R$ MIMO channel, the MSE metric is defined as

$$MSE = \sum_{u=1}^{N_R} \sum_{v=1}^{N_T} ||\boldsymbol{h}_{f,u,v} - \widehat{\boldsymbol{h}}_{f,u,v}||^2. \tag{5.62}$$

Figures 5.6 and 5.7 illustrate the MSE performance of the developed algorithm for different SNR conditions with the 6 path channel model. Performance is compared to the MSE results obtained from using the LSI method and the theoretical CRB.

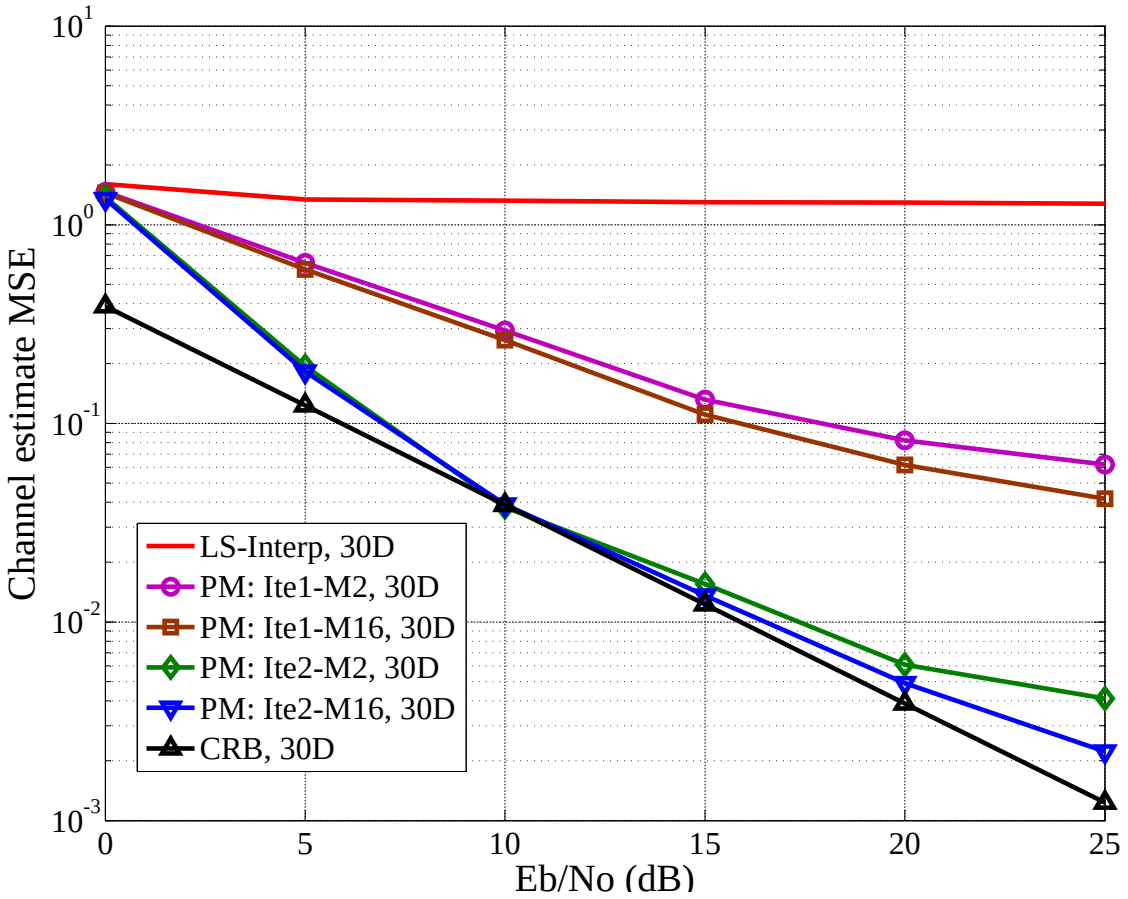

Figure 5.7: Channel estimation MSE performance with $\tau_{PD} = \tau_{L-1} = 30$, 6 path channel with exponential decay power.

Here, it is assumed that the maximum channel delay τ_{L-1} is equal to the maximum pre-defined delay τ_{PD}. As in Chapter 4, the notation 'PM' indicates the proposed method; 'Ite' indicates the number of iterations, 'M' indicates the value of the M factor utilized in the BDMA algorithm and '18D' or '30D' indicates the maximum channel delay of $\tau_{L-1} = 18$ and $\tau_{L-1} = 30$ respectively.

It can be seen from Fig. 5.6 and Fig. 5.7 that the proposed algorithm outperforms the LSI approach. The algorithm's performance is also very close to the CRB after only 2 iterations even though the maximum channel delay spread is far exceeding the CP (more than twice for $\tau_{L-1} = 18$ in Fig. 5.6 and more than three times for $\tau_{L-1} = 30$ as in Fig. 5.7). However, it can be seen that error floors start appearing

at high Eb/No values, especially at higher delays, due to residual interference. The figure also shows us that there is only a small performance degradation when the algorithm utilizes $M = 2$ instead of $M = 16$ (full complexity). The utilization of $M = 2$ leads to a significant complexity reduction, which improves the practicality of our method.

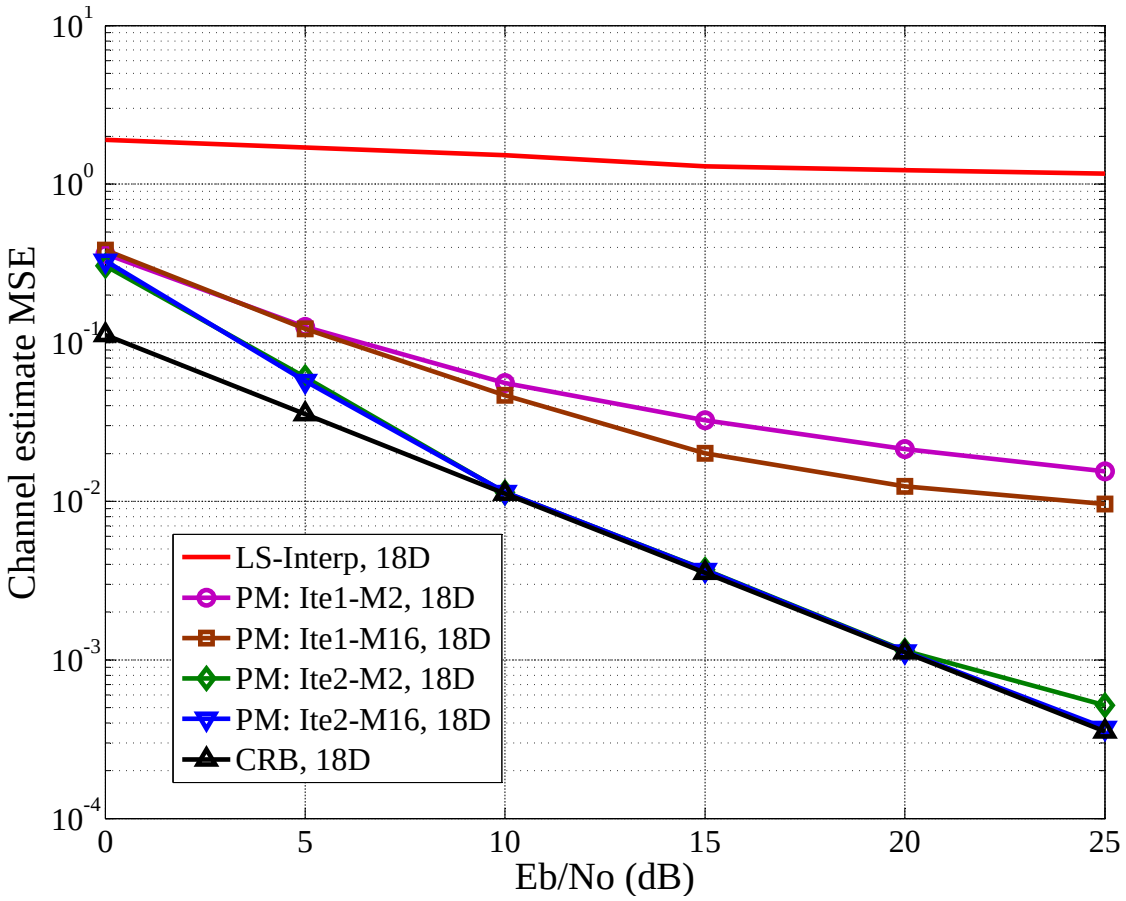

Figure 5.8: Channel estimation MSE performance with $\tau_{PD} = \tau_{L-1} = 18$, 2 equal power path channel.

Similar results can also be seen in Fig. 5.8 and Fig. 5.9, which shows our simulation results for channels with 2 equal power paths. Here, the proposed method is also significantly better than the LSI approach and is able to reach the CRB with 2 iterations. In general, our proposed method provides better estimation accuracy for this channel type than the 6 path channel. This is because it is easier for the esti-

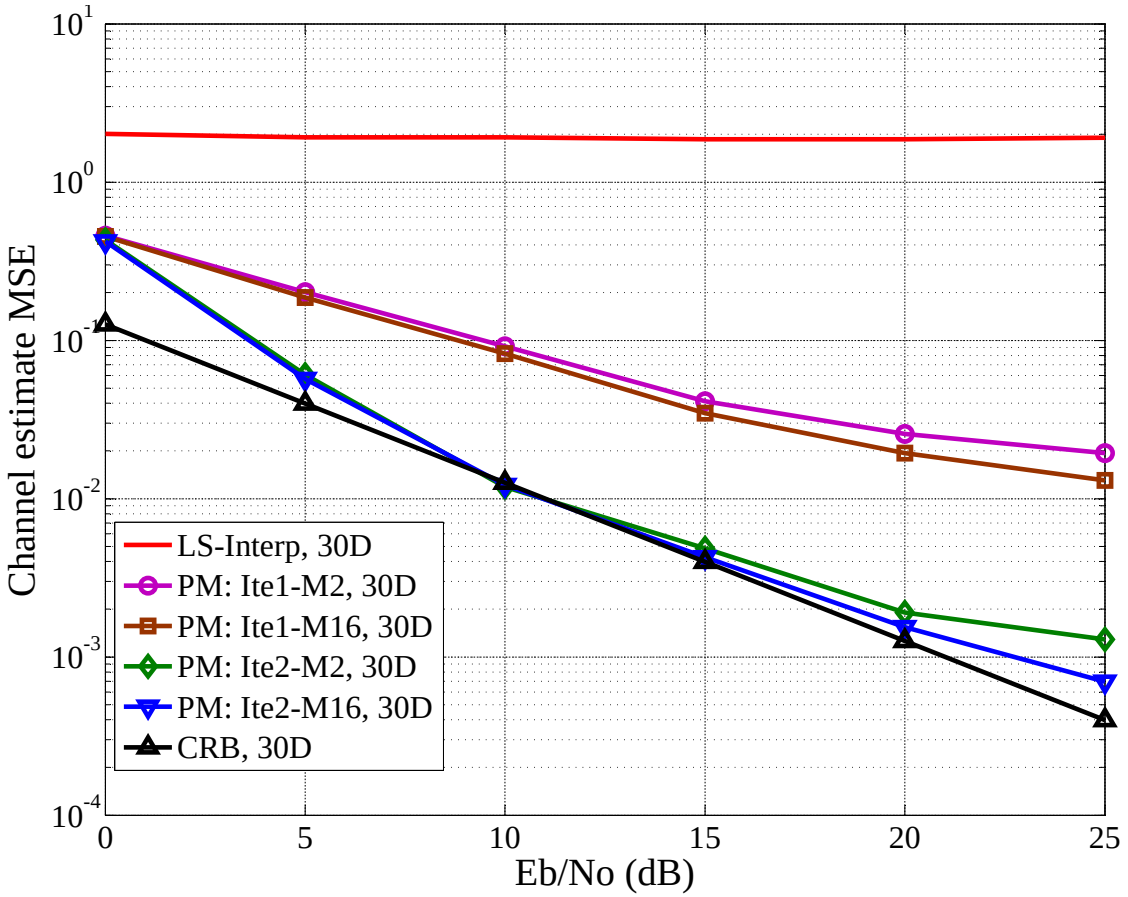

Figure 5.9: Channel estimation MSE performance with $\tau_{_{PD}} = \tau_{L-1} = 30$, 2 equal power path channel.

mation process to identify 2 major paths that are far apart in time, than to search for 6 paths that are considerably closer and have decreasing power. This causes the EPSB-MMSE estimator to have a better estimate of the channel covariance matrix, leading to a better overall channel estimation. Such advantage overcomes the increase in interference power when the 2 path channel is considered.

Figure 5.10 illustrates the proposed algorithm performance with respect to the variations in channel delay spread. It can be seen that the increase in channel delay spread has a negative effect on the proposed estimator. However, the degradation rate is not fast, especially for the 2 path channel. With only 2 iterations, the estimator is able to achieve the MSE values close to that of the sufficient CP case for

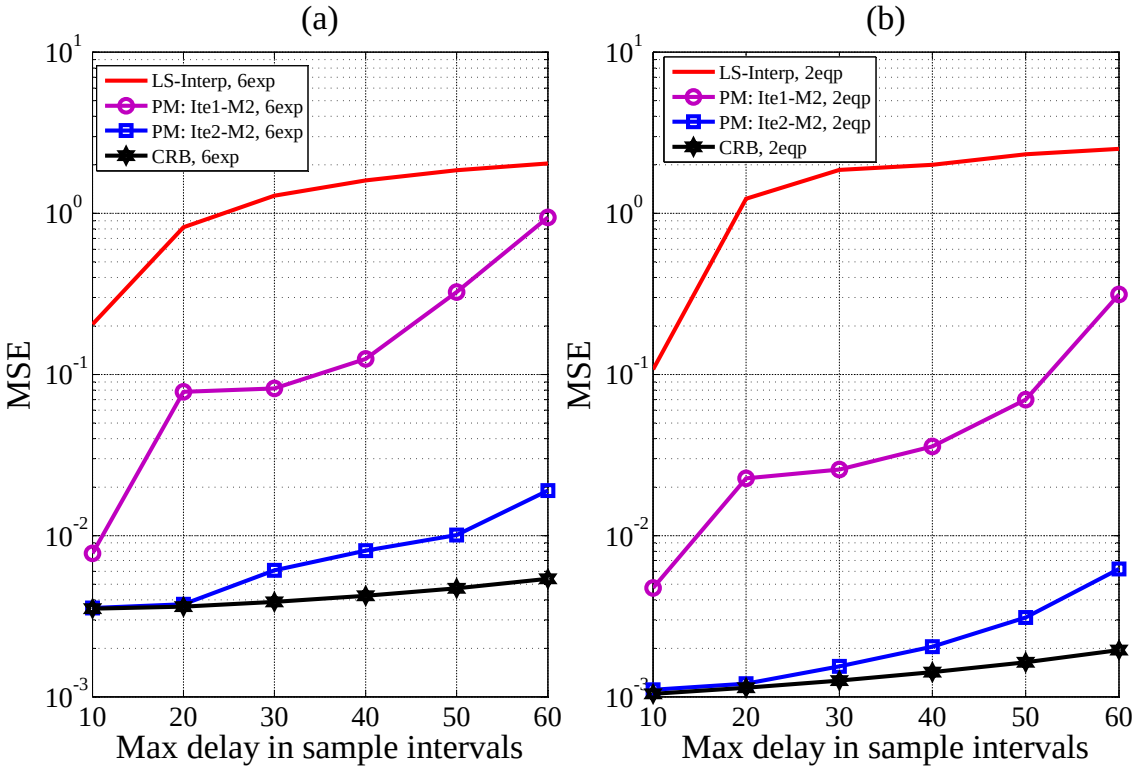

Figure 5.10: MIMO channel estimate MSE with SNR of 20 dB. Figure (a) considers 6 path channel with exponential decay power and figure (b) considers 2 path channel with equal power.

channel delay spread up to 30 sample intervals for the 6 path channel and up to 50 sample intervals for the 2 path channel. Such results are significant as these delay spread values are more than 3 and 5 times the CP length, respectively (so the interference power at these delay values are high leading to severe signal corruptions). There is a large difference in performance of the proposed technique after 1 and 2 iterations. This is because the estimator can only rely on the pilot sub-carriers for channel estimates in the first iteration while it utilizes both pilot sub-carriers and data sub-carrier estimates from the second iteration onward. In addition, ICI is not fully compensated in the initial iteration as there is no available knowledge about the currently received OFDM symbols. In comparison, the degradation caused by channel delay spread in Fig. 5.10 is significantly less than that in Fig. 4.10, which corresponds to the PSB-MMSE technique. This means that the EPSB-MMSE al-

gorithm provides much better tolerance against such increase in comparison to the PSB-MMSE algorithm proposed in Chapter 4.

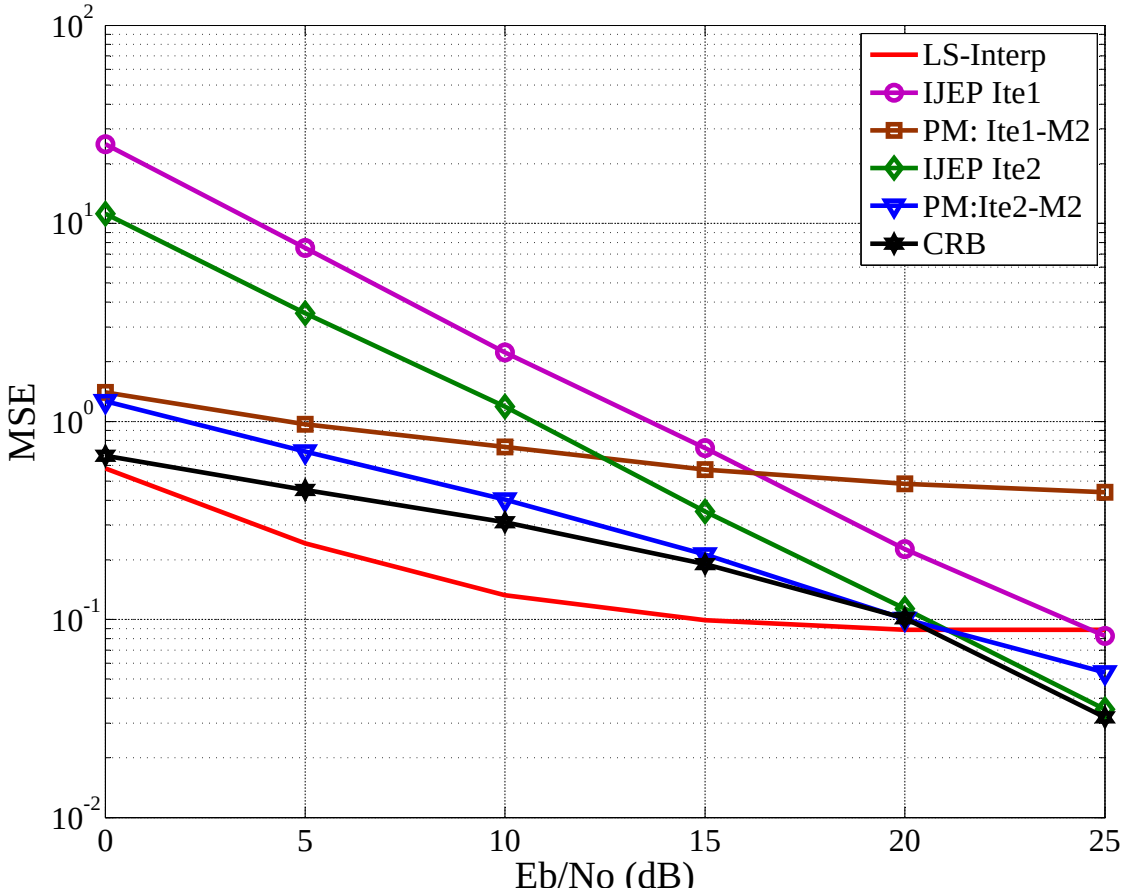

Figure 5.11: MIMO channel estimation MSE performance with $\tau_{_{PD}} = \tau_{L-1} = 5$, $G = 0$, and 6 path channel with exponential decay power.

Here, we also investigate the performance of the proposed method where there is no CP. In these simulations, we set $G = 0$ and the maximum delay spread to be $\tau_{L-1} = 5$. The IJEP algorithm in [22] is also included for performance comparison. The obtained MSE results are shown in Fig. 5.11. It can be seen that the LS method provides a better channel estimate than both our proposed methods and the IJEP for most of the considered SNR range. However, it soon faces a floor while the IJEP and our scheme do not. In comparison, for low to medium SNR range, our method generally provides lower MSE values than the IJEP scheme. It should be noted

that the IJEP algorithm requires a full OFDM symbol for providing pilots while the proposed scheme only needs a fraction of it (about 1/6 for the simulated LTE OFDM systems). For high SNR values, the IJEP with 1 iteration outperforms our scheme with 1 iteration. However, both schemes with 2 iterations have similar performance and they both converge to the CRB. It should be noted that our proposed method allows a reduction of 70% in the number of required pilot sub-carriers but it is 2 times more complex than the IJEP algorithm.

5.6.2 BER Results

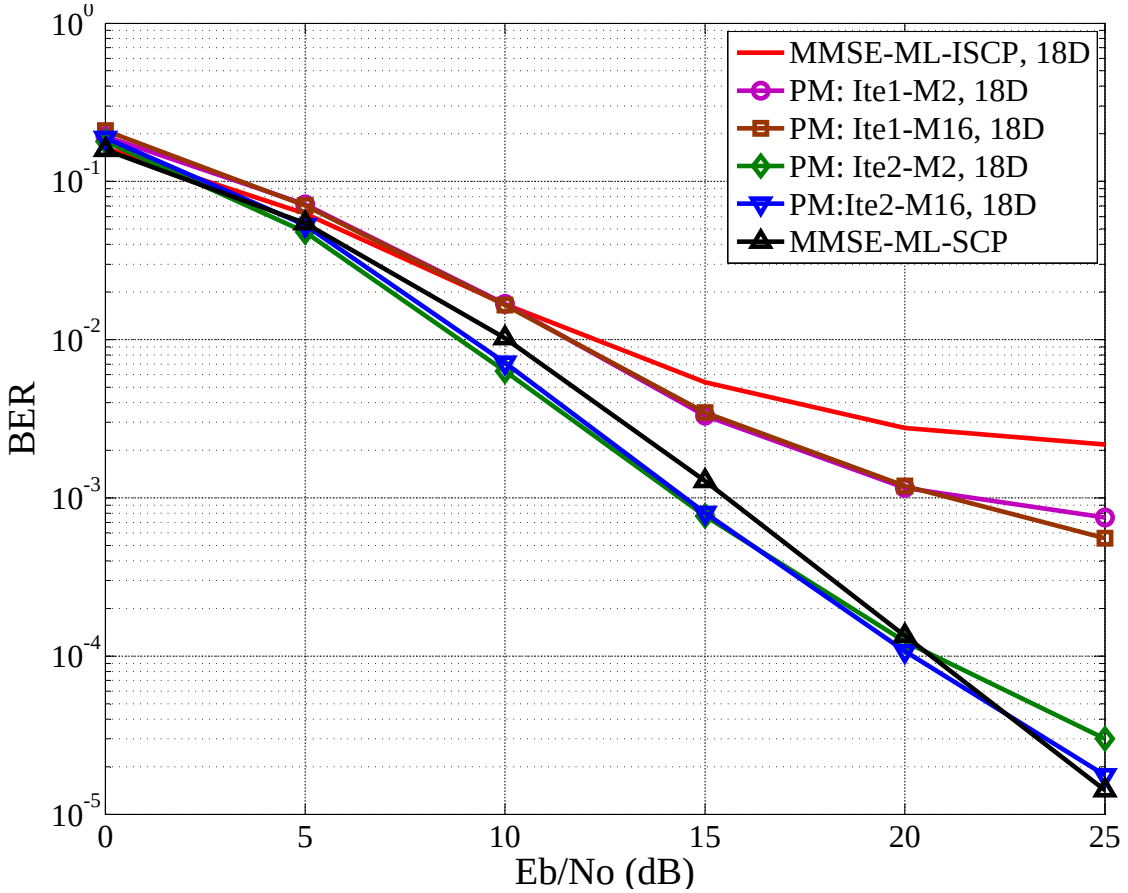

Figure 5.12: BER performance with maximum delay of $\tau_{_{PD}} = \tau_{L-1} = 18$ and 6 path channel with exponential decay power.

Figures 5.12 and 5.13 show the simulated BER results for maximum channel

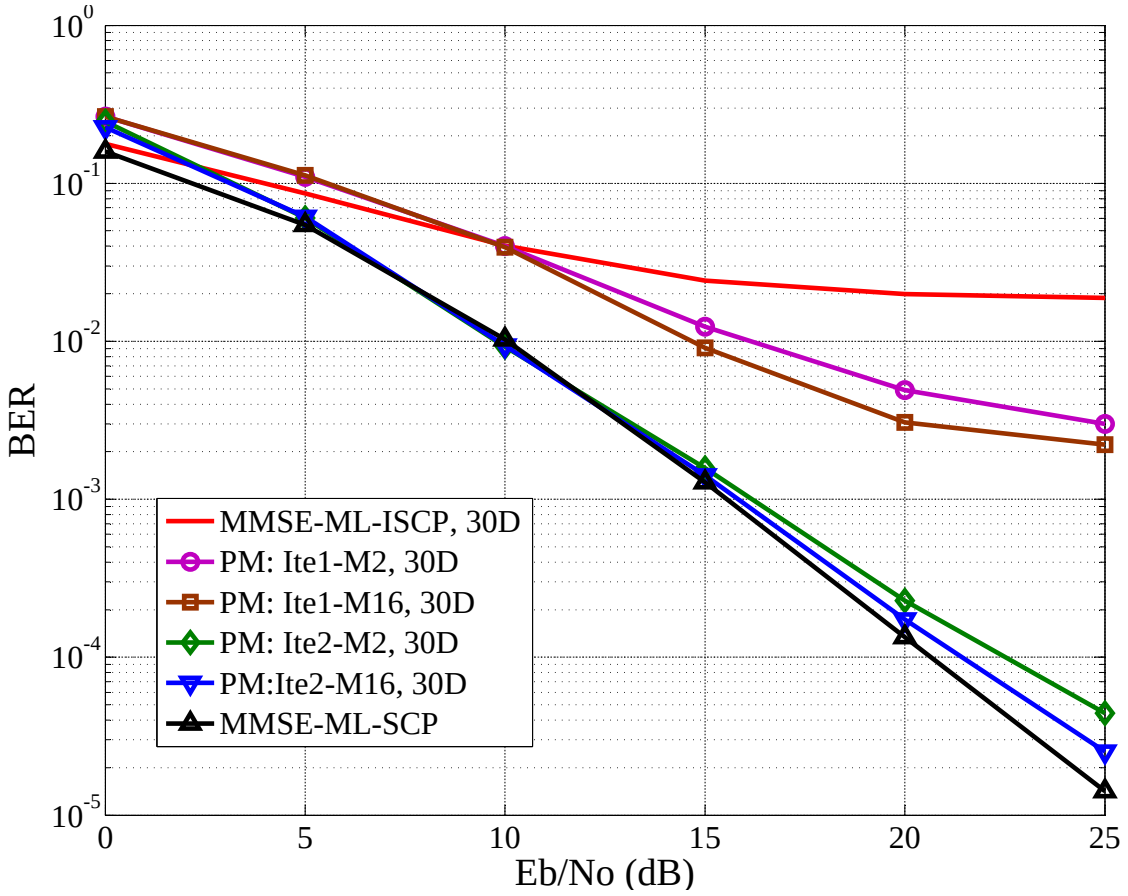

Figure 5.13: BER performance with maximum delay of $\tau_{PD} = \tau_{L-1} = 30$ and 6 path channel with exponential decay power.

delay of $\tau_{L-1} = 18$ and $\tau_{L-1} = 30$ for the 6 exponential decay power path channel, respectively. Here, our proposed scheme is compared with a reception process consisting of a standard MMSE channel estimator and a ML data detector described in Section 2.2.2. The standard MMSE estimator utilizes the available pilot sub-carriers to estimate the TD channel and the process assumes a known delay profile (so it only needs to estimate the channel path coefficients). The ML detector operates on individual sub-carriers. It searches for all possible combinations of symbols transmitted on sub-carriers from different transmit antennas and computes the corresponding MSEs for ML detection. The BER results for the MMSE-ML receiver are obtained for both scenarios of insufficient CP ('ISCP') and sufficient CP ('SCP'). In the first case, the CP is kept at $G = 9$ while it is extended to the maximum delay spread for

the latter.

It can be seen in the two figures that the proposed method achieves significant BER performance gain over the MMSE-ML receiver when the CP is insufficient. On the other hand, it is able to converge to performance near that of the sufficient CP case with only 2 iterations. Similarly to the MSE results, we can observe that the obtained BERs corresponding to $M = 2$ are not far from the BERs corresponding to $M = 16$. It is worth noting a particular aspect shown in Fig. 5.12. The curves corresponding to the proposed methods with 2 iterations show better BER than the sufficient CP BER at medium SNR. This is due to the data aided effect introduced to the estimation process in the second iterations while the MMSE-ML process only relies on pilot sub-carriers for channel estimation. However, at high SNR, this advantage diminishes due to residual interference. This is not observed in Fig. 5.13, because it is more difficult to estimate the longer delay spread channel as the interference power is higher.

Figures 5.14 and 5.15 show the simulated BER results for maximum channel delay of $\tau_{L-1} = 18$ and $\tau_{L-1} = 30$ for the 2 path with equal power channel, respectively. In general, it can be seen that the performance of our proposed method for this channel is similar to that of the 6 path channel. However, the data aided advantage shown in Fig. 5.12 is not observed in these two figures. This is because it is easier to estimate the 2 path channel than the 6 path channel. Therefore, the MMSE-ML receiver is able to acquire good channel estimates with only pilot sub-carriers.

Figure 5.16 illustrates the BER performance of the proposed iterative receiver with respect to channel delay spread. Similar to the MSE performance, the BER performance of the proposed method is considerably affected by the increase in channel delay spread. The proposed methods outperform the standard MMSE-ML receiver even with only 1 iteration. With 2 iterations, the proposed design is able to achieve the BER results close to those of the sufficient CP system for a channel delay spread up to 3 times the CP length for both channel types. This corresponds to a reduction of 70% of the required bandwidth needed for transmitting the CP. In addition, the degradation rate caused by the increase in channel delay spread is steady, but not fast. This indicates the resilience of the proposed method to extreme

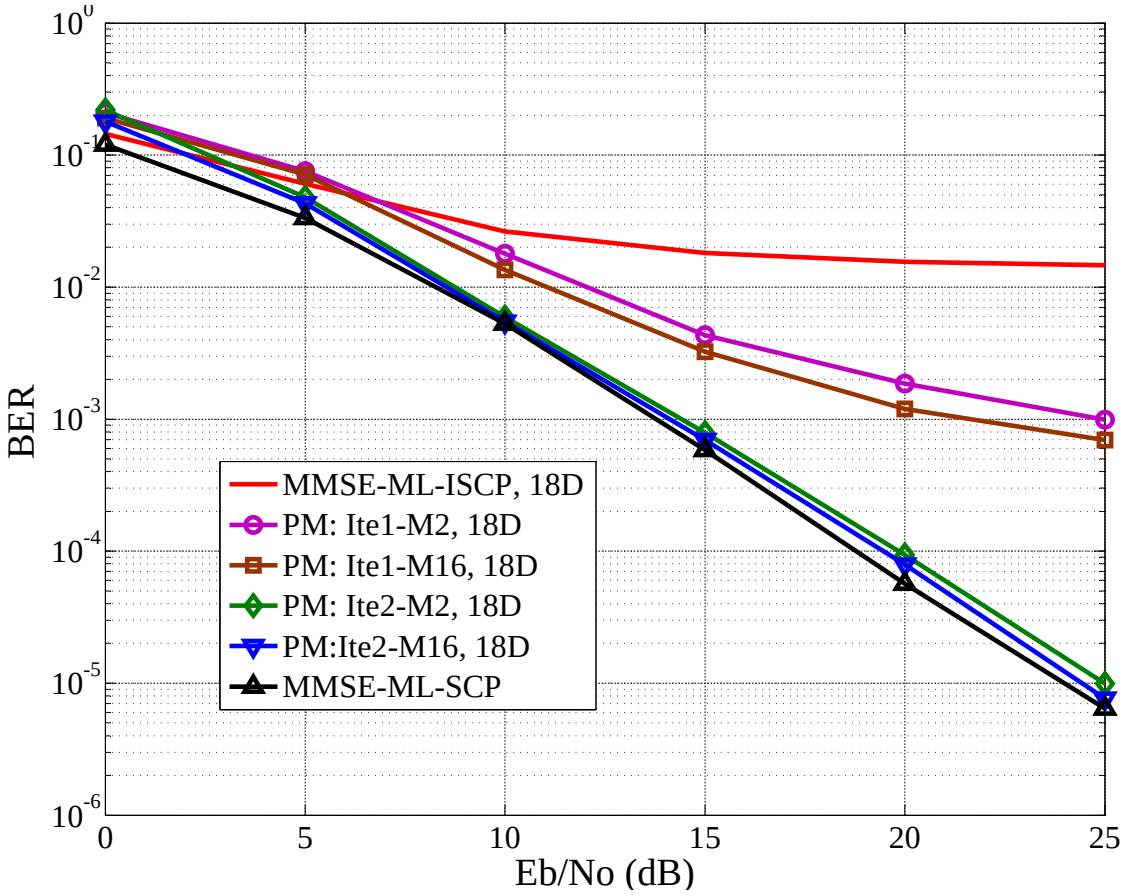

Figure 5.14: BER performance with maximum delay of $\tau_{PD} = \tau_{L-1} = 18$ and 2 path channel with equal power.

long delay spread conditions. The performance can be improved with the incorporation of an error control code into the transmission scheme.

Given the above results, it is also interesting to understand the capability of the developed BDMA equalization algorithm given perfect channel knowledge. Figure 5.17 presents such results. At sufficiently high SNRs, the BDMA algorithm provides much better BER than MMSE-ISCP and the RISIC algorithm [2], especially for the case of $\tau_{L-1} = 60$. With 2 iterations, the algorithm is also able to achieve interference free detection accuracy for a high delay spread channel ($\tau_{L-1} = 30$, more than 3 times the CP length) and near it for a very high delay spread channel ($\tau_{L-1} = 60$, more than 6 times the CP length). Such satisfactory performance is achieved because the

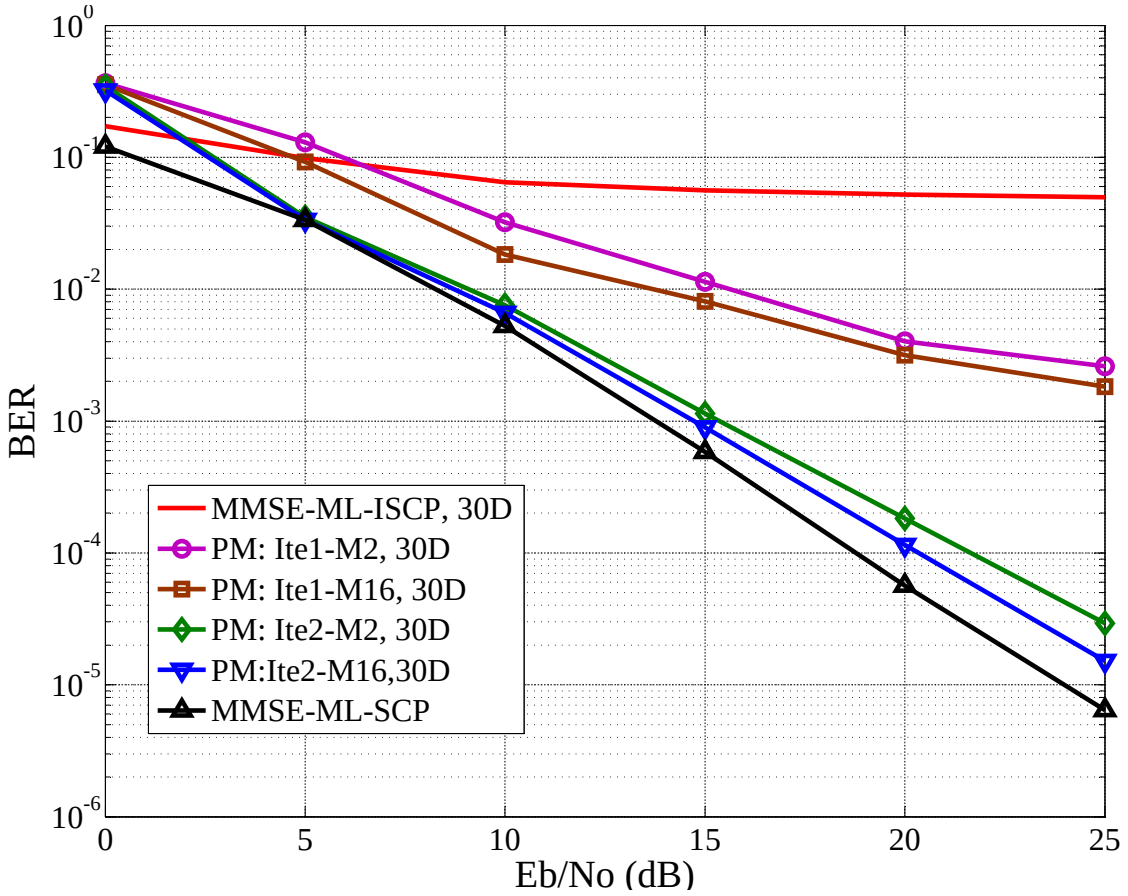

Figure 5.15: BER performance with maximum delay of $\tau_{_{PD}} = \tau_{L-1} = 30$ and 2 path channel with equal power.

BDMA algorithm is able to capture a sufficient number of neighbouring sub-carriers, which cause the majority of ICI on both sides of the considered sub-carrier.

5.7 Summary

In this chapter, a high performance iterative reception process consisting of channel estimation and trellis equalization has been presented. A high performance EPSB-MMSE channel estimator was developed based on the PSB-MMSE algorithm proposed in Chapter 4. Here, the channel estimation process was formulated into an optimization process, which can be solved by searching for an optimal solution among a finite number of possibilities. A low complexity, but efficient algorithm is

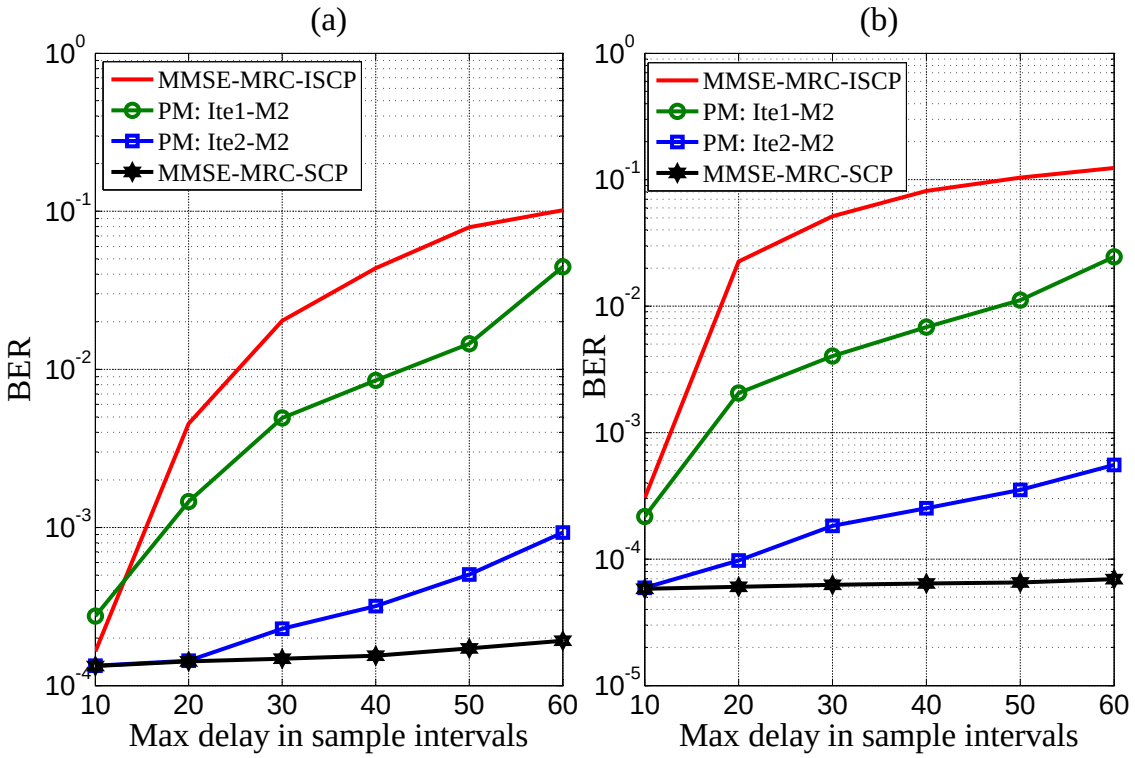

Figure 5.16: BER performance with SNR of 20 dB. Figure (a) considers 6 path channel with exponential decay power and figure (b) considers 2 path channel with equal power.

introduced to reduce the PSB-MMSE estimator complexity. Estimated data sub-carriers from the last iteration are also utilized to enhance the estimation accuracy. It was shown by simulations that the proposed channel estimator is significantly better than the standard LSI method and is comparable to the IJEP scheme, which requires a significantly higher number of pilot sub-carriers. On the other hand, the EPSB-MMSE estimator was also able to achieve the CRB for channel delay spread more than 4 times the CP length, which is difficult to achieve.

An effective trellis equalizer was also introduced in this chapter. The developed BDMA equalization algorithm utilizes a bidirectional procedure to include a sufficient number of sub-carriers for accurate detection while keeping the trellis size as small as possible. The M-algorithm was also incorporated into the process for fur-

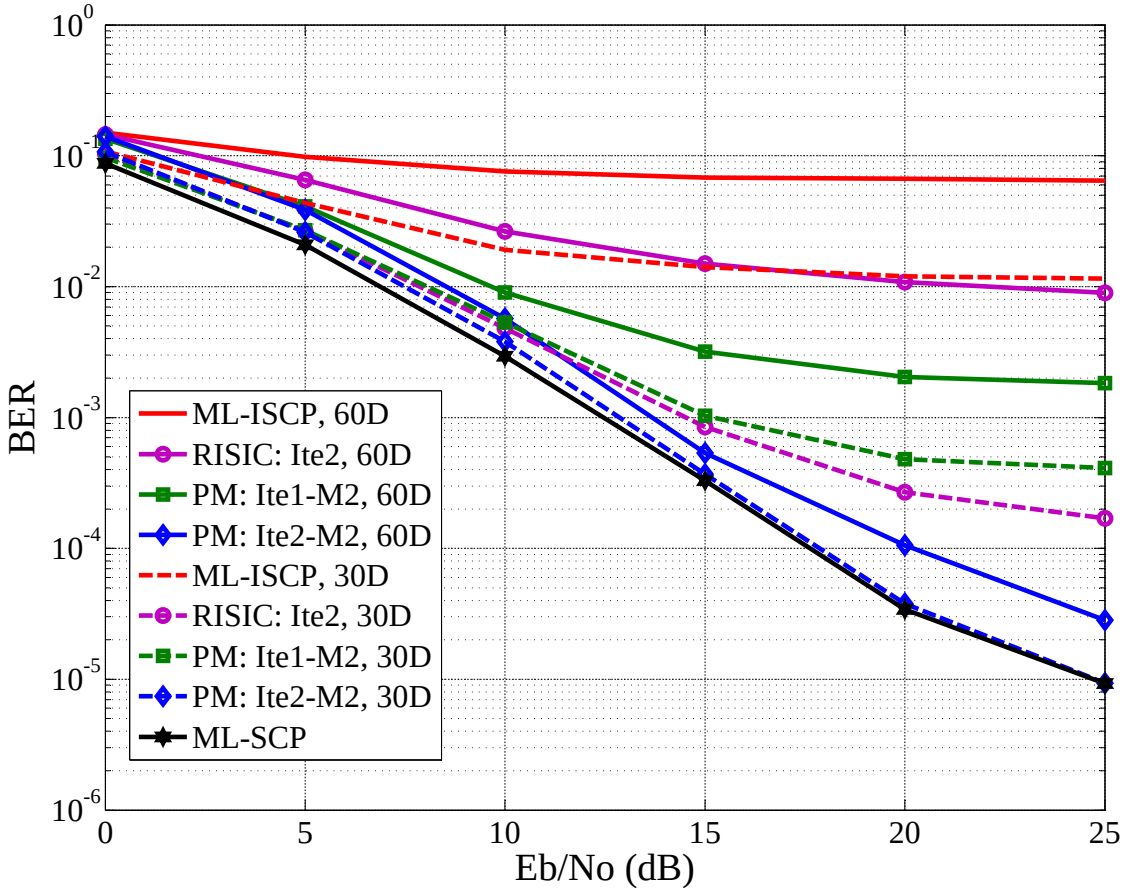

Figure 5.17: BER performance of BDMA algorithm, $\tau_{_{PD}} = \tau_{L-1} = 30$ or 60. Assuming perfect channel knowledge and 6 path channel with exponential decay power.

ther complexity reduction. The obtained simulation results showed that the BDMA algorithm is very effective in equalizing an insufficient CP MIMO-OFDM signal. It allows the iterative reception process to converge to the sufficient CP performance with only 2 iterations even when the channel delay spread is much higher than the CP length.

Chapter 6

Conclusions and Future Work

The main contribution of this thesis is the advanced receiver designs (consisting of channel estimation and data detection) for insufficient CP OFDM systems that enable OFDM transmissions over longer ranges, and/or with improved spectral efficiency. The developed receivers can work with channel delay spreads up to 3 times the CP duration. This corresponds to an approximately 70% reduction in the time period reserved for the CP in OFDM systems. In the context of LTE, an overall OFDM duration is 71.3 μs while the standard and extended CP lengths are 4.7 μs and 16.7 μs, respectively [1]. This means the temporal spectral efficiencies corresponding to the normal and extended CP are 93.4% and 76.5%. With the proposed designs, the normal CP could be used for situations where previously the extended CP was required in LTE networks. Specifically, the normal CP could be used on LTE networks with delay spread of up to the extended CP length. Thus, our methods can allow an increase of 16.9% in temporal spectral efficiency. On the other hand, the designs also allows LTE range extension for a given CP length given that the transmission power is sufficient.

In terms of complexity, the proposed receivers are more complex than the standard receivers using a one tap equalizer, but our receivers significantly outperform the standard receivers. In comparison with similar methods in literature such as the RISIC [2] and IJEP [22], our proposed methods offer comparable complexity with better performance in terms of data detection accuracy and bandwidth efficiency. For example, with the same number of iterations, the proposed methods can offer detection accuracy for delay spread up to 6 times the CP length while the

RISIC method struggles when the delay spread is 3 times the CP duration. On the other hand, our proposed methods only require a small number of pilot sub-carriers to achieve an accurate channel estimate while the IJEP algorithm requires a full OFDM symbol dedicated for the pilot. Hence, the proposed methods provide better bandwidth efficiency and flexibility than IJEP when applied to existing LTE systems.

In this thesis, our contributions include analysis of the interference arising in insufficient CP OFDM transmissions and the development of a number of effective reception techniques for such transmissions in SIMO and MIMO systems. An effective PSB-MMSE algorithm is developed for channel estimation in SIMO-OFDM systems with insufficient CP. For data detection, we proposed three detectors based on ZF, MMSE and trellis techniques. The PSB-MMSE estimator and the trellis based equalizer are extended to the EPSP-MMSE estimator and the BDMA equalizer for MIMO systems. For enhancing the data reception process, iterative receivers are constructed based on these designs and can provide excellent performance. In this chapter, the results obtained are summarized and possible future research directions are described, based on the findings of the research.

6.1 Interference Analysis

OFDM transmissions with insufficient CP suffer ISI and ICI, which distort the transmitted signal. In order to develop effective reception schemes, the insufficient CP interference is mathematically modelled and its characteristics are analyzed in Chapter 3. It can be seen that the interference has a severe effect on the transmission quality in the form of a reduction in SINR. There is a fast degradation in SINR when the channel delay increases beyond the CP length. Increasing the transmission power, and hence SNR, has little effect in compensating for such a reduction. Thus, it is necessary to have an efficient channel estimation, interference mitigation and equalization process for a reliable OFDM link.

The analysis also showed that ICI is a major degradation factor (nearly as severe as ISI) and most ICI energy comes from sub-carriers that are close to the sub-carrier of interest. It was found that across a wide range of channel delay spread, the majority of ICI energy is located in the closest 6 to 8 sub-carriers and a significant number of additional sub-carriers would be required to achieve meaningful gains

beyond that. This characteristic is important for designing the trellis based equalization as its process needs to involve a sufficient number of these sub-carriers to be effective.

It is also realized that the distribution of the insufficient CP induced interference is approximately Gaussian distributed with zero mean. This is because both ISI and ICI are the sums of a large number of scaled independent and identically distributed variables drawn from a finite QAM constellation. Such approximation is supported by interference histograms, which resemble a normal distribution, and the interference auto-correlation that is approximately a delta function. Yet, it is further proven by the Chi-Square goodness of fit test, which passes with a significance level of 1.5%. This property is important as it allows the channel estimators to compensate the interference effect in the initial estimation (when ICI is not yet mitigated) by treating it as an additional noise source with a known variance.

6.2 Reception Methods for Insufficient CP SIMO-OFDM

In Chapter 4, we proposed various iterative receiver designs for channel estimation and data detection of insufficient CP SIMO-OFDM transmission. In the context of insufficient CP, it is difficult to acquire an accurate channel estimate because the unknown data sub-carriers corrupt the pilot sub-carriers. In addition, it becomes more difficult when the channel statistics (in the form of the PDF matrix) are not available at the receiver side. The PSB-MMSE channel estimator was proposed to overcome these factors while using a limited number of pilot sub-carriers. The PSB-MMSE algorithm involves the processes of estimating the channel PDP matrix and identifying the channel coefficients. Simulated MSE results have indicated that the proposed PSB-MMSE channel estimator is an effective estimation technique as it is able to achieve an estimation accuracy near that of sufficient CP systems for a channel delay spread up to twice the CP length. However, the method is limited by the number of available pilot sub-carriers used to estimate long delay spread channels due to the inaccuracy in estimating the covariance matrix.

We also proposed effective data detection strategies in the form of ZF, MMSE and trellis based detectors. The two ZF and MMSE detectors are less complex than the proposed trellis equalizer. However, these techniques have a restriction regard-

ing the number of channel paths and the number of receive antennas; hence they are not as generalized as the trellis based technique. It can be observed that all the proposed detection methods provide much better performance than the standard MRC - one tap detector. In comparison, the trellis equalizer provides the best performance, which is followed by the MMSE detector and finally the ZF detector. The trellis equalizer is able to have detection accuracy close to that of sufficient CP transmission with only a few iterations. However, its performance degrades significantly as the channel delay spread exceeds 3 times the CP length because the major ICI contributed sub-carriers (in the forward direction) are not included in its process.

The complexities of the proposed channel estimation and data detection algorithms were also analyzed in Chapter 4. The analysis showed us that the complexity of the PSB-MMSE algorithm is approximately 75% of the complexity of the conventional MMSE algorithm. This is because the standard MMSE channel estimator needs to calculate the full TD channel response while the proposed method only needs to estimate the channel path coefficients. On the other hand, it can be seen that the RISIC algorithm is approximately 2.7 and 1.7 times more complex than the proposed ZF and MMSE detectors, respectively, while the proposed trellis equalizer is 1.6 times more complex than the RISIC algorithm [2]. However, the trellis equalizer provides significantly better BER performance than those of other methods. It is able to provide near sufficient CP detection accuracy with channel delay spread up to 3 times the CP duration while the other methods cannot do so when the delay spread exceeds 1.5 times the CP duration.

6.3 Reception Method for Insufficient CP MIMO-OFDM

In Chapter 5, a high performance iterative receiver consisting of channel estimation and trellis equalization was presented. Here, the high performance EPSB-MMSE algorithm was developed based on the PSB-MMSE estimator for estimating MIMO channels. The channel estimation process was formulated into an optimization process that searches for an optimal solution among a finite number of possibilities. An effective search method is developed to reduce the estimator complexity. The estimator also used aided data from the previous iteration to improve its performance. Obtained simulation results showed us that the proposed EPSB-MMSE method is significantly better than the standard LSI method [101] and is compatible to the

IJEP scheme [22], which needs a full OFDM symbol as pilot. On the other hand, the EPSB-MMSE estimator approaches the CRB for delay spread up to 4 times the CP length with only 2 iterations.

The BDMA equalization process was developed as an extension of the previously proposed trellis equalizer for MIMO systems. The developed algorithm utilizes a bidirectional process to include a necessary number of sub-carriers for accurate detection while keeping the trellis size minimal. For further complexity reduction, the equalization process incorporates the M-algorithm. It was shown via simulation results that the BDMA algorithm can provide excellent data detection accuracy for insufficient CP MIMO-OFDM transmissions. The BDMA algorithm significantly outperforms both the standard receiver and the RISIC algorithm [2]. It allows the iterative reception process to converge to the sufficient CP accuracy for channel delay spread up to 3 times the CP length with only 2 iterations. Simulation results also showed us that reduction in complexity by using the factor of 2 still provided performance close to that of the full complexity equalizer.

The complexity analysis in Chapter 5 showed us that the proposed EPSB-MMSE algorithm is approximately 1.95 times more complex than the IJEP algorithm. However, our method is applicable to the pilot setting used in LTE and offers better bandwidth efficiency by requiring a lot fewer pilot sub-carriers (a reduction of approximately 70% in comparison to the pilot requirement in the IJEP algorithm for the considered LTE systems) while achieving comparable performance. Our channel estimation method is more flexible in terms of pilot arrangement so it is applicable to a wide variety of OFDM systems. It was also shown that the BDMA is approximately 2.5 times more complex than the RISIC algorithm. However, our method provides significantly better BER performance as it provides more than 2 times the system tolerance for the excess delay spread achieved by the RISIC algorithm.

6.4 Suggestions for Future Research

In this section we give a list of possible areas for further research which should be considered to further enhance the performance of the systems we have developed in this thesis.

- The current research is limited to un-coded OFDM systems. This work could be extended to investigate the system performances with a forward error control code. The presence of an error control decoder in the receiver would allow us to construct an iterative process between the channel estimator, equalizer and decoder. A suitable soft information generation algorithm such as the SOVA algorithm [112, 113] could be applied to the trellis equalizer and the decoder for enhancing their performance via the exchange of soft information. The interference mitigation process could also benefit from the computed soft information. However, such iterative structure can become computationally expensive. Hence, complexity reduction techniques may need to be investigated for the receiver to be practical.

- Space-time coding is an important feature in LTE MIMO-OFDM systems. The incorporation of space-time coding into the MIMO-OFDM systems may provide the receiver with additional information to effectively detect data from insufficient CP MIMO-OFDM transmission. The additional information comes from the strong correlation between the transmitted space-time encoded OFDM symbols. Our research can be extended to explore this.

- The work in this thesis considers block fading channels in which the channel coefficients stay constant for a duration of a few OFDM symbols. A possible extension on our work is to investigate insufficient CP OFDM systems with a fading channel in which its coefficients vary (slowly) over an OFDM symbol duration. Due to the limited number of available pilot sub-carriers, it would be very difficult to directly estimate such a channel. Therefore, a possible solution is to use the basis expansion model to approximate the channel [37]. The pilot sub-carriers can be used to estimate/tune the model parameters (which are much fewer in number compared to the channel coefficients) so that it can be as close to the transmission channel as much as possible. Given that the channel statistics such as fade rate can be known at the receiver as prior knowledge, we could investigate suitable channel prediction algorithms for enhancing the reception process.

- In this work, we assume perfect synchronization. However, in practical sys-

tems, an OFDM receiver can suffer carrier offset due to the imperfections in local oscillators and Doppler effect present in mobile radio channels. Such frequency offset can be reliably approximated via the use of pilot OFDM symbols in OFDM systems. However, in our considered insufficient CP OFDM systems, pilot OFDM symbols are not available. In addition, the small number of available pilot sub-carriers are corrupted by ISI and ICI, thus causing imperfections in frequency offset estimation. As an extension to this work, we can develop high performance iterative methods for joint frequency offset, channel estimation and data detection over doubly (time and frequency) selective channels for insufficient CP OFDM systems.

- It was shown in this work that employing an insufficient CP or suppressing the CP can significantly increase the spectral efficiency of an OFDM system, especially for long range transmissions. Spectral efficiency can also be improved by using full-duplex transmission, where bidirectional communications is carried out over the same temporal and spectral resources. It is expected that a system utilizing both full duplex and insufficient CP OFDM can achieve very high spectral efficiency. Such capacity gain is desired for current and future wireless networks. The work in this thesis can be extended to establish a high performance receiver that can reliably detect transmitted data in insufficient CP OFDM full duplex systems.

Appendix A

Proof for Property of Inner Summation in ICI and ISI Expressions

In this section, we will show the proof for the equality in (3.18), which is given by

$$\sum_{k=0,k\neq a}^{N-1}\left|\frac{\rho_{k-a}^{\tau_l-G}-1}{1-\rho_{k-a}}\right|^2=\frac{|e^{j\pi(\tau_l-G)}-1|^2}{4}+2\sum_{k=1}^{N/2-1}\left|\frac{\rho_k^{\tau_l-G}-1}{1-\rho_k}\right|^2. \tag{A.1}$$

Let us denote

$$B(k)=\frac{\rho_k^{\tau_l-G}-1}{1-\rho_k}=\frac{e^{j2\pi k(\tau_l-G)/N}-1}{1-e^{j2\pi k/N}} \tag{A.2}$$

for $-N+1\leq n\leq N-1$. The function $B(n)$ has the properties $|B(k)|^2=|B(-k)|^2$ and $|B(N/2-k)|^2=|B(N/2+k)|^2$. The proofs for these properties are shown below: From (A.2), we have

$$\begin{aligned}|B(-k)|^2 &= \left|\frac{\cos(2\pi k(\tau_l-G)/N)-j\sin(2\pi k(\tau_l-G)/N)-1}{1-\cos(2\pi k/N)+j\sin(2\pi k/N)}\right|^2\\ &= \frac{|\cos(2\pi k(\tau_l-G)/N)-1|^2+|\sin(2\pi k(\tau_l-G)/N)|^2}{|1-\cos(2\pi k/N)|^2+|\sin(2\pi k/N)|^2}\end{aligned} \tag{A.3}$$

and

$$\begin{aligned}|B(k)|^2 &= \left|\frac{\cos(2\pi k(\tau_l-G)/N)+j\sin(2\pi k(\tau_l-G)/N)-1}{1-\cos(2\pi k/N)-j\sin(2\pi k/N)}\right|^2\\ &= \frac{|\cos(2\pi k(\tau_l-G)/N)-1|^2+|\sin(2\pi k(\tau_l-G)/N)|^2}{|1-\cos(2\pi k/N)|^2+|\sin(2\pi k/N)|^2}.\end{aligned} \tag{A.4}$$

A. PROOF FOR PROPERTY OF INNER SUMMATION IN ICI AND ISI EXPRESSIONS

As the final expressions in (A.3) and (A.4) are the same, the property $|B(k)|^2 = |B(-k)|^2$ is true. On the other hand,

$$\begin{aligned}
& |B(N/2-k)|^2 \\
= & \left|\frac{e^{j2\pi(N/2-k)(\tau_l-G)/N}-1}{1-e^{j2\pi(N/2-k)/N}}\right|^2 = \left|\frac{e^{-j2\pi k(\tau_l-G)/N}e^{j2\pi N/2(\tau_l-G)/N}-1}{1-e^{-j2\pi k/N}e^{j2\pi N/2/N}}\right|^2 \\
= & \left|\frac{e^{-j2\pi k(\tau_l-G)/N}e^{j\pi(\tau_l-G)}-1}{1-e^{-j2\pi k/N}e^{j\pi}}\right|^2 = \left|\frac{e^{-j2\pi k(\tau_l-G)/N}(-1)^{\tau_l-G}-1}{1+e^{-j2\pi k/N}}\right|^2 \\
= & \frac{\left|\cos(2\pi k(\tau_l-G)/N)(-1)^{\tau_l-G}-1\right|^2+\left|\sin(2\pi k(\tau_l-G)/N)\right|^2}{\left|1-\cos(2\pi k/N)(-1)^{\tau_l-G}\right|^2+\left|\sin(2\pi k/N)\right|^2} \qquad \text{(A.5)}
\end{aligned}$$

and

$$\begin{aligned}
& |B(N/2+k)|^2 \\
= & \left|\frac{e^{j2\pi(N/2+k)(\tau_l-G)/N}-1}{1-e^{j2\pi(N/2+k)/N}}\right|^2 = \left|\frac{e^{j2\pi k(\tau_l-G)/N}e^{j2\pi N/2(\tau_l-G)/N}-1}{1-e^{j2\pi k/N}e^{j2\pi N/2/N}}\right|^2 \\
= & \left|\frac{e^{j2\pi k(\tau_l-G)/N}e^{j\pi(\tau_l-G)}-1}{1-e^{j2\pi k/N}e^{j\pi}}\right|^2 = \left|\frac{e^{j2\pi k(\tau_l-G)/N}(-1)^{\tau_l-G}-1}{1+e^{j2\pi k/N}}\right|^2 \\
= & \frac{\left|\cos(2\pi k(\tau_l-G)/N)(-1)^{\tau_l-G}-1\right|^2+\left|\sin(2\pi k(\tau_l-G)/N)\right|^2}{\left|1-\cos(2\pi k/N)(-1)^{\tau_l-G}\right|^2+\left|\sin(2\pi k/N)\right|^2}. \qquad \text{(A.6)}
\end{aligned}$$

Hence, $|B(N/2-k)|^2 = |B(N/2+k)|^2$. Using the above properties of $B(k)$, for $0 \le a \le N/2-1$, we have

$$\begin{aligned}
\sum_{k=0,k\neq a}^{N-1}|B(k-a)|^2 &= \sum_{k=-a}^{N-1-a}|B(k)|^2 \\
&= |B(N/2)|^2+\sum_{k=-a,z\neq 0}^{a}|B(k)|^2+\sum_{k=a+1,z\neq N/2}^{N-1-a}|B(k)|^2 \\
&= |B(N/2)|^2+2\sum_{k=1}^{a}|B(k)|^2+\sum_{k=a+1,z\neq N/2}^{N-1-a}|B(k)|^2
\end{aligned} \qquad \text{(A.7)}$$

and

$$\begin{aligned}\sum_{z=a+1,k\neq N/2}^{N-1-a}|B(k)|^2 &= \sum_{k=-N/2+a+1}^{-1}|B(N/2+k)|^2+|B(N/2-k)|^2\\ &= 2\sum_{k=-N/2+a+1}^{-1}|B(N/2+k)|^2\\ &= 2\sum_{k=a+1}^{N/2-1}|B(k)|^2. \qquad \text{(A.8)}\end{aligned}$$

Hence,

$$\sum_{k=0}^{N-1}|B(k-a)|^2=|B(0)|^2+|B(N/2)|^2+2\sum_{k=1}^{N/2-1}|B(k)|^2. \qquad \text{(A.9)}$$

Substituting (A.2) into (A.9), we obtain

$$\begin{aligned}\sum_{k=0}^{N-1}\left|\frac{\rho_{k-a}^{\tau_l-G}-1}{1-\rho_{k-a}}\right|^2 &= \left|\frac{\rho_{N/2}^{\tau_l-G}-1}{1-\rho_{N/2}}\right|^2+2\sum_{k=1}^{N/2-1}\left|\frac{\rho_k^{\tau_l-G}-1}{1-\rho_k}\right|^2\\ &= \frac{|e^{j\pi(\tau_l-G)}-1|^2}{4}+2\sum_{k=1}^{N/2-1}\left|\frac{\rho_k^{\tau_l-G}-1}{1-\rho_k}\right|^2. \qquad \text{(A.10)}\end{aligned}$$

So our proof is complete.

Bibliography

[1] E. Dahlman, S. Parkvall, and J. Skold, *4G LTE/LTE-Advanced for Mobile Broadband*. Elsevier Ltd., Oxford, 2011.

[2] D. Kim and G. L. Stuber, "Residual ISI cancellation for OFDM with applications to HDTV broadcasting," *IEEE J. Sel. Areas Commun.*, vol. 16, pp. 1590–1599, Oct. 1998.

[3] L. J. Cimini, "Analysis and simulation of a digital mobile radio channel using orthogonal frequency division multiplexing," *IEEE Trans. Commun.*, vol. 33, pp. 665–765, July 1985.

[4] IEEE 802.11 WG, "IEEE 802.11 wireless local area networks (WLAN)."

[5] K. Fazel and S. Kaiser, *Multi-Carrier and Spread Spectrum Systems: From OFDM and MC–CDMA to LTE and WiMAX*. John Wiley & Sons, 2nd ed., 2008.

[6] E. Dahlman, S. Parkvall, J. Skold, and P. Beming, *3G Evolution: HSPA and LTE for Mobile Broadband*. Elsevier Ltd., Oxford, 2nd ed., 2008.

[7] J. A. C. Bingham, "Multicarrier modulation for data transmission: An idea whose time has come," *IEEE Commun. Mag.*, vol. 28, pp. 5–14, May 1990.

[8] L. M. Correia and R. Prasad, "An overview of wireless broadband communications," *IEEE Commun. Mag.*, vol. 17, pp. 28–33, Jan. 2000.

[9] Z. Wang and G. B. Giannakis, "Wireless multicarrier communications," *IEEE Signal Process. Mag.*, vol. 17, pp. 29 – 48, May 2000.

[10] J. U. Shanker, *OFDM Towards Broadband Wireless Access*. Artech House, Norwood, 2007.

[11] H. Sari, G. Karam, and I. Jeanclaude, "Transmission techniques for digital terrestrial TV broadcasting," *IEEE Commun. Mag.*, vol. 33, pp. 100–109, Feb. 1995.

[12] X. Ma, M. K. Oh, and G. B. Giannakis, "Hopping pilots for estimation of frequency-offset and multiantenna channels in MIMO-OFDM," *IEEE Trans. Commun.*, vol. 53, pp. 162–172, Jan. 2005.

[13] N. Gejoh and Y. Karasawa, "OFDM transmission characteristics in multipath environment where the delay spreading exceeds the guard interval analyzed based on the ETP model," *Electronics Commun. Jap.*, vol. 87, pp. 1–10, Jan. 2004.

[14] Y. Karasawa, N. Gejoh, and T. Izumi, "Modeling and analysis of OFDM transmission characteristics in rayleigh fading environment in which the delay profile exceeds the guard interval," *IEICE Trans. Commun.*, vol. E88-B, pp. 3020–3027, July 2005.

[15] X. Nguyen, T. Taniguchi, and Y. Karasawa, "Statistical characteristics of MIMO-OFDM transmission systems in a multipath environment where the delay spreading exceeds the guard interval," *Electronics Commun. Jap.*, vol. 88, pp. 29–39, Dec. 2005.

[16] S. Suyama, H. Suzuki, and K. Fukawa, "An OFDM receiver with smoothed FFT-window and RLS-MLSE for fast multipath fading environments with large delay spread," in *Proc. of IEEE 7th Inter. Symp. on Spread Spectrum Tech. & App.*, vol. 2, pp. 353–357, 2002.

[17] K. Hayashi and H. Sakai, "A simple interference elimination scheme for single carrier block transmission with insufficient cyclic prefix," in *Proc. of 17th Inter. Symp. Wireless Per. Multi. Commun.*, 2004, Sydney, Australia.

[18] M. D. Nisar, W. Utscick, H. Nottensteiner, and T. Hindelang, "On channel estimation and equalization of OFDM systems with insufficient cyclic prefix," in *Proc. of IEEE 65th Veh. Tech. Conf.*, pp. 1445–1449, Apr. 2007, Dublin.

[19] V. Nguyen, M. Patzold, F. Maehara, H. Haas, and M. Pham, "Channel estimation and interference cancellation for MIMO-OFDM systems," *IEICE Trans. Commun.*, vol. E-90-B, pp. 277–290, Feb. 2007.

[20] C. Prieto, V. P. Gil, and M. J. F. Garcia, "Joint channel and frequency offset estimation in MIMO-OFDM systems with insufficient cyclic prefix," *Phys. Commun.*, vol. 4, pp. 254–265, Dec. 2011.

[21] C. Prieto and M. J. F. Garcia, "Suppression of cyclic prefix in down-link LTE like systems to increase capacity," in *Proc. of IEEE 77th Veh. Tech. Conf.*, Jun. 2013, Desden, Germany.

[22] C. Prieto and M. J. F. Garcia, "Iterative joint estimation procedure for channel and frequency offset in multi-antenna OFDM systems with an insufficient cyclic prefix," *IEEE Trans. Veh. Tech.*, vol. 62, pp. 3653–3662, Oct. 2013.

[23] H. C. Won, J. H. Jang, and G. H. Im, "Iterative cyclic prefix reconstruction and channel estimation for space-time block coded frequency division multiplexing," in *Proc. of IEEE Inter. Conf. on Commun.*, vol. 4, pp. 16–20, May. 2005.

[24] H. C. Won and G. H. Im, "Iterative cyclic prefix reconstruction and channel estimation for a STBC OFDM system," *IEEE Commun. Let.*, vol. 9, pp. 307–309, Apr. 2005.

[25] X. Wang, P. Ho, and Y. Wu, "Robust channel estimation and ISI cancellation for OFDM systems with suppressed features," *IEEE J. Sel. Areas Commun.*, vol. 23, pp. 963–972, May 2005.

[26] J. B. Lim, E. S. Kim, C. J. Park, H. C. Won, K. H. Kim, and G. H. Im, "Bandwidth-efficient OFDM transmission with iterative cyclic prefix reconstruction," *IEEE J. Commun. and Netw.*, vol. 10, pp. 239–252, Sept. 2008.

[27] M. Yoshida, Y. Amezawa, S. Sonobe, and A. Sugitani, "Laboratory experiment of OFDM transmission using VLP and pre-FFT equalizer over ISI channels," in *Proc. of IEEE 59th Veh. Tech. Conf.*, vol. 1, pp. 540–544, 2004.

[28] C. Li and S. Roy, "Subspace based blind channel estimation for OFDM by exploiting virtual carrier," in *Proc. of IEEE Global Telecommun. Conf.*, vol. 1, pp. 295–299, Nov. 2001, San Antonio, Texas.

[29] C. Li and S. Roy, "Subspace-based blind channel estimation for OFDM by exploiting virtual carriers," *IEEE Trans. Wireless Commun.*, vol. 2, pp. 1536–1276, Jan. 2003.

[30] C. Shin and E. J. Powers, "Blind channel estimation for MIMO-OFDM systems using virtual carriers," in *Proc. of IEEE Global Telecommun. Conf.*, vol. 4, pp. 2465–2469, Dec. 2004.

[31] C. Shin, R. W. Heath, and E. J. Powers, "Blind channel estimation for MIMO-OFDM systems," *IEEE Trans. Veh. Tech.*, vol. 56, pp. 670–685, Feb. 2007.

[32] Y. Sagae, S. Suyama, H. Suzuki, and K. Fukawa, "An OFDM turbo equalizer for scattered pilot signals in multipath environments with delay difference greater than guard interval," in *Proc. of IEEE 59th Veh. Tech. Conf.*, vol. 1, pp. 425–429, May 2004.

[33] J. G. Kim and J. T. Lim, "MAP-based channel estimation for MIMO-OFDM over fast rayleigh fading channels," *IEEE Trans. Veh. Tech.*, vol. 57, pp. 1963–1968, May 2008.

[34] H. Nguyen-Le, T. Le-Ngoc, and C. C. Ko, "Joint channel estimation and synchronization for MIMO-OFDM in the presence of carrier and sampling frequency offsets," *IEEE Trans. Broadcast.*, vol. 58, pp. 3075–3081, July 2008.

[35] H. Nguyen-Le, T. Le-Ngoc, and C. C. Ko, "Turbo processing for joint channel estimation, synchronization, and decoding in coded MIMO–OFDM systems," *EURASIP J. Wireless Commun. and Netw.*, vol. 2009.

[36] H. Nguyen-Le, T. Le-Ngoc, and C. C. Ko, "RLS-based joint estimation and tracking of channel response, sampling and carrier frequency offsets for OFDM," *IEEE Trans. Broadcast.*, vol. 55, pp. 84–94, Mar. 2009.

[37] H. Nguyen-Le, T. Le-Ngoc, and C. C. Ko, "Iterative receiver design with joint doubly selective channel and CFO estimation for coded MIMO–OFDM transmissions," *IEEE Trans. Veh. Tech.*, vol. 60, pp. 4052–4057, May 2011.

[38] E. P. Simon, H. H. L. Ros, and M. Ghogho, "Joint carrier frequency offset and channel estimation for OFDM systems via the EM algorithm in the presence of very high mobility," *IEEE Trans. Sig. Process.*, vol. 60, pp. 754–765, Feb. 2012.

[39] K. C. Hung and D. W. Lin, "Pilot-based LMMSE channel estimation for OFDM systems with power delay profile approximation," *IEEE Trans. Veh. Tech.*, vol. 59, pp. 150–159, Jan. 2010.

[40] P. Melsa, R. Younce, and C. Rohrs, "Impulse response shortening for discrete multitone transceivers," *IEEE Trans. Commun.*, vol. 44, pp. 1662–1672, Dec. 1996.

[41] W. Henkel and T. Kessleer, "Maximizing the channel capacity of multicarrier transmission by suitable adaptation of the time domain equalizer," *IEEE Trans. Commun.*, vol. 48, pp. 2000–2004, Dec. 2000.

[42] B. Farhang-Boroujeny and M. Ding, "Design methods for time-domain equalizers in dmt transceivers," *IEEE Trans. Commun.*, vol. 49, pp. 554–562, Mar. 2001.

[43] K. Vanbleu, G. Ysebaert, G. Cuypers, M. Moonen, and K. V. Acker, "Bitrate maximizing time-domain equalizer design for DMT-based systems," *IEEE Trans. Commun.*, vol. 52, pp. 871–876, June 2004.

[44] T. Tang and R. W. Heath, "Space-time interference cancellation in MIMO-OFDM systems," *IEEE Trans. Veh. Tech.*, vol. 54, pp. 1802–1816, Sept. 2005.

[45] I. Barhumi, G. Leus, and M. Moonen, "Equalization for OFDM over doubly selective channels," *IEEE Trans. Sig. Process.*, vol. 54, pp. 1445–1458, Apr. 2006.

[46] R. K. Martin, G. Ysebaert, and K. Vanbleu, "Bit error rate minimizing channel shortening equalizers for cyclic prefixed systems," *IEEE Trans. Commun.*, vol. 55, pp. 2605–2616, June 2007.

[47] M. Shaodan and T. S. Ng, "Semi-blind time-domain equalization for MIMO-OFDM systems," *IEEE Trans. Veh. Tech.*, vol. 57, pp. 2219–2227, July 2008.

[48] C. Toker and G. Altin, "Blind, adaptive channel shortening equalizer algorithm which can provide shortened channel state information (BACS–SI)," *IEEE Trans. Sig. Process.*, vol. 57, pp. 1483–1493, Apr. 2009.

[49] T. Miyajima and Z. Ding, "Sub-carrier nulling algorithms for channel shortening in uplink OFDMA systems," *IEEE Trans. Sig. Process.*, vol. 60, pp. 2374–2385, May 2012.

[50] D. Darsena, G. Gelli, L. Paura, and F. Verde, "Blind channel shortening for space-time-frequency block coded MIMO-OFDM systems," *IEEE Trans. Wireless Commun.*, vol. 11, pp. 1022–1033, Mar. 2012.

[51] G. Leus and M. Moonen, "Per-tone equalization for MIMO-OFDM systems," *IEEE Trans. Sig. Process.*, vol. 51, pp. 2965–2975, Nov. 2003.

[52] I. Barhumi, G. Leus, and M. Moonen, "Equalization for OFDM over doubly selective channels," *IEEE Trans. Sig. Process.*, vol. 54, pp. 1445–1458, Apr. 2006.

[53] N. Al-Dhahir, "FIR channel-shortening equalizers for MIMO ISI channels," *IEEE Trans. Wireless Commun.*, vol. 49, pp. 213–218, Feb. 2001.

[54] S. D. Ma and T. S. Ng, "Time domain signal detection based on second order statistics for MIMO–OFDM systems," *IEEE Trans. Sig. Process.*, vol. 55, pp. 1150–1158, Mar. 2007.

[55] S. D. Ma and T. S. Ng, "Semi blind time domain equalization for MIMO–OFDM systems," *IEEE Trans. Veh. Tech.*, vol. 57, pp. 2219–2227, July 2008.

[56] M. Budsabathon, Y. Hara, and S. Hara, "Optimum beamforming for pre-FFT OFDM adaptive antenna array," *IEEE Trans. Veh. Tech.*, vol. 53, pp. 945–955, July 2004.

[57] C. Y. Liu, Y. F. Chen, and C. P. Li, "Blind beamforming schemes in SC-FDMA systems with insufficient cyclic prefix and carrier frequency offset," *IEEE Trans. Veh. Tech.*, vol. 58, pp. 4848–4859, Nov. 2009.

[58] C. Y. Lin, J. Y. Wu, and T. S. Lee, "Robust constrained optimization based linear receiver for high-rate MIMO-OFDM against channel estimation errors," *IEEE Trans. Sig. Process.*, vol. 55, pp. 2628–2645, June 2007.

[59] Y. Jin and X. G. Xia, "An interference nulling based channel independent precoding for MIMO-OFDM systems with insufficient cyclic prefix," *IEEE Trans. Commun.*, vol. 61, pp. 131–143, Jan. 2013.

[60] Y. Jin and X. G. Xia, "A robust precoder design based on channel statistics for MIMO-OFDM systems with insufficient cyclic prefix," *IEEE Trans. Commun.*, vol. 62, pp. 1249–1257, Apr. 2014.

[61] A. S. Bedi, J. Akhtar, K. Rajawat, and A. K. Jagannatham, "BER optimized precoders for OFDM systems with insufficient cyclic prefix," *IEEE Commun. Let.*, vol. 99, pp. 1–4, Dec. 2015.

[62] C. Kosanyakun and C. Kotchasarn, "A study of insufficient cyclic prefix by using precoding for MIMO-OFDM systems," in *IEEE 17th Int. Conf. Adv. Commun. Tech.*, jul 2015.

[63] A. Okazaki, K. Motoyoshi, M. Higashinaka, T. Nagayasu, H. Kubo, and A. Shibuya, "Frequency domain equalization incorporated with frequency domain redundancy for OFDM systems," in *IEEE 17th Inter. Symp. on Per., Indoor and Mobile Radio Commun.*, vol. 1, pp. 1–5, Sep. 2006, Helsinki.

[64] S. Suyama, H. Suzuki, and K. Fukawa, "An OFDM receiver employing turbo equalization for multipath environments with delay spread greater than the guard interval," in *Proc. of IEEE 57th Veh. Tech. Conf.*, vol. 1, pp. 632–636, apr 2003.

[65] S. Chen and C. Zhu, "ICI and ISI analysis and mitigation for OFDM systems with insufficient cyclic prefix in time-varying channels," *IEEE Trans. Consumer Electronics*, vol. 50, pp. 78–83, Feb. 2004.

[66] M. Yoshida and T. Taniguchi, "An LDPC-coded OFDM receiver with pre-FFT iterative equalizer for ISI channels," in *Proc. of IEEE 61st Veh. Tech. Conf.*, vol. 2, pp. 767–772, May 2005.

[67] J. B. Lim, C. H. Choi, and G. H. Im, "MIMO-OFDM with insufficient cyclic prefix," *IEEE Commun. Let.*, vol. 10, pp. 356–358, May 2006.

[68] M. Grossmann, C. Schneider, and R. S. Thoma, "Turbo equalisation for MIMO-OFDM transmission with insufficient guard interval," in *Proc. of IEEE Int. Zurich Sem. Commun.*, pp. 114–117, 2006, Zurich.

[69] A. F. Molisch, M. Toeltsch, and S. Vermani, "Iterative methods for cancellation of intercarrier interference in OFDM systems," *IEEE Trans. Veh. Tech.*, vol. 56, pp. 2158–2167, July 2007.

[70] J. B. Lim, E. S. Kim, C. J. Park, H. C. Won, K. H. Kim, and G. H. Im, "Bandwidth-efficient OFDM transmission with iterative cyclic prefix reconstruction," *IEEE Jo. Commun. Net.*, vol. 10, pp. 239–252, Sept. 2008.

[71] Z. Chen, C. Yongyu, and D. Yang, "Low-complexity turbo equalization for MIMO-OFDM system without cyclic prefix," in *IEEE 20th Inter. Symp. on Per., Indoor and Mobile Radio Commun.*, pp. 310–314, Sep. 2009, Tokyo.

[72] H. Lee, Y. Lee, and H. Park, "An efficient CP compensation for SC–FDE with insufficient CP symbols," *IEEE Commun. Let.*, vol. 14, pp. 548–550, June 2010.

[73] S. Suyama, Y. Hara, H. Suzuki, Y. Kamio, and K. Fukawa, "A maximum likelihood OFDM receiver with smoothed FFT-window for large multipath delay difference over the guard interval," in *Proc. of IEEE 55th Veh. Tech. Conf.*, vol. 3, pp. 1247–1251, 2002.

[74] S. Suyama, H. Suzuki, and K. Fukawa, "A MIMO-OFDM receiver employing the low-complexity turbo equalization in multipath environments with delay difference greater than the guard interval," *IEICE Trans. Commun.*, vol. E88-B, pp. 39–46, Jan. 2005.

[75] P. Alexander, D. Haley, and A. Grant, "Outdoor mobile broadband access with 802.11," *IEEE Commun. Mag.*, vol. 45, pp. 108–114, Nov. 2007.

[76] D. N. Liu and M. P. Fitz, "Iterative MAP equalization and decoding in wireless mobile coded OFDM," *IEEE Trans. Commun.*, vol. 57, pp. 2042–2051, July 2009.

[77] G. K. Walker, J. Wang, C. Lo, X. Zhang, and G. Bao, "Relationship between LTE broadcast/eMBMS and next generation broadcast television," *IEEE Trans. Broadcast.*, vol. 60, pp. 185–192, June 2014.

[78] T. Pham, T. Le-Ngoc, G. Woodward, and P. A. Martin, "Channel estimation and data detection for insufficient cyclic prefix MIMO-OFDM," *submitted to IEEE Trans. Veh. Tech.*, Mar. 2016.

[79] T. M. Pham, P. A. Martin, and G. Woodward, "Channel estimation and data detection for insufficient cyclic prefix SIMO-OFDM with pilot sub-carriers," in *IEEE 16th Aus. Comm. Theory Workshop*, Jan. 2016, Melbourne, Australia.

[80] T. M. Pham, P. A. Martin, G. Woodward, K. P. Kongara, and C. Horn, "Receiver design for SIMO-OFDM systems with insufficient cyclic prefix," in *IEEE 80th Veh. Tech. Conf.*, Sep. 2014, Vancouver, Canada.

[81] T. Pham, T. Le-Ngoc, G. Woodward, P. A. Martin, and K. T. Phan, "Equalization for MIMO-OFDM systems with insufficient cyclic prefix," in *IEEE 83th Veh. Tech. Conf.*, May 2016, Nanjing, China.

[82] M. C. Jeruchim, P. Balaban, and K. S. Shanmugan, *Simulation of Communication Systems*. New York, Kluwer Academic/Plenum, 2nd ed., 2000.

[83] J. B. Anderson, "Instrumentable tree encoding of information sources," *M.Sc. Thesis. School of Electrical Engineering,* Cornell University, 1969.

[84] T. S. Rappaport, *Wireless Communications Principles and Practice*. New York: Prentice-Hall, 2nd ed., 2002.

[85] D. Tse and P. Viswanath, *Fundamentals of Wireless Communication*. Cambridge University Press, 1st ed., 2005.

[86] J. M. Wozencraft and I. M. Jacobs, *Principles of Communication Engineering*. New York: Wiley, 1st ed., 1965.

[87] J. G. Proakis, *Digital Communications*. McGraw Hill, Boston, 2nd ed., 2001.

[88] 3GPP Organisational Partners, "3GPP TS 36.201 Ver. 8.0.0." `http://www.quintillion.co.jp/3GPP/Specs/36201-800.pdf`.

[89] A. Goldsmith, *Wireless Communications*. Cambridge University Press, 1st ed., 2005.

[90] W. C. Jakes, *Microwave Mobile Communications*. New York: IEEE Press, 1st ed., 2074.

[91] D. O. Reudink, "Properties of mobile radio propagation above 400 MHz," *IEEE Trans. Veh. Tech.*, vol. 23, pp. 1–20, Nov. 1974.

[92] H. Suzuki, "A statistical model for urban radio propagation," *IEEE Trans. Commun.*, vol. 25, pp. 673–680, July 1977.

[93] E. Biglieri, J. G. Proakis, and S. Shamai, "Fading channels: Information theoretic and communications aspects," *IEEE Trans. Inform. Theory*, vol. 44, pp. 2619–2692, Oct. 1998.

[94] J. Fuhl, J. P. Rossi, and E. Bonek, "High resolution 3-D direction of arrival determination for urban mobile radio," *IEEE Trans. Ant. & Prop.*, vol. 45, pp. 672–682, Apr. 1997.

[95] M. Toeltsch, J. Laurila, K. Kalliola, A. F. Molisch, P. Vainikainen, and E. Bonek, "Statistical characterization of urban spatial radio channels," *IEEE J. Sel. Areas in Commun.*, vol. 20, pp. 539–549, Apr. 2002.

[96] Y. Kai, M. Bengtsson, B. Ottersten, D. McNamara, P. Karlsson, and M. Beach, "Modeling of wideband MIMO radio channels based on NLoS indoor measurements," *IEEE Trans. Veh. Tech.*, vol. 53, pp. 655–665, May 2004.

[97] S. S. Ghassemzadeh, L. J. Greenstein, T. Sveinsson, A. Kavcic, and V. Tarokh, "UWB delay profile models for residential and commercial indoor environments," *IEEE Trans. Veh. Tech.*, vol. 54, pp. 1235–1244, July 2005.

[98] V. Erceg, D. G. Michelson, S. S. Ghassemzadeh, L. J. Greenstein, A. J. Rustako, P. B. Guerlain, M. K. Dennison, R. Roman, D. J. Barnickel, S. C. Wang, and R. R. Miller, "A model for the multipath delay profile of fixed wireless channels," *IEEE J. Sel. Areas in Commun.*, vol. 17, pp. 399–410, Mar. 1999.

[99] T. Yucek and H. Arslan, "Time dispersion and delay spread estimation for adaptive OFDM systems," *IEEE Trans. Veh. Tech.*, vol. 57, pp. 1715–1722, May 2008.

[100] S. Haykin, *Communication Systems.* John Wiley & Sons, 4th ed., 2001.

[101] J. Rime and M. Renfors, "Pilot spacing in orthogonal frequency division multiplexing system on practical channels," *IEEE Trans. Consumer Electronics*, vol. 42, pp. 959 – 962, Nov. 1996.

[102] D. G. Brennan, "Linear diversity combining techniques," *IEEE Proc.*, vol. 91, pp. 331–356, Feb. 2003.

[103] M. Abramowitz and I. A. Stegun, *Handbook of Mathematical Functions with Formulas, Graphs, and Mathematical Tables.* New York: Dover, 9th ed., 1972.

[104] K. A. Hamdi, "On the statistics of signal to interference plus noise ratio in wireless communications," *IEEE Trans. Commun.*, vol. 57, pp. 3199–3204, Nov. 2009.

[105] S. Coleri, M. Ergen, A. Puri, and A. Bahai, "Channel estimation techniques based on pilot arrangement in OFDM systems," *IEEE Trans. Broadcast.*, vol. 45, pp. 223–229, Mar. 1999.

[106] R. G. Brown and P. Y. C. Hwang, *Introduction to Random Signals and Applied Kalman Filtering.* New York: John Wiley & Sons, 3rd ed., 2008.

[107] H. Minn and V. K. Bhargava, "An investigation into time domain approach for OFDM channel estimation," *IEEE Trans. Broadcast.*, vol. 46, pp. 240–248, Mar. 2000.

[108] W. Zhou and W. H. Lam, "A fast LMMSE channel estimation method for OFDM systems," *EURASIP Journal on Wireless Commun. And Networking*, pp. 1–13, 2009.

[109] S. M. Kay, *Fundamentals of Statistical Signal Processing, Vol. 1, Estimation Theory*. Englewood Cliffs, NJ: Prentice-Hall, 1993.

[110] J. Shao, *Mathematical Statistics*. New York: Springer, 1998.

[111] A. V. D. Bos, *Parameter Estimation for Scientists and Engineers*. Hoboken: John Wiley & Sons, 2007.

[112] J. Hagenauer and P. Hoeher, "A Viterbi algorithm with soft-decision outputs and its applications," in *Proc. of IEEE Global Telecommun. Conf.*, vol. 3, pp. 1680 – 1686, Nov. 1989, Dallas, Texas.

[113] T. M. Pham, P. A. Martin, D. P. Taylor, and C. Horn, "Soft detection of CPM in multipath fading," in *Proc. of IEEE 55th Veh. Tech. Conf.*, pp. 2–5, Jun. 2013, Desden, Germany.